Universidade Federal de Santa Catarina
Campus de Florianópolis
Programa de Pós-Graduação em Engenharia Elétrica

Rogério Pereira Junior

Filter bank based waveforms for modern wireless communication systems

Florianópolis/SC

2022

Filter bank based waveforms for modern wireless communication systems

Rogério Pereira Junior

Tese de Doutorado submetida ao Programa de Pós-Graduação em Engenharia Elétrica (PPGEEL), da Universidade Federal de Santa Catarina para a obtenção do título de Doutor em Engenharia Elétrica.
Orientador: Prof. Carlos Aurélio Faria da Rocha, Dr.
Co-orientadores:
Prof. Bruno Sens Chang, Dr.
Prof. Didier Le Ruyet, Ph.D

Florianópolis/SC

2022

Ficha de identificação da obra elaborada pelo autor,
através do Programa de Geração Automática da Biblioteca Universitária da UFSC.

Junior, Rogério Pereira
Filter bank based waveforms for modern wireless communication systems / Rogério Pereira Junior ; orientador, Carlos Aurélio Faria da Rocha, coorientador, Bruno Sens Chang, coorientador, Didier Le Ruyet, 2023.
106 p.

Tese (doutorado) - Universidade Federal de Santa Catarina, Centro Tecnológico, Programa de Pós-Graduação em Engenharia Elétrica, Florianópolis, 2023.

Inclui referências.

1. Engenharia Elétrica. 2. Banco de filtros. 3. Ortogonalidade complexa. 4. Pré-Codificação. 5. Alta mobilidade. I. Faria da Rocha, Carlos Aurélio . II. Sens Chang, Bruno . III. Le Ruyet, Didier IV. Universidade Federal de Santa Catarina. Programa de Pós-Graduação em Engenharia Elétrica. V. Título.

Rogério Pereira Junior

Filter bank based waveforms for modern wireless communication systems

O presente trabalho em nível de doutorado foi avaliado e aprovado por banca examinadora composta pelos seguintes membros:

Prof. Carlos Aurélio Faria da Rocha, Dr.
Universidade Federal de Santa Catarina

Prof. Richard Demo Souza, Dr.
Universidade Federal de Santa Catarina

Prof. Leonardo Silva Resende, Dr.
Universidade Federal de Santa Catarina

Prof. Glauber Gomes de Oliveira Brante, Dr.
Universidade Tecnológica Federal do Paraná

Prof. Cristiano Magalhães Panazio, Dr.
Universidade de São Paulo

Certificamos que esta é a **versão original e final** do trabalho de conclusão que foi julgado adequado para obtenção do título de Doutor em Engenharia Elétrica

Documento assinado digitalmente
Telles Brunelli Lazzarin
Data: 21/03/2023 17:15:46-0300
CPF: ***.400.719-**
Verifique as assinaturas em https://v.ufsc.br

Prof. Telles Brunelli Lazzarin, Dr.
Coordenação do Programa de Pós-Graduação

Documento assinado digitalmente
CARLOS AURELIO FARIA DA ROCHA
Data: 17/03/2023 11:32:09-0300
CPF: ***.075.032-**
Verifique as assinaturas em https://v.ufsc.br

Prof. Carlos Aurélio Faria da Rocha, Dr.
Orientador

Florianópolis, 2022.

Para Samantha e Kauê, amo vocês.

Agradecimentos

Deixo meus sinceros agradecimentos a todos aqueles que de alguma forma contribuíram para que fosse possível o desenvolvimento desse trabalho, em especial:

Aos meus pais Rogério e Maria do Carmo pelo amor, confiança e ensinamentos que sempre me passaram em todos os momentos de minha vida;

A minha amada Samantha pelo companheirismo, amor e principalmente compreensão nos momentos de ausência;

A meu orientador Carlos Aurélio Faria da Rocha pelos ensinamentos acadêmicos, pelo privilégio de trabalhar sob sua orientação, paciência e motivação para que fosse possível a realização deste trabalho. Fica aqui, todo o meu respeito e admiração.

A meus coorientadores Bruno Sens Chang e Didier Le Ruyet, mesmo com a distância, exerceram um papel imprescindível com suas disponibilidades, colaborações e inspirações para realização desta tese.

A todos os demais professores do PPGEEL que contribuíram para construção do meu conhecimento em especial aos professores Richard Demo Souza, Bartolomeu Ferreira Uchôa Filho e Leonardo Silva Resende.

A Capes pelo apoio financeiro

A todos, Muito obrigado.

O caminho para o progresso não é rápido nem fácil.

Marie Curie

Resumo

Os novos sistemas de comunicação sem fio têm como objetivo cobrir uma ampla gama de cenários de aplicação. Estas aplicações vão desde a conectividade de milhares de dispositivos com baixo consumo energético até cenários de alta mobilidade com alta taxa de transmissão. Neste sentido, é necessário que todos os recursos tempo-frequência disponíveis sejam alocados da melhor maneira possível. Devido a problemas como alta emissão fora de banda (OOB) e sensibilidade a desvio Doppler, a Multiplexação por Divisão de Frequência Ortogonal (OFDM), escolhida como a forma de onda para a quinta geração de tecnologia móvel, não é a técnica mais eficiente para atender todas as demandas requeridas. Assim, busca-se técnicas que possam minimizar essas limitações. A modulação *orthogonal time frequency space* (OTFS) apresenta robustez em cenários de alta mobilidade com a detecção dos símbolos no domínio delay-Doppler, no entanto, mantém os problemas de emissão OOB. Alternativamente, o sistema Multiportadora de Bancos de Filtros (FBMC) ganhou atenção científica pelo uso de filtros digitais em cada subportadora. Deste modo, obtém-se uma melhor separação entre os canais e consequentemente uma redução da OOB. Entretanto, o processo de filtragem induz interferência intrínseca no sistema gerando a perda da ortogonalidade complexa.

Neste trabalho são propostas esquemas constituídos por técnicas de pré e pós-codificação em sistemas de banco de filtros com o objetivo de recuperar a ortogonalidade complexa. Tais técnicas são baseadas no espalhamento dos símbolos tanto no domínio da frequência como no domínio do tempo e trazem consigo características adicionais requeridas nos sistemas de comunicação sem fio modernos. Destaca-se além da melhor localização espectral, a robustez a cenários de alta mobilidade e baixa relação de potência pico-média (PAPR). Além disso, também é apresentado receptores de cancelamento de interferência no formato iterativo que aumentam consideravelmente o desempenho do sistema. Por fim, é desenvolvida uma proposta para tornar o projeto da forma de onda mais flexível através da introdução de um parâmetro chamado fator de taxa. Este fator possibilita que o sistema obtenha maior robustez em cenários de alta mobilidade de forma a ser uma alternativa ao sistema OTFS. Outra característica do sistema proposto é o bom desempenho de erro nestes mesmos cenários utilizando um equalizador simples no domínio da frequência, desempenho que não pode ser obtido com a modulação OTFS. São desenvolvidas soluções de forma fechada para relação sinal-interferência validando os resultados obtidos.

Palavras-chave: Banco de Filtros. Ortogonalidade complexa. Pré-Codificação. Alta mobilidade.

Abstract

The new wireless communication systems are intended to cover a wide range of application scenarios. These applications range from the connectivity of thousands of devices with low energy consumption to high mobility scenarios with high transmission rate. In this sense, it is necessary that all available time-frequency resources are allocated in the best possible way. Due to problems such as high out-of-band emission (OOB) and Doppler shift sensitivity, orthogonal frequency division multiplexing (OFDM), chosen as the waveform for the fifth generation (5G) of mobile technology, is not the most efficient technique for meet all required demands. Thus, techniques are sought that can minimize these limitations. The orthogonal time frequency space (OTFS) modulation presents robustness in high mobility scenarios with the detection of symbols in the delay-Doppler domain, however, it maintains the OOB emission problems. Alternatively, the multicarrier filter bank (FBMC) system has gained scientific attention for the use of digital filters on each subcarrier. In this way, a better separation between the channels is obtained and consequently a reduction of the OOB. However, the filtering process induces intrinsic interference in the system generating the loss of complex orthogonality.

In this work, schemes consisting of pre- and post-coding techniques in filter bank systems are proposed in order to recover the complex orthogonality. Such techniques are based on the spreading of symbols in both frequency and time domains and bring with them additional features required in modern wireless communication systems. Besides the better spectral localization, the robustness to high mobility and low peak-to-average power ratio (PAPR) scenarios stands out. In addition, interference canceling receivers are also presented in iterative format that considerably increase the performance of the system. Finally, a proposal is developed to make the waveform design more flexible by introducing a parameter called rate factor. This factor allows the system to obtain greater robustness in high mobility scenarios in order to be an alternative to the OTFS system. Another characteristic of the proposed system is the good error performance in these same scenarios using a simple frequency domain equalizer, a performance that cannot be obtained with OTFS modulation. Closed-form solutions are developed for the signal-interference relationship, validating the obtained results.

Keywords: Filter Bank. Complex Orthogonality. Precoding. High Mobility.

Resumo Expandido

Introdução

A multiplexação por divisão de frequência ortogonal (OFDM) é um dos esquemas de modulação mais difundidos e foi considerado parte fundamental em diversos sistemas de comunicação. Suas características de robustez contra canais seletivos em frequência, capacidade de evitar interferência entre símbolos com o prefixo cíclico (CP), equalização simples no domínio da frequência e sua implementação digital eficiente usando a transformada rápida de Fourier (FFT) demonstram o porque de sua popularidade. Entretanto, apesar de todas as suas qualidades, a técnica OFDM possui certas características indesejáveis que dificultam sua implementação em alguns cenários. Primeiro, há uma perda na eficiência espectral devido à inserção do prefixo cíclico. Em segundo lugar, o OFDM é muito sensível a desvios de frequência e tempo que podem ser geradas por uma sincronização defeituosa, ou até mesmo pelo efeito Doppler. Em terceiro lugar, o OFDM possui um valor elevado da razão entre a potência de pico e a potência média (PAPR) do sinal que pode levar o amplificador a operar em uma região não linear, resultando num consumo ineficiente de energia. Além disso, o OFDM utiliza um pulso formatador retangular o que leva a uma representação espectral do tipo *sinc* que causa grandes lóbulos laterais em cada subportadora. Assim, os subcanais na borda da largura de banda de transmissão podem ser uma fonte de interferência para outros sistemas vizinhos, devido a esta emissão fora da banda (OOB). Nesse sentido a técnica OFDM não é a técnica mais eficiente para os diversos cenários de aplicações que estão surgindo e sendo propostos para os novos sistemas sem fio. É necessário uma forma de onda que consiga obter alta tolerância a interferências, baixa latência, baixo consumo energético e robustez a erros de sincronização tempo-frequência.

Várias técnicas alternativas foram intensamente estudadas e algumas se mostraram mais promissoras e vêm competindo diretamente para se afirmar como padrão internacional para novas tecnologias. Dentre as técnicas propostas na literatura, pode-se destacar as técnicas SC-FDMA (*single carrier frequency division multiple access*), FBMC (*filter bank multi-carrier*) e a recente OTFS (*orthogonal time-frequency space*). Os sistemas SC-FDMA utilizam uma pré-codificação baseada no espalhamento dos símbolos de dados via transformada de Fourier discreta (DFT) antes do modulador OFDM. Desta forma, emula-se um sistema de portador única obtendo uma baixa PAPR e uma baixa sensibilidade ao deslocamento de frequência da portadora. No entanto, os problemas de emissão fora de banda persistem no sistema. Já nos sistemas FBMC executa-se uma filtragem em cada subportadora fornecendo um espectro bem localizado e uma rejeição significativa das emissões OOB. O uso desses filtros especialmente projetados, faz com que a interferência

entre símbolos e entre subportadoras sejam evitadas sem o uso de CP. Isso permite que o FBMC alcance uma eficiência espectral mais alta em comparação com o sistema OFDM. Além disso, uma implementação eficiente de baixa complexidade é possível por meio de redes polifásicas (PPN). No entanto, o teorema de *Balian-Low* diz que funções base com ortogonalidade complexa possuem necessariamente dispersão infinita no tempo ou na frequência. De fato, para o caso OFDM, temos no domínio da frequência o pulso *sinc* que se estende ao infinito. No caso do FBMC, a filtragem faz com que isso não ocorra e os símbolos são sobrepostos no tempo acarretando em uma interferência intrínseca imaginária por não possuir ortogonalidade complexa. Para cumprir o teorema a condição de ortogonalidade é reduzida ao campo real. Isto motivou o uso da modulação de amplitude em quadratura com offset (OQAM), que consiste em dividir os símbolos na transmissão em parte real e imaginária para serem modulados em símbolos consecutivos, de maneira que os símbolos reais e imaginários são alternados no tempo. Assim, para o esquema FBMC/OQAM, alternativamente, podemos enxerga-lo como um sistema onde a taxa de símbolo é dobrada, utilizando alternadamente a parte real e a parte imaginária de um símbolo QAM. Porém, a restrição da ortogonalidade para o plano real causa problemas para adaptar os sistemas FBMC-OQAM a certos esquemas de múltiplas antenas como multiplexação espacial com detecção de máxima verossimilhança e codificação em bloco espaço-temporal de Alamouti. Além disso, os problemas de sensibilidade ao Doppler e alta PAPR também estão presentes no sistema FBMC.

Nos últimos anos, a modulação OTFS recebeu significativa atenção como alternativa ao OFDM, especialmente para cenários de alta mobilidade. Usando uma pré-codificação via transformada simplética de Fourier (SFFT), a OTFS converte canais variantes no tempo em canais invariantes em um domínio chamado delay-Doppler (DD). Basicamente os símbolos de informação são inicialmente descritos no domínio DD, e então são mapeados para o domínio tempo-frequência (TF) pela inversa da SFFT (ISFFT) e, finalmente, transmitidos pelo canal usando o modulador OFDM. No receptor o processo inverso é realizado aplicando a SFFT. Através deste mapeamento, pode-se assumir que todos os símbolos em um bloco de transmissão experimentam o mesmo ganho de canal, proporcionando uma alta ordem de diversidade. No entanto, a detecção de dados é movida de um equalizador simples no domínio tempo-frequência para receptores no domínio DD com maior complexidade. Em termos de OOB, pelo uso do modulador OFDM como núcleo do sistema, a técnica apresenta o mesmo problema de localização espectral.

Objetivos

O objetivo central deste trabalho é propor e estudar um novo esquema baseado em banco de filtros pré-codificado com características de ortogonalidade complexa entre os pulsos base, robustez a canais duplamente seletivos, baixa PAPR e menores emissões fora da banda. Nosso primeiro objetivo é resgatar a ortogonalidade complexa e com suas

consequências, agregar outras funcionalidades benéficas para a construção de um esquema atraente para sistemas sem fios modernos. A pré-codificação é baseada no espalhamento dos símbolos por meio de pares DFT/IDFT semelhantes as vistas nos sistema SC-FDE e OTFS.

Metodologia

O trabalho desenvolvido tem início com uma profunda análise do estado da arte dos sistemas multiportadoras principalmente do OFDM por sua grande popularidade. Investigou-se suas desvantagens e as proposições existentes na literatura (mencionadas anteriormente) para minimiza-las. Percebe-se que as técnicas SC-FDMA e OTFS representam uma pré-codificação do sistema OFDM, trazendo algumas características interessantes em termos de PAPR e robustez ao Doppler. Por outro lado, o sistema FBMC modifica o núcleo do sistema removendo o prefixo cíclico e utilizando um banco de filtros de modo a obter uma vantagem em termos de localização espectral, entretanto perdendo a ortogonalidade complexa. O maior desafio para a aplicação de sistemas FBMC é o cancelamento da interferência intrínseca do filtro permitindo a restauração da ortogonalidade complexa. Espalhar os símbolos de dados em toda a faixa de tempo ou em todas as subportadoras pode ser usado para essa finalidade. Tal espalhamento é feito indiretamente nos sistemas SC-FDMA e OTFS, porém com objetivos distintos. Partindo desta premissa, nosso foco inicial foi a recuperação da ortogonalidade complexa. Nesse sentido, introduzimos no sistema FBMC uma pré-codificação baseada no espalhamento dos símbolos no domínio da frequência via DFT. Combinada com um estágio de compensação de interferência e uma estratégia de alocação dos dados, consegue-se obter a ortogonalidade complexa. Desta forma, obtemos a técnica que chamamos de *precoded DFT filter bank* que apresenta as vantagens do SC-FDMA e FBMC como, melhor localização espectral, baixa PAPR além de recuperar a ortogonalidade complexa.

A técnica OTFS utiliza o modulador OFDM como núcleo para transmissão dos dados. No entanto, outras técnicas multiportadoras também podem ser utilizadas para implementar esta transmissão, desde que a ortogonalidade complexa entre os pulsos do transmissor/receptor seja garantida. Assim, para usar o OTFS com um transceptor FBMC como núcleo, é necessário eliminar a interferência proveniente dos filtros para recuperar a ortogonalidade complexa. Conforme relatado anteriormente, esse objetivo pode ser alcançado usando pré-codificação via DFT. O ponto crucial aqui é que a restauração da ortogonalidade complexa pode ser feita usando parte do ISFFT (com mudanças estratégicas) aplicada no OTFS, visto que a mesma é uma transformada bidimensional (2D) formada pela combinação do par DFT/IDFT. Assim, apresentamos uma nova estrutura de banco de filtros pré-codificados baseada na modulação OTFS, na qual chamamos de *2D-FFT filter bank*. O esquema apresenta vantagens significativas em canais duplamente seletivos e eficiência espectral.

As contribuições propostas neste trabalho consideram a análise dos sistemas propostos sob diferentes aspectos: eficiência espectral, desempenho de erro em termos de taxa de erro de bit, PAPR, complexidade dos equalizadores e para implementação do esquema. Para se chegar em ambas as proposições, desenvolveu-se uma notação matricial para formular todo o modelo do sistema. Obteve-se uma notação concisa que permite entender principalmente o processo de compensação do filtro, devido à possibilidade de desmembrar o processo de modulação multiportadora por implementação via redes polifásicas. A partir desta notação foram desenvolvidas expressões analíticas de taxa de erro de bit (BER), relação sinal-interferência (SIR) e relação sinal-ruido-interferência (SINR) para ambos os esquemas validando os resultados obtidos.

Resultados e Discussão

A partir de simulações numéricas e das expressões analíticas obtidas, os sistemas propostos foram comparados com os outros esquemas discutidos na literatura. Primeiramente, mostrou-se que os resultados teóricos coincidem com os simulados validando o desempenho do sistema. Enfatizando o 2D-FFT filter bank visto que é a proposta final do trabalho, temos que o esquema possui uma estrutura semelhante à técnica OTFS e apresenta um bom desempenho de erro mesmo utilizando equalizadores simples no domínio da frequência, fato que não ocorre no próprio OTFS. Explorando esse comportamento, introduzimos receptores iterativos que usam um estágio inicial de equalização no domínio da frequência. Com estes receptores, o desempenho do erro é obtido nos mesmos níveis dos receptores da técnica OTFS no domínio DD que exigem maior complexidade. Em termos de eficiência espectral, nosso esquema apresenta vantagens em vista ser utilizado um banco de filtros. Já em termos de PAPR e BER utilizando o mesmo tipo de receptor no domínio DD, os sistemas apresentam resultados praticamente iguais. Por fim, a recuperação da ortogonalidade complexa permitiu a flexibilização da forma de onda introduzido um fator taxa para obter ainda mais robustez em cenários de alta mobilidade.

Considerações Finais

A transmissão por canais que variam no tempo e com alta dispersão Doppler é um desafio. A robustez da técnica OTFS para estes tipos de cenários torna a atraente o uso em futuras comunicações sem fio que suportam uma ampla gama de aplicações. Este trabalho visou obter um sistema com a mesma robustez do OTFS, mas com a vantagem de obter uma equalização com bom desempenho e baixa complexidade no domínio TF, além de menor OOB e PAPR. Apresentou-se uma estrutura de banco de filtros pré-codificado com tais características baseando-se no espalhamento dos símbolos via pares de DFT/IDFT.

Palavras-chave: Banco de Filtros, Ortogonalidade complexa, Pré-Codificação, Alta Mobilidade.

List of Figures

List of Tables

List of abbreviations and acronyms

AMP-FO: Approximate message passing simplified by first-order

BER: Bit error rate

IB-DFE: Iterative block decision feedback equalizer

CP: Cyclic prefix

DFT: Discrete Fourier transform

FB: Filter bank

FBMC: Filter bank multi-carrier

FFT: Fast Fourier transform

ICI: InterCarrier interference

IDFT: Inverse discrete Fourier transform

IFFT: Inverse fast Fourier transform

IIC: Iterative interference cancellation

ISFFT: Inverse symplectic finite Fourier transform

ISI: InterSymbol interference

ITU: International telecommunication union

LTE: Long term evolution

MIMO: Multiple input multiple output

ML: Maximum likelihood

MRC: Maximum ratio combining

MMSE: Minimum mean square error

MMSE-DD: Minimum mean square error in delay-Doppler domain

MMSE-TF: Minimum mean square error in time-frequency domain

mMTC: Massive machine type communication

MSE: Mean square error

PPN: Polyphase network

PHYDYAS: PHYsical layer for DYnamic AccesS

OFDM: Orthogonal frequency-division multiplexing

OOB: Out-of-band

OQAM: Offset quadrature amplitude modulation

OTFS: Orthogonal time frequency space

PAM: Pulse amplitude modulation

PAPR: Peak-to-average power ratio

QAM: Quadrature amplitude modulation

QPSK: Quadrature phase shift keying

SC-FDMA: Single carrier frequency division multiple access

SFFT: symplectic finite Fourier transform

SIR: Signal-to-interference ratio

SINR: Signal-to-interference-plus-noise ratio

SISO: Single input single output

SIMO: Single input multiple output

SM: Space multiplexing

SNR: Signal to noise ratio

URLLC: Ultra Reliable Low Latency Communication

TDL: Tapped delay line

ZF: Zero Forcing

List of symbols

$\mathbf{W}_n$	DFT matrix of n points.
$\mathbf{I}_n$	The identity matrix of size $n \times n$.
$\mathbf{0}_{n\times m}$	The square zero matrix of size $n \times m$.
$\mathbf{0}_n$	The square zero matrix of size $n \times n$.
j	imaginary number, $\sqrt{-1}$
$\mathbf{A}$	Capital and bold letter to represent an array.
$\mathbf{a}$	Lowercase and bold to represent a vector.
$log(.)$	The base 2 logarithm.
$\mathbf{A}^T$	The transpose operator.
$\mathbf{A}^H$	The complex conjugate (Hermitian) transpose operator.
$\mathbf{A}^{-1}$	The inverse of matrix $\mathbf{A}$.
$\mathbf{A}_{i,j}$	to refer to the $(i;j)$-th element of a matrix $\mathbf{A}$.
$\mathbf{a}_i$	to i-th element of the vector $\mathbf{a}$.
$\mathbb{C}^{p\times n}$,$\mathbb{R}^{p\times n}$	The set of matrices with p rows and n columns, with complex and real elements.
vec($\mathbf{A}$)	column vectorization of a matrix $\mathbf{A}$.
diag($\mathbf{A}$)	produces a new vector with the same elements as the main diagonal of $\mathbf{A}$.
diag($\mathbf{a}$)	represents the generation of a diagonal matrix of the elements of the vector $\mathbf{a}$.
$\oplus$	Kronecker product.
$\langle a, b\rangle$	Inner product operator between a and b.
$\Delta\tau$	Spacing in the delay domain.
$\Delta\nu$	Spacing in the Doppler domain.
L	Number of subcarriers in multicarrier modulations.

K	Number of OFDM symbols.
K'	Number of filter bank symbols.
L_{CP}	Cyclic prefix length in OFDM.
T	Symbol duration.
F	Subcarrier Spacing.
B	Total available bandwidth.
T_s	Sampling period.
f_s	Sampling frequency.
$g(m)$	Prototype filter function.
O	Overlapping factor in FBMC.
l	Subcarrier index.
k	Time index of a multicarrier symbol.
m	Sample time index.
$x_{l,k}$	Sample on the l-th subcarrier at time k.
E_b/N_0	Energy per bit to noise power spectral density ratio

Contents

1 Introduction

Wireless communication has revolutionized information transport in the world. Due to this evolution, traffic on mobile networks grows exponentially and there is a growing demand for higher and higher transmission rates. In addition, a broad convergence of processing and messaging technologies is emerging. We are currently experiencing the fifth generation of mobile networks (5G), which not only promises higher transmission rates and capacity, but also targets or operates in a diverse range of scenarios [3]. Among them are highlighted [4, 5]:

- Enhanced Mobile Broadband (eMBB): provides high data rates plus better service coverage for applications and reliability;
- Ultra-reliable, low-latency communication (URLLC): focuses on services that need to be extremely reliable and low-latency, such as autonomous vehicles, industrial manufacturing control, smart grids, and remote medical surgery;
- Massive Machine Type Communication (mMTC): connects a large number of power-constrained devices.

Applications for Industry 4.0 such as Internet of Things, communications between devices and between machines, are examples of new communication systems that are marking the transition from a centralized communication system to a distributed one. With the emergence of these new applications, a waveform that provides low latency, high interference tolerance and better spectral confinement is sought. In addition, the available electromagnetic spectrum is increasingly restricted, reinforcing the need for a good allocation of resources in frequency and even the use of millimeter waves [6, 7].

Multicarrier systems aim to divide the available spectrum into several subchannels so that each subchannel has an approximately flat frequency response. Orthogonal Frequency Division Multiplexing (OFDM) is currently the most widespread class of multicarrier systems. Its main features are:

- High spectral efficiency and robustness to frequency selective channels using orthogonal subcarriers;
- Ability to avoid intersymbol interference (ISI) and intercarrier interference (ICI) by attaching a cyclic prefix (CP) greater than the maximum propagation delay of the channel;
- Simple and low-complexity equalization in the frequency domain;

- Efficient digital implementation using the fast Fourier transform (FFT), thus facilitating its implementation in hardware.

Due to these properties, OFDM is present in various wireless communication systems such as the DVB digital television standard [8], Wi-Fi based on the IEEE 802.11 standard [9] and the fourth generation (4G) LTE standard [10]. However, despite all its qualities the OFDM technique has certain undesirable characteristics that makes it difficult to implement in some scenarios. First, there is a loss in spectral efficiency due to the insertion of the cyclic prefix. In fact, the cyclic prefix is a copy of part of the transmitted OFDM symbol and this redundancy reduces the effective throughput. Another problem in the OFDM system is the sensitivity to frequency shifts generated by the Doppler effect. Mainly present in high mobility scenarios, these deviations cause ICI and consequently a break in the orthogonality between the subcarriers. Furthermore, OFDM uses a rectangular shaping pulse which leads to a sinc spectral representation that causes large side lobes on each subcarrier. Thus, we have a spectrum leakage producing out-of-band (OOB) emissions such that subchannels at the edge of the transmission bandwidth can be a source of interference to other neighboring systems. In addition to frequency deviation problems, OOB can also generate significant ICI and again the breakdown of complex orthogonality. Lastly, the OFDM signal has high peak power to average power ratio (PAPR), which can cause the amplifier to operate in a non-linear region, resulting in inefficient power consumption and additional OOB emission.

With some minor modifications, the OFDM system was chosen as the waveform adopted for 5G [11]. Although this decision makes sense in terms of compatibility with 4G systems, it is not the most efficient technique for the variety of application scenarios that the technology proposes. It is expected that the sixth generation (6G) will bring with it the objective of further expanding data capacity, and being able to effectively encompass and improve the range of applications envisaged beyond 5G [12]. In this sense, changes are needed in the OFDM transmission structure, such as the adoption of a specific formatting filter to meet the metrics imposed by modern wireless systems.

The filter bank multicarrier system (FBMC) is an alternative to combat the high OOB emissions inherent to OFDM [13]. Based on filtering on each subcarrier, a good separation between the subchannels is obtained and consequently a significant rejection of OOB emissions [14, 15]. The application of these specially designed filters avoids ISI and ICI without the need to use the cyclic prefix. This allows the FBMC to achieve higher spectral efficiency compared to the OFDM system and robustness to interference. Furthermore, an efficient implementation with low complexity is possible through the polyphase decomposition [16]. However, according to the Balian-Low theorem [17] base functions with complex orthogonality necessarily have infinite dispersion in time or in frequency. In fact, for the OFDM case we have in the frequency domain the pulse sinc

that extends to infinity. In the case of FBMC, filtering guarantees a well located spectrum and the symbols are superimposed in the time domain, resulting in an imaginary intrinsic interference because it does not have complex orthogonality. To fulfill the theorem, it is necessary to relax the complex orthogonality criterion for the real field. Thus, if we transmit only real symbols it is possible to retrieve the data at the receiver by taking only the real part of the received signal. However, if the objective of the system is to provide the maximum information transfer rate, it would be best to transmit simultaneously in phase and quadrature, as is done in OFDM through complex symbols coming from a Quadrature Amplitude Modulation (QAM) constellation. As a way of providing full capacity, even with restriction of orthogonality for the real field, the FBMC scheme is preferably used with Offset-QAM (OQAM) modulations, giving rise to FBMC/OQAM [13]. OQAM modulation consists of dividing the symbols in the transmission into real and imaginary parts to be modulated into consecutive symbols, so that the real and imaginary symbols are alternated in time [18]. As a consequence, imaginary symbols through a phase shift suffer a half-symbol period delay in relation to real symbols, preventing their simultaneous transmission [19]. For the FBMC/OQAM scheme, alternatively, we can see it as a system where the symbol rate is doubled per subchannel, using alternately the real part and the imaginary part of it. Thus, a transmission of only real symbols is generated at a doubled rate while maintaining the maximum transmission capacity free of filter interference. Using OQAM causes the data on the receiver side to be detected only by the real (or imaginary) component of the signal and the imaginary (or real) part appears as an intrinsic interference term [2]. However, even if this interference is orthogonal to the data symbols, the loss of complex orthogonality makes the channel estimation process complicated in multiple input/output (MIMO) techniques such as spacetime block encoding and space multiplexing (SM) with maximum likelihood (ML) detection [20]. To facilitate channel estimation, it is necessary that the system needs more processing and a greater number of pilot subcarriers [21]. In short, the FBMC system solves spectral localization problems by using the restricted available spectrum more efficiently. However, problems arise for application in MIMO systems, in addition to maintaining the problems of high PAPR and Doppler sensitivity of OFDM.

There is a great interest in research that proposes new waveforms for these wireless communication systems in order to overcome the highlighted limitations [22]. Several techniques have been intensively studied and some have shown to be more promising and have been directly competing to assert themselves as an international standard for new technologies. In the literature, pre-coded versions of OFDM and FBMC systems stand out for this purpose. Related to OFDM, solutions such as single carrier frequency division multiple access (SC-FDMA) [23] and orthogonal space-time-frequency modulation (OTFS) [24] have been proposed, targeting applications that require high baud rate, lower PAPR and robustness to doubly selective channels. The SC-FDMA technique uses discrete

Fourier transform (DFT) spreading before the OFDM modulator, while OTFS uses a similar approach but using a two-dimensional (2D) DFT. Thus, SC-FDMA and OTFS systems can be seen as DFT spread OFDM and 2D-DFT spread OFDM, respectively. The purpose of SC-FDMA is to reduce PAPR while maintaining frequency domain equalization. In turn, OTFS has significant advantages in doubly selective channels compared to OFDM, making it a possible solution for new systems in high mobility scenarios. It is known that an OFDM system can be seen as a transmission of a block represented by a grid in the time-frequency (TF) domains where on the frequency axis we have the regularly spaced subcarriers and in time the transmitted multicarrier symbols. In OTFS, information symbols are initially described in a grid in the delay-Doppler (DD) domain, then mapped to symbols on a TF domain grid by a two-dimensional DFT, and finally transmitted over the channel using the OFDM modulator [25]. In this context, OTFS provides a high diversity order, converting a doubly dispersive channel into a near-flat fading channel in the DD domain [26]. However, data detection is moved from simple equalizer in the TF domain to estimation in the DD domain, with greater complexity. It is possible to cite as an example the equalizer based on the minimum mean square error (MMSE) criterion with the traditional matrix inversion approach [27]. This matrix inversion can be avoided by exploiting the sparse characteristics of the channel impulse response in the DD domain, through the use of detectors based on message passing algorithms (MPA) [28, 29, 30]. There are also other computationally less complex receivers proposed for OTFS, such as those seen in [31, 32, 33]. However, all of them are generally more complex than simple equalization in the TF domain. Symbol detection in OTFS is a topic of much study and discussion. In terms of OOB, by using the OFDM modulator as the core of the system, both techniques present the same spectral localization problems.

Precoding techniques can also be introduced and analyzed in FBMC system. However, its application also aims to eliminate the intrinsic interference of the filter to allow an efficient implementation of MIMO techniques, even if it is not as direct as in OFDM. Similar to the precodings proposed for OFDM, the spreading of data symbols is also beneficial in FBMC allowing the recovery of complex orthogonality. In [34], the authors show that Alamouti coding can be performed restoring complex orthogonality, but only when combined with code division multiple access (CDMA). However, the scheme still depends on an OQAM transmission and it was observed that this combination must be constructed taking into account the particular characteristics of the transmission channel. The idea was improved in [35], where complex orthogonality is guaranteed by spreading the symbols in time or frequency through Hadamard matrices. However, this orthogonality is valid only if the channel has an approximately flat frequency response within the scattering length, requiring the use of protective subcarriers slightly reducing the spectral efficiency. Another solution is to consider a precoding based on OFDM itself, that is, spreading the symbols in time via inverse DFT (IDFT) [36]. This so-called FFT-FBMC scheme analyzes

the intrinsic interference of the filter as coefficients of a multipath channel. Thus, the authors aim to isolate and eliminate the intrinsic interference of the filter, transforming the FBMC system into an equivalent system formulated as OFDM. An improvement of the FFT-FBMC was recently proposed in [37] and is called block-filtered OFDM (BF-OFDM). The upgrade consists of attaching a filter pre-compensation stage to the transmitter, so that no filtering is required on the receiver side, which offers the possibility to implement a simple receiver based only on an FFT. However, the time symbol-spreading generates sensitivity in time-varying channels. Thus, both techniques are sensitive to Doppler shift. In the same thread, the authors in [38] presented the FBMC Pruned DFT-spread, which is based on frequency scattering using a DFT combined with a filter compensation stage. Compared to the SC-FDMA system, the proposed system in [38] has many similarities. It is worth mentioning that the use of an IDFT of the OFDM modulator with a size larger than the pre-coding DFT must be used in order to avoid critical sampling. The differences consist in adding a filter compensation stage and switching the system core from an OFDM modulator to an FBMC/OQAM transmitting at double rate. Thus, the system presents the main characteristics of SC-FDMA and FBMC, such as low PAPR, better spectral localization and certain robustness to Doppler scattering, in addition to restoring the complex orthogonality. Its limitations are related to the length of the filter used, which needs to be limited to a certain value, and the use of the OQAM structure in the filter bank. As we will see in this work, we can improve this structure and add features seen in OTFS. The idea is to combine the benefits of FBMC filtering with the robustness to high mobility scenarios of OTFS. Additionally, a good error performance is obtained with simple receivers in the TF domain, avoiding complex algorithms in the delay-Doppler domain.

Filter bank-based systems have great potential for new emerging technologies. However, mainly due to the constraint of orthogonality to the real plane, the technique still does not have a great impact on the industry for its adoption. Using specific pre-codings, it is possible to eliminate this restriction, in addition to adding desirable features in order to make the technique more attractive for new technologies. It should be noted that all the techniques mentioned above are based on the use of precoding, spreading the symbols in time or frequency while the system core, that is, OFDM or FBMC/OQAM, remains unchanged. However, we will see with the propositions of this work that this can be changed in order to obtain significant advantages in terms of performance.

1.1 Objective

1.1.1 General Objective

The general objective of this work is to propose new schemes based on a precoded filter bank system with characteristics of complex orthogonality between the base pulses, robustness to doubly selective channels, low PAPR and lower OOB emissions. Our first goal is to recover the complex orthogonality and with its consequences, adding functionality within the project that fits what is intended. Precoding is based on spreading symbols via DFT/IDFT pairs. The proposal has a structure similar to the OTFS technique and has a good performance even using simple equalizers in the frequency domain, a fact that does not occur in the OTFS itself.

1.1.2 Specific Objectives

Considering the development of the work and the general objective presented, the following specific objectives are highlighted:

- Description of the filter bank implementation via polyphase decomposition in matrix format. Such description helps in understanding the process of compensation for both filter and channel interference.
- System evaluation through an analysis of the signal-to-noise ratio plus interference (SINR), signal-to-interference ratio (SIR) and bit error rate (BER). Closed-form solutions for SINR on doubly selective channels are developed and show that in many cases, one-tap equalizers are sufficient.
- Proposal of iterative receivers for cases of more hostile environments.
- Comparative analysis of performance with other multicarrier techniques proposed in the literature.
- Introduction of the rate factor for generalization of the proposed system as a consequence of the elimination of filter interference. Such generalization allows a considerable improvement in performance in high mobility scenarios.

1.2 Organization

This work is organized as follows:

Chapter 2: The concepts related to multicarrier systems will be addressed, as well as the matrix representation necessary for modeling the techniques proposed later.

Chapter 3: The description of the pre-coded filter bank system via DFT is contextualized. We will discuss how to eliminate interference from the filter bank through precoding combined with a data transmission strategy.

Chapter 4: The introduction of two iterative receivers with hybrid performance in terms of domain are presented. Such receivers are applied to the schemes proposed in chapters 3 and 5 bringing some alternatives in terms of filtering and error performance.

Chapter 5: With the results obtained in Chapter 3, we have the proposition of a new scheme called Two-Dimensional FFT Precoded Filter Bank (2D-FFT FB). Such a scheme employs similar characteristics of the OTFS technique, in addition to a good spectral localization and efficient equalization in the time-frequency domain.

Chapter 6: By recovering the complex orthogonality, the implementation of the filter bank via polyphase networks can be generalized in order to obtain better characteristics in the pre-coded schemes. A generalized version of the schemes proposed in chapters 3 and 5 is described in this chapter.

Conclusion: Finally, the final considerations and future works that intend to be elaborated are presented.

1.3 Scientific Contributions

The following is a list of accepted/submitted submissions resulting from the contents presented in this work.

1. Junior, R. P., da Rocha, C. A., Chang, B. S. and Le Ruyet, D. A novel DFT precoded filter bank system with iterative equalization. IEEE Wireless Communications Letters, v. 10, n. 3, p. 478-482, 2020.

2. Junior, R. P., da Rocha, C. A., Chang, B. S. and Le Ruyet, D. Receptor baseado em cancelamento de interferência para sistema de banco de filtros pré-codificado. In: 2021 39th Brazilian Symposium on Telecommunications and Signal Processing (SBrT).

3. Junior, R. P., da Rocha, C. A., Chang, B. S. and Le Ruyet, D. Iterative interference cancellation for the DFT Precoded Filter Bank System. In: 2021 17th International Symposium on Wireless Communication Systems (ISWCS). IEEE, 2021. p. 1-6.

4. Junior, R. P., da Rocha, C. A., Chang, B. S. and Le Ruyet, D. A Generalized DFT Precoded Filter Bank System. IEEE Wireless Communications Letters, v. 11, n. 6, p. 1176-1180, 2022.

5. Junior, R. P., da Rocha, C. A., Chang, B. S. and Le Ruyet, D. IB-DFE receiver for generalized SIMO DFT precoded filter bank systems in doubly selective channels. IEEE Latin-American Conference on Communications (LATINCOM), 2022.

6. Junior, R. P., da Rocha, C. A., Chang, B. S. and Le Ruyet, D. A Two-Dimensional FFT Precoded Filter Bank Scheme. Submitted for IEEE Transactions on Wireless Communications.

7. Junior, R. P., da Rocha, C. A., Chang, B. S. and Le Ruyet, D. A Generalized Two-Dimensional FFT Precoded Filter Bank Scheme with Low Complexity Equalizers in Time-Frequency Domain. Ready for submission.

2 Multicarrier Systems

One of the most challenging problems in wireless communications systems is to combat ISI caused by multipath channels. In order to achieve high baud rate communication with acceptable performance, this interference must be drastically reduced. Multicarrier transmission combined with frequency domain equalization techniques proved to be an efficient approach for these situations. In addition to reducing or even eliminating the ISI, it is possible to perform the equalization process in a simple and low-complexity way in the frequency domain.

In this chapter, the OFDM multicarrier system and its variations are presented and analyzed to combat interference from multipath channels, as well as to provide several characteristics necessary for a modern wireless transmission system. A detailed comparative analysis between the systems is also presented.

2.1 OFDM system

The effects of the multipaths responsible for the frequency selectivity of the communication channels make the detection of transmitted symbols a very complex process. In general, the various paths received at different times of the same signal cause ISI and make it necessary to have an equalizer of significant length for the elimination of this interference and the correct recovery of the transmitted information. One solution is to split the bandwidth of a frequency-selective channel into several subchannels with flat fading via parallel data transmission over several subcarriers. This type of transmission is commonly called multicarrier transmission.

Orthogonal frequency division multiplexing, or OFDM, is the most widespread modulation among all multicarrier systems. In general, as illustrated by Figure 1, the idea is to split a bit stream of rate R into different parallel beams of rate R/L, and transmit them after mapping the data on different orthogonal subchannels evenly spaced every F Hz. This operation leads to a division of the available bandwidth into L subchannels, where this number L is chosen to be large enough to guarantee that each subchannel has a bandwidth smaller than the coherence bandwidth of the transmission channel. Equivalently, this operation makes the duration of the T symbol in each beam much longer than the time spread of the channel. Thus, each subchannel is narrow enough to guarantee a flat fading effect and consequently the ISI in each subchannel is small. Basically, a high data rate $(1/T)$ transmission is partitioned into several parallel transmissions, but each with lower data rates $(1/LT)$. In these parallel transmissions, an equalizer of one coefficient per subchannel that can be implemented by a simple multiplier is sufficient to compensate for

channel effects, thus eliminating the need for an equalizer of relatively large length.

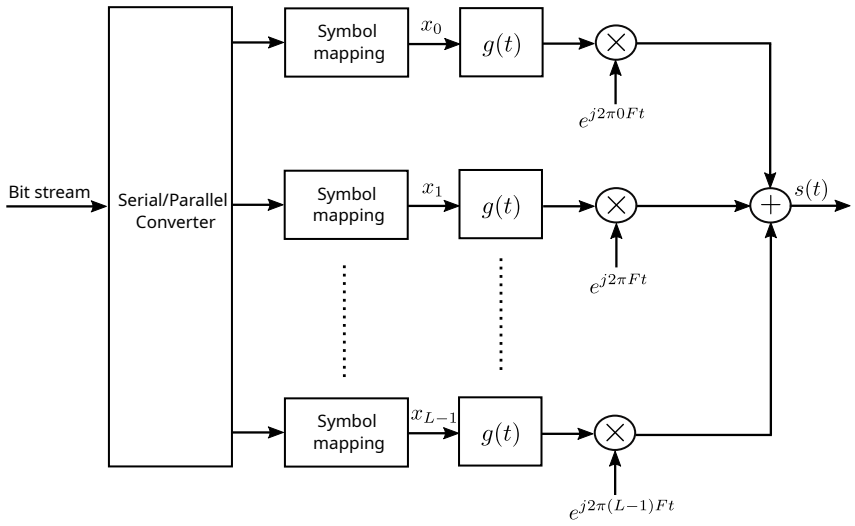

Figure 1 – Multicarrier Transmitter.

2.1.1 OFDM Principles

In multicarrier transmissions, the transmitted symbols can be visualized as a block represented by a time-frequency grid or plane. This grid is composed of K OFDM symbols transmitted at each instant of time, each with L evenly spaced subcarriers. Let us denote by $x_{l,k}$ the sequence of complex symbols arising from a QAM modulation on the lth subcarrier at the time instant k. After the serial/parallel conversion, the data is summed and transmitted. The resulting signal $s(t)$ can be written in baseband as follows:

$$\begin{aligned} s(t) &= \sum_{l=0}^{L-1} \sum_{k} x_{l,k} g(t - kT) e^{j2\pi lF(t-kT)}, \\ &= \sum_{l=0}^{L-1} \sum_{k} x_{l,k} g_{l,k}(t) \end{aligned} \tag{2.1}$$

where F is the spacing between each subchannel, $g(t)$ corresponds to the prototype filter used to separate the subchannels, which in this case is a rectangular window, defined by

$$g(t) = \begin{cases} \frac{1}{\sqrt{L}}, & 0 \leq t < T \\ 0, & \text{otherwise} \end{cases} \tag{2.2}$$

and $g_{l,k}(t)$ is the base synthesis function defined as

$$g_{l,k}(t) = g(t - kT) e^{j2\pi lF(t-kT)} \tag{2.3}$$

which is essentially a time and frequency shifted version of the $g(t)$ prototype filter. As the impulse response of the prototype filter is a rectangular window, in the frequency

domain each symbol has the shape of a sinc function and therefore they overlapping. Even with this overlapping, information from each subcarrier can be extracted individually and retrieved [39]. For this to be true, the orthogonality condition between the subcarriers must be respected. Orthogonality is the ability to cancel interference induced by the waveform itself and not by other sources such as the communication channel, for example. The perfect reconstruction of complex symbols is obtained by imposing the condition of complex orthogonality given by

$$\begin{aligned} \langle g_{l,k}(t), g^*_{l',k'}(t)\rangle &= \int_{\mathbb{R}} g(t-kT)g(t-k'T)e^{j2\pi lF(t-kT)}e^{-j2\pi l'F(t-k'T)}dt \\ &= \delta_{k-k'}\delta_{l-l'}, \end{aligned} \tag{2.4}$$

where $\langle u, v\rangle$ corresponds to the inner product between u and v, while δ_n is the unit impulse is defined by:

$$\delta_n = \begin{cases} 1, & \text{if } n = 0 \\ 0, & \text{otherwise.} \end{cases} \tag{2.5}$$

On the receiver side, assuming a channel without distortion, that is, without the presence of ISI and other interferences, the transmitted signal can be perfectly recovered, that is:

$$\begin{aligned} & \frac{1}{T}\int_0^T s(t)g(t-k'T)e^{-j2\pi l'F(t-k'T)}dt \\ = & \frac{1}{T}\int_0^T \left(\sum_{l'=0}^{L-1}\sum_{k'} x_{l',k'}g(t-k'T)e^{-j2\pi l'F(t-k'T)}\right)g(t-kT)e^{-j2\pi lF(t-kT)}dt \\ = & \sum_{j=0}^{N-1} x_{l',k'}\delta_{k-k'}\delta_{l-l'} \\ = & x_{l,k} \end{aligned} \tag{2.6}$$

Analyzing in more detail equation (2.4), it can be concluded that the smallest spacing between the frequencies that guarantees the complex orthogonality between them is $F = 1/T$. Therefore, this spacing should be used to obtain the best spectral efficiency and a symbol density $TF = 1$. Again, it is worth noting that the formatting pulse of the symbols $a_{l,k}$ is a rectangular pulse of duration T. Thus, spectrally, the transmitted signal $s(t)$ is composed of functions sincs spaced by $F = 1/T$ Hz, as shown in Figure 2. It is clear from the Figure that in OFDM transmission, the communication channel is subdivided into subchannels centered on frequencies lF and in each subchannel data is transmitted at rates R/L. OFDM transmission is based on this principle, making the difference between the frequencies of two adjacent subcarriers as small as possible, maintaining the orthogonality between them. In this way, there is an overlapping of the spectra of each subchannel, thus achieving a spectral efficiency greater than that of a conventional multicarrier transmission.

Our discussion of OFDM so far has focused on the continuous or analog model. Although mathematically this is the best approach to understand the concepts, this model

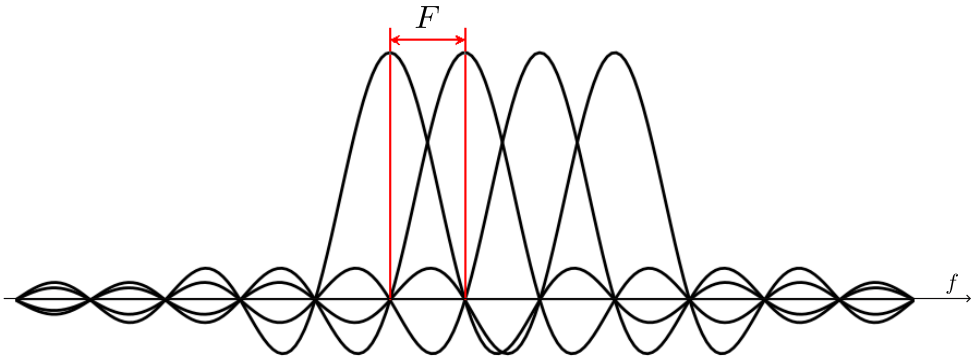

Figure 2 – Sinc functions spaced from each other every F Hz.

requires sets of oscillators, making its implementation impossible due to complexity. In practice, $s(t)$ is the analog signal obtained from discrete-time samples $s[m] = s(mTs)$ using the Nyquist sampling theorem, where $Ts = T/L$ is the sampling period. Consequently, the sampling frequency is given by $fs = FL$. Therefore, the discrete-time transmitted signal can be expressed as follows:

$$s[m] = \sum_{l=0}^{L-1} \sum_{k} x_{l,k} g[m - kL] e^{\frac{j2\pi l}{L}(m-kL)} \tag{2.7}$$

The expression (2.7) can be efficiently implemented using the inverse discrete Fourier transform (IDFT). Consider a discrete time sequence $f[m], 0 \leq m < L$. The discrete Fourier transform (DFT) and its IDFT of L points are given respectively by [40]

$$F[l] = \frac{1}{\sqrt{L}} \sum_{m=0}^{L-1} f[m] e^{\frac{-j2\pi ml}{L}}, \quad \text{l} = 0, 1, ..., L-1 \tag{2.8}$$

and

$$f[m] = \frac{1}{\sqrt{L}} \sum_{l=0}^{L-1} F[k] e^{\frac{j2\pi lm}{L}}, \quad \text{m} = 0, 1, ..., L-1. \tag{2.9}$$

DFT/IDFT operations are calculated using L^2 operations from equations (2.8) and (2.9). This number can be reduced using efficient algorithms, the most common being the fast Fourier transform and its inverse (FFT/IFFT). With this algorithm, the number of calculations can be reduced to $L \log_2 L$ [40]. Without loss of generality, we only consider the time position $k = 0$ (slight abuse of notation), that is, we only have a single multicarrier symbol ($K = 1$). Thus, the expression of the transmitted signal $s[m]$, given in (2.7), becomes:

$$s[m] = \frac{1}{\sqrt{L}} \sum_{l=0}^{L-1} x_{l,0} e^{\frac{j2\pi lm}{L}} \quad \text{m} = 0, 1, ..., L-1. \tag{2.10}$$

According to the definition of IDFT given by (2.9), we conclude that an OFDM symbol is the IDFT of the data sequence $x_{l,0}$, $0 \leq l < L - 1$. It is also simple to show that the

OFDM transmitter can be represented by simple matrix multiplication. Note that the l-th element of the DFT of the sequence $f[m]$ given in (2.8) can be written as the inner product of two vectors, that is

$$F[l] = \frac{1}{\sqrt{L}}\begin{bmatrix} W_L^0 & W_L^l & W_L^{2l} & \dots & W_L^{(L-1)l} \end{bmatrix}\begin{bmatrix} f[0] \\ f[1] \\ f[2] \\ \vdots \\ f[L-1] \end{bmatrix} \tag{2.11}$$

where $W_L = e^{-j2\pi/L}$, and therefore $W_L^l = e^{-j(2\pi/L)l}$. Thus, the DFT of L points of the sequence $f[m]$ can be written as

$$\begin{bmatrix} F[0] \\ F[1] \\ F[2] \\ \vdots \\ F[L-1] \end{bmatrix} = \frac{1}{\sqrt{L}}\begin{bmatrix} 1 & 1 & 1 & \dots & 1 \\ 1 & W_L & W_L^2 & \dots & W_L^{L-1} \\ \vdots & \vdots & \ddots & & \vdots \\ 1 & W_L^{L-1} & W_L^{2(L-1)} & \dots & W_L^{(L-1)^2} \end{bmatrix}\begin{bmatrix} f[0] \\ f[1] \\ f[2] \\ \vdots \\ f[L-1] \end{bmatrix} \tag{2.12}$$

or in a simplified way using matrices such as

$$\mathbf{f} = \mathbf{W}_L\tilde{\mathbf{f}} \tag{2.13}$$

where $\mathbf{f} \in \mathbb{C}^{L\times 1}$ e $\tilde{\mathbf{f}} \in \mathbb{C}^{L\times 1}$ are vectors that represent the sequences $F[l]$ and $f[m]$ and $\mathbf{W}_L \in \mathbb{C}^{L\times L}$

$$\mathbf{W}_L = \frac{1}{\sqrt{L}}\begin{bmatrix} 1 & 1 & 1 & \dots & 1 \\ 1 & W_L & W_L^2 & \dots & W_L^{L-1} \\ \vdots & \vdots & \ddots & & \vdots \\ 1 & W_L^{L-1} & W_L^{2(L-1)} & \dots & W_L^{(L-1)^2} \end{bmatrix} \tag{2.14}$$

is known as the L-points DFT matrix. We can also represent this DFT matrix for any order as follows

$$[\mathbf{W}_n]_{l,k} = e^{j2\pi kl/n} \text{ for } k,l = 0,\dots,n-1 \tag{2.15}$$

where $\mathbf{W}_n \in \mathbb{C}^{n\times n}$ is the DFT matrix of n points. An important property of this matrix is that it is an orthonormal matrix or unitary matrix, as it satisfies the following condition [41]:

$$\mathbf{W}_L\mathbf{W}_L^H = \mathbf{W}_L^H\mathbf{W}_L = \mathbf{I}_L, \tag{2.16}$$

where $\mathbf{I}_L \in \mathbb{R}^{L\times L}$ is the identity matrix of order L and $(.)^H$ indicates Hermitian transposition. Thus, the matrix $\mathbf{W}_L^{-1} \in \mathbb{C}^{L\times L} = \mathbf{W}_L^H \in \mathbb{C}^{L\times L}$ and, consequently, one can represent the IDFT of the vector $\mathbf{f}$ of the equation (2.9) as:

$$\tilde{\mathbf{f}} = \mathbf{W}_L^H\mathbf{f}. \tag{2.17}$$

With this idea in mind, we denote $\mathbf{x}_k \in \mathbb{C}^{L\times 1} = [x_{0,k}, x_{1,k}, \ldots, x_{L-1,k}]^T$ as the vector whose elements are the L data symbols at the k-th instant of time. Thus, the vector $\mathbf{s}_k = [s_{0,k}, s_{1,k}, \ldots, s_{L-1,k}]^T \in \mathbb{C}^{L\times 1}$ representing the k-th OFDM symbol can be given by

$$\mathbf{s}_k \;=\; \mathbf{W}_L^H \mathbf{x}_k. \tag{2.18}$$

Therefore, the entire transmitted signal $s[m]$, given in (2.10), can be seen as a succession of blocks obtained by executing the IDFT on the data block $x_{l,k}$. Thus, as shown in the Figure 3, the OFDM transmitter can be implemented using an IDFT and, for the same reason, the receiver can be implemented using a DFT. With the help of the FFT algorithm, the design of the OFDM technique becomes very simple and with low complexity [42]. At the transmitter, OFDM symbols are generated efficiently through the IFFT ($\mathbf{W}_L^H$), while at the receiver, an FFT ($\mathbf{W}_L$) is used to retrieve the transmitted symbols. With this transmission technique, it is noted that the equalization process can be performed in the frequency domain. Next, we will see that by adding a guard interval to each transmitted symbol, this transmission scheme becomes highly robust to severely time-dispersive channels.

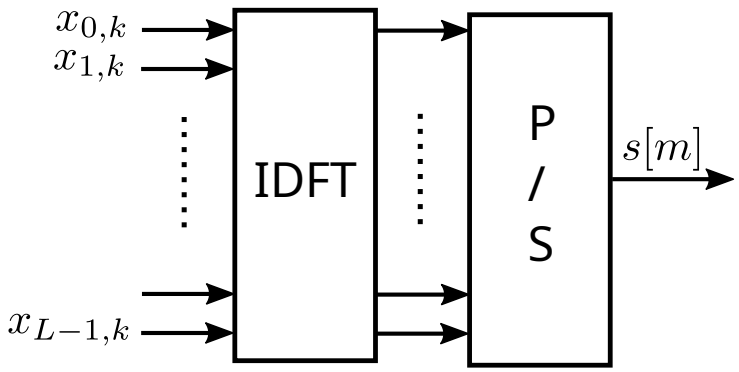

Figure 3 – OFDM Transmitter Structure.

2.1.2 Cyclic Prefix

As much as the OFDM technique is efficient in combating ISI, the signal spread caused by the mobile channel can cause part of the adjacent multicarrier symbols to interfere with each other. The cyclic prefix (CP), introduced by Peled and Ruiz [43] is a very efficient method to avoid this interference between multicarrier symbols. It is the simple resource of inserting at the beginning of each transmitted symbol, a copy of duration T_{CP} of a set of final samples of the respective symbol, as illustrated by Figure 4. Specifically, the last L_{CP} samples of each multicarrier symbol are repeated at the beginning of the transmitted symbol, as shown by

$$\mathbf{s}_{-i,k} = \mathbf{s}_{L-i,k} \;\text{ for }\; i = 0, 1, \ldots, L_{CP} - 1 \tag{2.19}$$

The cyclic prefix function can be divided into two parts. First, it acts as a guard interval to prevent interference between multicarrier symbols. Thus, interference can be considered

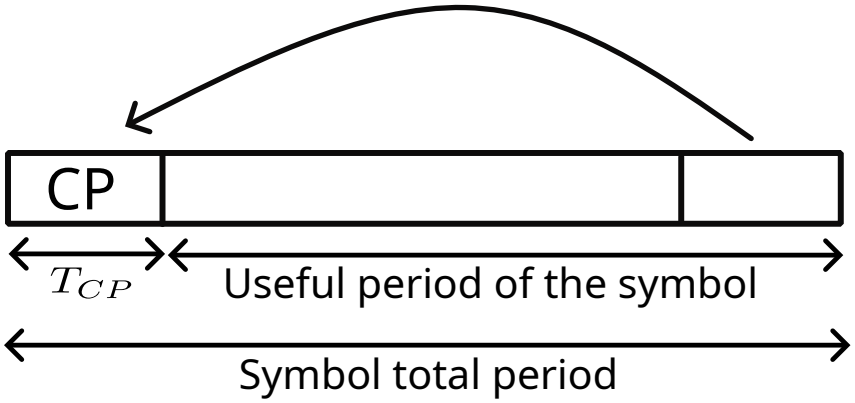

Figure 4 – Addition of the cyclic prefix in an OFDM symbol.

negligible or completely eliminated as long as the cyclic prefix has a duration greater than or equal to the duration of the channel impulse response. Second, its use converts the linear convolution of the transmitted data with the channel impulse response into a circular convolution. Consequently, analyzing in the frequency domain and using the property of circular convolution of the DFT, each block can be equalized independently and in a simple way [44]. To exploit this second advantage, let us first consider, again, the transmission of a single OFDM symbol, that is, $K = 1$. In this sense, we can exchange $\mathbf{s}_k$ for just $\mathbf{s} \in \mathbb{C}^{L\times 1}$. Now, adding a cyclic prefix of size L_{CP} in $\mathbf{s}$ creates a new vector $\mathbf{s}^{CP} \in \mathbb{C}^{(L+L_{CP})\times 1}$ which can be described as

$$\mathbf{s}^{cp} = [s_{L-L_{CP}}, s_{L-L_{CP}+1}, ..., s_{L-1}, s_0, s_1, \ldots, s_{L-1}]^T. \tag{2.20}$$

This vector is now transmitted over a channel of length V, whose impulse response is given by vector $\tilde{\mathbf{h}} = [h_0, h_1, ..., h_{V-1}] \in \mathbb{C}^{V\times 1}$. Assuming that the channel is fixed during the transmission of one symbol OFDM and the length of the cyclic prefix is exactly equal to the length of the channel, i.e. $L_{CP} = V - 1$, the matrix description of the signal after the convolution process and the sum by the noise vector $\tilde{\mathbf{n}} \in \mathbb{C}^{(L+L_{CP})\times 1}$ can be expressed as follows:

$$\begin{bmatrix} \tilde{r}_{L-1} \\ \tilde{r}_{L-2} \\ \vdots \\ \tilde{r}_0 \end{bmatrix} = \begin{bmatrix} h_0 & h_1 & \ldots & h_{V-1} & 0 & \ldots & 0 \\ 0 & h_0 & \ldots & h_{V-2} & h_{V-1} & \ldots & 0 \\ \vdots & \vdots & \ddots & \ddots & \ddots & \ddots & \vdots \\ 0 & \ldots & 0 & h_0 & \ldots & h_{V-2} & h_{V-1} \end{bmatrix} \begin{bmatrix} s_{L-1} \\ \vdots \\ s_0 \\ s_{L-1} \\ \vdots \\ s_{L-L_{CP}} \end{bmatrix} + \begin{bmatrix} n_{L-1} \\ n_{L-2} \\ \vdots \\ n_0 \end{bmatrix} \tag{2.21}$$

At the receiver, to eliminate interference between symbols, the first L_{CP} samples corresponding to the cyclic prefix are discarded. In this way, it can be shown that the matrix representation presented in (2.21) is equivalent to the following representation [41]:

$$\begin{bmatrix} \tilde{r}_{L-1} \\ \tilde{r}_{L-2} \\ \vdots \\ \vdots \\ \vdots \\ \vdots \\ \tilde{r}_0 \end{bmatrix} = \begin{bmatrix} h_0 & h_1 & \dots & h_{V-1} & 0 & \dots & 0 \\ 0 & h_0 & \dots & h_{V-2} & h_{V-1} & \dots & 0 \\ \vdots & \vdots & \ddots & \ddots & \ddots & \ddots & \vdots \\ 0 & \dots & 0 & h_0 & \dots & h_{V-2} & h_{V-1} \\ \vdots & \vdots & \ddots & \ddots & \ddots & \ddots & \vdots \\ h_2 & h_3 & \dots & h_{V-3} & \dots & h_0 & h_1 \\ h_1 & h_2 & \dots & h_{V-2} & \dots & 0 & h_0 \end{bmatrix} \begin{bmatrix} s_{L-1} \\ s_{L-2} \\ \vdots \\ \vdots \\ \vdots \\ \vdots \\ s_0 \end{bmatrix} + \begin{bmatrix} \tilde{n}_{L-1} \\ \tilde{n}_{L-2} \\ \vdots \\ \vdots \\ \vdots \\ \vdots \\ \tilde{n}_0 \end{bmatrix} \tag{2.22}$$

which can be rewritten more compactly as:

$$\tilde{\mathbf{r}} = \mathbf{H}'\mathbf{s} + \tilde{\mathbf{n}}. \tag{2.23}$$

From this definition, we can clearly see that the matrix $\mathbf{H}' \in \mathbb{C}^{L\times L}$ has the following structure: the first line corresponds to the impulse response of the channel $\tilde{\mathbf{h}}$ appended with $(L-V)$ zeros. Every row of the matrix is obtained by applying a right shift to the previous row, with the additional condition that the last element of the previous row is twisted in the shift process to be circled back to the leftmost element of the new row. Consequently, the matrix $\mathbf{H}'$ is called a circulant matrix, which is characteristic of circular convolutions. With the brief description of the DFT of the section 2.1.1 and considering the circulant matrix $\mathbf{H}'$ of the equation (2.23), an important property of $\mathbf{H}'$ is that a spectral decomposition can be applied to this matrix to obtain [45]:

$$\mathbf{H}' = \mathbf{W}_L^H \bar{\mathbf{H}} \mathbf{W}_L, \tag{2.24}$$

where $\bar{\mathbf{H}} \in \mathbb{C}^{L\times L}$ is a diagonal matrix with its (i,i)-th entry $H_{i,i}$ corresponding to the frequency response of the i-th coefficient of the channel impulse response $\tilde{\mathbf{h}}$. Indicating these transform values by $H_0, H_1, \dots, H_{L-1}$, one can express $\bar{\mathbf{H}}$ as:

$$\bar{\mathbf{H}} = \begin{bmatrix} H_0 & 0 & \dots & 0 \\ 0 & H_1 & \dots & 0 \\ \vdots & \vdots & \ddots & \vdots \\ 0 & 0 & \vdots & H_{L-1} \end{bmatrix} \tag{2.25}$$

Thus, the l-th diagonal element of $\bar{\mathbf{H}}$ is given by $H_l = \sum_{i=0}^{V-1} h_i e^{-\frac{j2\pi li}{L}}$ where $0 \leq l < L$ and h_i denotes the channel coefficient of the i-th tap in the time domain. Given the output vector $\tilde{\mathbf{r}}$, after removing the cyclic prefix, the OFDM demodulator consists of a DFT of L points, in this way it is possible to define a representation of the OFDM symbol received in the frequency domain $\mathbf{r} \in \mathbb{C}^{L\times 1}$ as:

$$\mathbf{r} = \mathbf{W}_L \tilde{\mathbf{r}}. \tag{2.26}$$

Substituting $\tilde{\mathbf{r}}$ by the equation (2.23) and defining the noise $\tilde{\mathbf{n}}$ using the equation (2.17), we have

$$\mathbf{r} = \mathbf{W}_L(\mathbf{H}'\mathbf{s} + \mathbf{W}_L^H\mathbf{n}) \tag{2.27}$$

where $\mathbf{n} \in \mathbb{C}^{L\times 1}$ represents the noise vector with zero mean and variance σ_n^2 in the frequency domain. Finally, using equations (2.18) and (2.24) we simply obtain

$$\mathbf{r} = \bar{\mathbf{H}}\mathbf{x} + \mathbf{n} \tag{2.28}$$

In extended matrix form we have:

$$\begin{bmatrix} r_0 \\ r_1 \\ \vdots \\ \vdots \\ \vdots \\ r_{L-1} \end{bmatrix} = \begin{bmatrix} H_0 & 0 & \dots & \dots & \dots & 0 \\ 0 & H_1 & 0 & \dots & \dots & \dots \\ \vdots & 0 & H_2 & 0 & \dots & \dots \\ \vdots & \dots & 0 & \ddots & \dots & \dots \\ \vdots & \dots & \dots & \dots & \ddots & \dots \\ 0 & \dots & \dots & \dots & \dots & H_{L-1} \end{bmatrix} \times \begin{bmatrix} x_0 \\ x_1 \\ \vdots \\ \vdots \\ \vdots \\ x_{L-1} \end{bmatrix} + \begin{bmatrix} n_0 \\ n_1 \\ \vdots \\ \vdots \\ \vdots \\ n_{L-1} \end{bmatrix}. \tag{2.29}$$

Note that in the frequency domain there is only one sample-by-sample multiplication between the transmitted symbols and the channel coefficients. With the corrupted samples discarded and given that the remaining symbols in the block are of sufficient size L to guarantee a flat-natured fading on each subchannel, equalizers with only one coefficient are usually sufficient to compensate for the effects introduced by the channel. Such equalizers can be realized by a simple multiplier per subchannel and are usually called one-tap equalizers [44].

The cyclic prefix is fundamental to the OFDM system. It avoids interference between adjacent multicarrier symbols and also makes it possible to transform the linear convolution between the channel impulse response and the transmitted block into a circular convolution. As shown earlier, circular convolution in the time domain is equivalent in the frequency domain to a multiplication of the DFTs of the channel impulse response and transmitted data. The baseband discrete OFDM system using the cyclic prefix (CP-OFDM) is illustrated by Figure 5. Initially the L complex symbols from a QAM

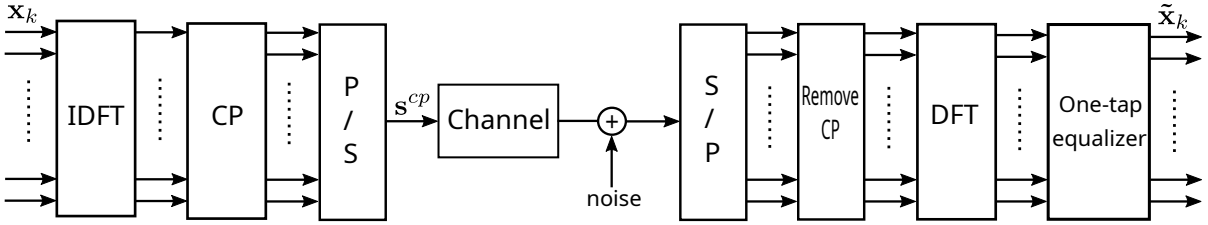

Figure 5 – Block diagram of the OFDM system with cyclic prefix.

constellation $\mathbf{x}_k$ at the $k-$th instant of time are transformed to the time domain through

an IDFT of L points. Then, the CP is added to each OFDM symbol with a length greater than the maximum spread delay of the channel. Finally, the parallel-serial conversion is performed in order to transmit the OFDM symbols in the time domain through the noise added channel. On reception, the symbols are resumed in parallel format, the CP is removed from each symbol and multicarrier demodulation is performed using a DFT of L points. Finally, the estimated symbols $\tilde{\mathbf{x}}_k$ are obtained after the frequency domain equalization process which will be defined later.

The cyclic prefix OFDM technique is possibly one of the most successful transmission schemes for digital communications. Its robustness against frequency selective channels combined with low-complexity equalization in the frequency domain constitutes the main motivation for its use [46]. However, despite all its benefits, this approach has some disadvantages. To eliminate ISI and ICI, the cyclic prefix is added to the OFDM symbol whose length is equal to or greater than the channel delay propagation. Although the use of CP guarantees ISI and ICI free transmission, however, the effective E_b/N_0 is reduced. Note that an OFDM symbol has duration $T + T_{CP}$ where T_{CP} is the additional period related to the CP. This OFDM symbol consists of L data subcarriers spaced between each $F = 1/T$ as shown in Figure 6 for $T_{CP} = 0$. For each area $(T + T_{CP}) \times F$, we have a

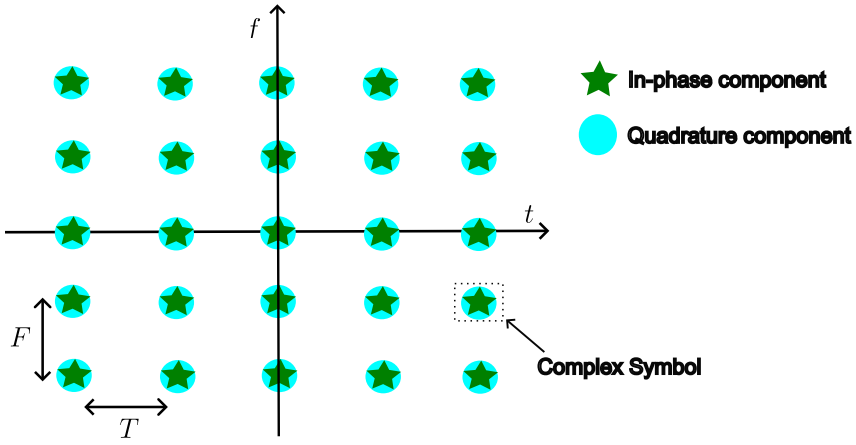

Figure 6 – Time-frequency representation of data in the OFDM system.

complex symbol. Thus, for the CP-OFDM system the data symbol density, that is, the maximum useful rate, can be expressed by [47]

$$\frac{1}{(T + T_{CP})F} = \frac{T}{T + T_{CP}} \leq 1. \tag{2.30}$$

The loss in E_b/N_0 is evident, due to the need to reserve a transmission time for the CP in order to avoid channel interference. The shape of the transmit pulse for each subcarrier is another source of system limitation. As it is a rectangular window, the spectral shape of the sinc type generates a high out-of-band emission. This fact makes the OFDM system sensitive to the Doppler shift associated with the Doppler spread due to the movement

of the mobile. Such a shift can cause severe interference between subcarriers, due to the break in orthogonality and consequently ISI. Another problem is the high value of the Peak Power to Average Power Ratio (PAPR) of the OFDM signal. Considering the transmitted symbols $\mathbf{x}_k$ independent and identically distributed of zero mean and unity power, the PAPR of an OFDM symbol can reach a value equal to the length of the symbol L [48]. However, this does not mean that it will always be this value; in general, the PAPR measurement is more statistical. A low PAPR allows the power amplifier in the transmitter to operate efficiently. On the other hand, a high PAPR forces the power amplifier to have a high backoff in order to ensure a linear amplification of the signal. Finally, OFDM systems have sensitivity in high mobility scenarios generating a great loss of performance by Doppler spreading. In this sense, these problems need to be tackled by demanding changes in the OFDM transmission structure, such as additional filtering or pre-processing applications to meet the metrics imposed by modern wireless systems.

2.2 FBMC/OQAM system

The use of the CP at each OFDM symbol allows the elimination of the ISI caused by multipaths. However, ICI remains a problem because of the large leakage in spectrum on each subcarrier. The need for better resource allocation in the frequency domain motivated the adoption of filtering in the OFDM technique. This filtering can be performed in several ways, originating schemes such as filtered OFDM (F-OFDM) [49], Universal Filtered MultiCarrier (UFMC) [50] and Filter Bank Multicarrier (FBMC). In F-OFDM, filtering is effectively performed on the transmitted signal, that is, in the entire band, while in UFMC a group of subcarriers is filtered, creating several subbands. In FBMC, filtering is performed individually on each subcarrier, so that interference between them occurs only for adjacent subchannels due to the drastic reduction of the secondary lobes of the spectrum. In addition, OOB emissions are also reduced by the filtering process. Thus, using a well-designed filter, the use of the CP is eliminated and a greater number of subcarriers can be used within the allocated band. However, multicarrier transmissions have fundamental limitations which are specified by the Balian-Law theorem [51]. The theorem says that it is impossible to simultaneously satisfy the property of complex orthogonality (according to equation (2.4)) and the use of well-localized band-limited filters with characteristic $TF = 1$ in channel separation. The concept of complex orthogonality was seen in section 2.1.1 and its importance is clear to allow the individual extraction of data from each interference-free subcarrier. When $TF = 1$, we have the maximum spectral efficiency, that is, we have the maximum data rate and the duration of a symbol is exactly the spacing between the subcarriers. If we consider an ideal channel, the OFDM technique maintains the complex orthogonality and $TF = 1$ (see (2.30)) since there is no need for the cyclic prefix in this scenario. However, spectral localization is sacrificed, since in the frequency

domain there is a sinc function. In short, base functions with complex orthogonality necessarily have infinite dispersion in time or in frequency. Thus, it is not possible to obtain a waveform with properties of complex orthogonality and good localization in the time and frequency domains with maximum transmission capacity. All these properties are desired, however, they cannot be fully satisfied simultaneously, being necessary to sacrifice some of them. For the adoption of filters well located in time and frequency without compromising the spectral efficiency, it is necessary to relax the complex orthogonality criterion and adopt the real orthogonality between base functions. This fact motivated the use of offset-QAM modulation (OQAM), which separates the real and imaginary part of complex QAM symbols by an offset $T/2$ (half a symbol period) and uses a transmit and receive rate doubled over the rates with conventional QAM modulations. In this way, the spacing between the subcarriers of $F = 1/T$ is preserved; however, the transmission of the now real symbols is performed every $T/2$ seconds in order to maintain the same data rate of the OFDM system. This is possible since every $TF = 0.5$ a real value data symbol is transmitted, leading to an equivalent time-frequency spacing of $TF = 1$ for a complex symbol. This means that the density in the time-frequency plane is twice as high in FBMC/OQAM compared to OFDM as shown in Figure 7. Therefore, the information carried by one complex-valued OFDM symbol with duration T is now carried by two real-valued symbols FBMC/OQAM each with duration $T/2$.

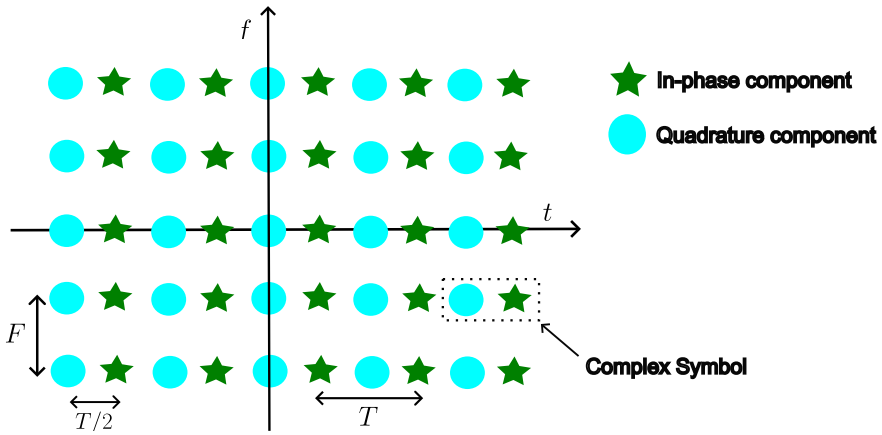

Figure 7 – Time-frequency representation of data in the FBMC/OQAM system.

The set of the filter bank with the OQAM modulation gives rise to the FBMC/OQAM which is often just called FBMC. Their proposal aims to remove the use of CP, limit out-of-band emission through the use of well-designed filters and achieve interference-free detection of symbols [15].

2.2.1 Principles

According to the OQAM transmission, we denote $x_{l,k} = a_{l,k}e^{j\frac{\pi}{2}(l+k)}$ where $a_{l,k}$ corresponds to data symbols transmitted on the lth subcarrier and at the time instant

k. However, now these symbols are represented by a constellation from Pulse Amplitude Modulation (PAM), that is, real symbols. In fact, in OQAM modulation, each complex data symbol is divided into its phase components (real part) and its quadrature components (imaginary part). These parts can be considered as elements of a pair of sequences of PAM symbols which are then transmitted with a time offset $T/2$. The phase term $e^{j\frac{\pi}{2}(l+k)}$ is to guarantee the phase shift of $\pi/2$ between adjacent symbols along the time-frequency axis. Thus, any pair of adjacent PAM symbols along the time and frequency axes are transmitted with a phase shift of $\pi/2$. Therefore, we directly consider the PAM symbols instead of the scaled QAM symbols since, due to the adopted OQAM transmission strategy, only real signals are sent in each sample of $a_{l,k}$. From this definition, the transmitted baseband FBMC/OQAM signal can be written as

$$s[m] = \sum_{l=0}^{L-1} \sum_{k} x_{l,k} g_{l,k}[m] \tag{2.31}$$

where

$$g_{l,k}[m] = g\Big[m - kL/2\Big] e^{j\frac{2\pi l}{L}\left(m - \frac{kL}{2}\right)} \tag{2.32}$$

and is essentially a time and frequency-shifted version of the prototype filter $g[m]$. The pulse used in the filtering process has unit energy and has a length of OL, where O denotes the filter's overlapping factor. This term defines the number of symbols that are overlapping in the time domain. We assume that the prototype filter $g[m]$ is zero outside the time interval $0 \leq m < OL - 1$. Note that the pulse duration is controlled by the overlapping factor O. The transmitted signal $s[m]$ can be divided into two signals, the even signal $s_e[m]$ and the odd signal $s_o[m]$, given by:

$$\begin{aligned} s[m] &= s_e[m] + s_o[m - L/2] \\ &= \sum_{l=0}^{L-1} \sum_{k} x_{l,2k} g[m - kL] e^{\frac{j2\pi l}{L}(m - kL)} \\ &+ \sum_{l=0}^{L-1} \sum_{k} x_{l,2k+1} g[m - kL - L/2] \\ &\times e^{\frac{j2\pi l}{L}(m - kL - L/2)}, \end{aligned} \tag{2.33}$$

where $s_o[m] = \sum_{l=0}^{L-1} \sum_k x_{l,2k+1} g[m - kL] e^{\frac{j2\pi l}{L}(m-kL)}$ and $s_e[m]$ is the first term of (2.33). Thus, $s[m]$ can be viewed as two streams transmitted with a time offset of $L/2$. This notation of the transmitted signal will be important in the continuity and development of the work in future sections.

The central idea of FBMC/OQAM is to allow the use of filters well located in the time-frequency plane, maintaining maximum transmission capacity, however, sacrificing complex orthogonality. Thus, the prototype filter is designed to satisfy the orthogonality

in the real field, that is:

$$\Re\Big\{ < g_{l,k}[m], g_{l',k'}[m] > \Big\} = \Re\Bigg\{ \sum_{m=-\infty}^{+\infty} g_{l,k} g^*_{l',k'} \Bigg\} = \delta_{l,l'}\delta_{k,k'} \tag{2.34}$$

where $< u, v >$ is the inner product of u and v, expressed by

$$\sum_{i=-\infty}^{+\infty} u^*[i]v[i]. \tag{2.35}$$

Based on this property and assuming an ideal channel, we have that the demodulated signal $r_{l,k}$ on the lth subcarrier at the instant k can be given by

$$\begin{aligned} r_{l,k} &=< s, g_{l,k} >= \sum_{m=-\infty}^{+\infty} s[m] g^*_{l,k}[m] \\ &= \sum_{l=0}^{L-1} \sum_{k'} a_{l',k'} \sum_{m=-\infty}^{+\infty} g_{l',k'}[m] g^*_{l,k}[m] \end{aligned} \tag{2.36}$$

Applying the real orthogonality condition described in equation (2.34), we can rewrite (2.36) as [52]:

$$r_{l,k} = a_{l,k} + \underbrace{\sum_{(l',k')\neq(l,k)} a_{l',k'} \sum_{m=-\infty}^{+\infty} g_{l',k'}[m] g^*_{l,k}[m]}_{I_{l,k}} \tag{2.37}$$

where $I_{l,k}$ is a term of intrinsic interference between symbols and between subcarriers (ISI/ICI) due to filtering. As all transmitted symbols $a_{l,k}$ are PAM symbols (symbols of a real constellation) and due to the real orthogonality condition defined in equation (2.34), the intrinsic interference term $I_{l,k}$ is purely imaginary, that is, $I_{l,k} = ju_{l,k}$ with $u_{l,k}$ being a real number. Therefore, equation (2.37) is rewritten as [52]:

$$r_{l,k} = a_{l,k} + ju_{l,k} \tag{2.38}$$

So the transmitted symbol $a_{l,k}$ can be obtained by retrieving the real part of the received signal $r_{l,k}$ as shown below

$$\hat{a}_{l,k} = \Re\{r_{l,k}\} = a_{l,k} \tag{2.39}$$

In the presence of the communication channel, in the case of a filter well located in the frequency domain, we have that the bandwidth is much smaller than the coherence band of the channel. Thus, even without the use of the cyclic prefix, a one-tap equalizer may be sufficient to minimize ISI problems. In terms of ICI, it is limited to adjacent subchannels according to the prototype filter used. We will see that some filters have better time localization so that interference is more present between the subcarriers, while others are band limited, bringing interference between the transmitted symbols. The idea is to obtain a filter with both characteristics so that the pulse energy is concentrated in both domains, limiting interference in the vicinity of a data symbol.

2.2.2 Efficient Digital Implementation

The purpose of the filter bank is to decompose the spectrum of a signal into a specified number of channels or recombine them using filters. A filter bank with L evenly spaced channels in a set of L filters, offset from each other by a uniform factor. Figure 8 exemplifies the decomposition of a filter $F[z]$ into L filters with uniform displacement every $1/L$. Its implementation can be done efficiently with low complexity via polyphase

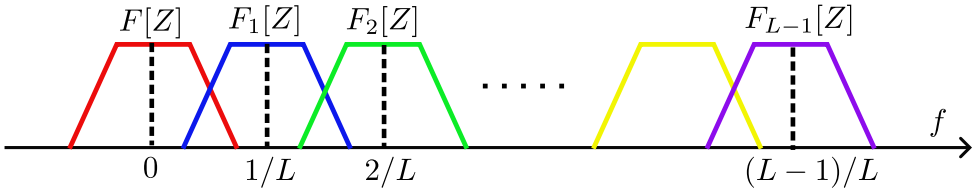

Figure 8 – Uniform overall frequency response of filter bank.

decomposition, a technique proposed by Bellanger [53]. This decomposition leads to the natural appearance of the DFT/IDFT operation, making it possible to preserve these operations present in the OFDM modulator and demodulator. The difference is that in FBMC systems the DFT is complemented by a set of digital filters forming a polyphase network (PPN) [16]. In transmission, the polyphase network combined with the IDFT composes the synthesis filter bank (SFB) expressed by the equation (2.32) and, in the reception, the polyphase network combined with the DFT forms the analysis filter bank (AFB), expressed by the conjugate of equation (2.32). As mentioned, the task of SFB is to divide the total bandwidth into equal L subchannels, while AFB has the task of recombining these L subchannels. Let us consider the sequence $g[i]$ as the impulse response of a filter with $D = OL$ coefficients. Filtering a sequence $x[m]$ by the filter $g[i]$ is defined by the convolution sum given by

$$y[m] = \sum_{i=0}^{D-1} g[i]x[m-i] \tag{2.40}$$

The frequency response of the filter can be expressed by:

$$G(f) = \sum_{i=0}^{D-1} g[i]e^{-j2\pi if} \tag{2.41}$$

Defining the filter transfer function $G(z)$, we have

$$G(z) = \sum_{i=0}^{D-1} g[i]z^{-i} \tag{2.42}$$

Because the filter length is a product of two factors, in the case OL, and we already know that O corresponds to the filter overlapping factor and L the number of subcarriers in the system, the filter sequence can be decomposed into L interleaved sequences of O

coefficients. Thus, the transfer function $G(z)$ can be redefined as

$$G(z) = \sum_{l=0}^{L-1} z^{-l} E_l(z^L) \tag{2.43}$$

where $E_l(z^L)$ are the so-called polyphase components of $G(z)$ and can be expressed by [40]:

$$E_l(z^L) = \sum_{o=0}^{O-1} g[oL + l] z^{-oL} \tag{2.44}$$

From this structure, the filter $G(z)$ is decomposed into L filters. By the equations (2.43) and (2.44), the impulse response of $E_1(z^L)$ contains each sample of $g[i]$ with index multiple of L, the impulse response of $E_2(z^L)$ contains each sample with index one unit above a multiple of L, and so on. Note that each filter element, $E_l(z^L)$, has the frequency response of a phase shifter, hence the name polyphase decomposition and polyphase network for the complete set. Defining $G_d(f)$ as the frequency response of the filter $G(z)$ shifted from $1/L$ in the frequency domain, we have

$$G_d(f) = G\left(f - \frac{1}{L}\right) = \sum_{i=0}^{D-1} g[i] e^{-j2\pi i(f-1/L)} \tag{2.45}$$

The corresponding transfer function is:

$$G_d(z) = \sum_{i=0}^{D-1} g[i] e^{-\frac{j2\pi i}{L}} z^{-i} \tag{2.46}$$

Using the polyphase representation, we rewrite $G_d(z)$ as

$$\begin{aligned} G_d(z) &= \sum_{l=0}^{L-1} \sum_{o=0}^{O-1} g[oL + l] e^{\frac{j2\pi l}{L}(oL+l)} z^{-(oL+l)} \\ &= \sum_{l=0}^{L-1} e^{\frac{j2\pi l}{L}} z^{-l} E_l(z^L) \end{aligned} \tag{2.47}$$

The key point here is that the $E_l(z^L)$ functions are not affected by the frequency shift. Thus, a uniform filter bank is obtained by shifting the frequency response of the prototype filter $G(z)$ on the frequency axis. Such a bank of filters is called a prototype filter [18]. Therefore, considering all displacements by multiples of $1/L$ and the associated filters we have the following expression

$$\begin{bmatrix} G_0(z) \\ G_1(z) \\ \vdots \\ G_{L-1}(z) \end{bmatrix} = \underbrace{\begin{bmatrix} 1 & 1 & 1 & \dots & 1 \\ 1 & W_L & W_L^2 & \dots & W_L^{L-1} \\ \vdots & \vdots & \ddots & & \vdots \\ 1 & W_L^{L-1} & W_L^{2(L-1)} & \dots & W_L^{(L-1)^2} \end{bmatrix}}_{L-\text{IDFT}} \underbrace{\begin{bmatrix} E_0(z^L) \\ z^{-1}E_0(z^L) \\ \vdots \\ z^{-(-L-1)}E_{L-1}(z^L) \end{bmatrix}}_{\text{PPN}}. \tag{2.48}$$

Note that we can represent the sequence $G_o(z), G_1(z), ...G_{L-1}(z)$ by multiplying the IDFT matrix $\mathbf{W}_L^H$ (see equation (2.8)) by the sequence $E_0(z^L), z^{-1}E_1(z^L), ..., z^{-(L-1)}E_{L-1}(z^L)$. According to (2.48) and using the noble identities [18], we obtain Figure 9 that summarizes the strategy presented so far, illustrating an efficient and simplified way of implementing a transmitter via polyphase networks. Note that OQAM modulation has not yet been applied, so that in Figure 9 we have a single data steam referring to one of the terms of the equation (2.33) where we divide the transmitted signal $s[m]$ into two signals. The

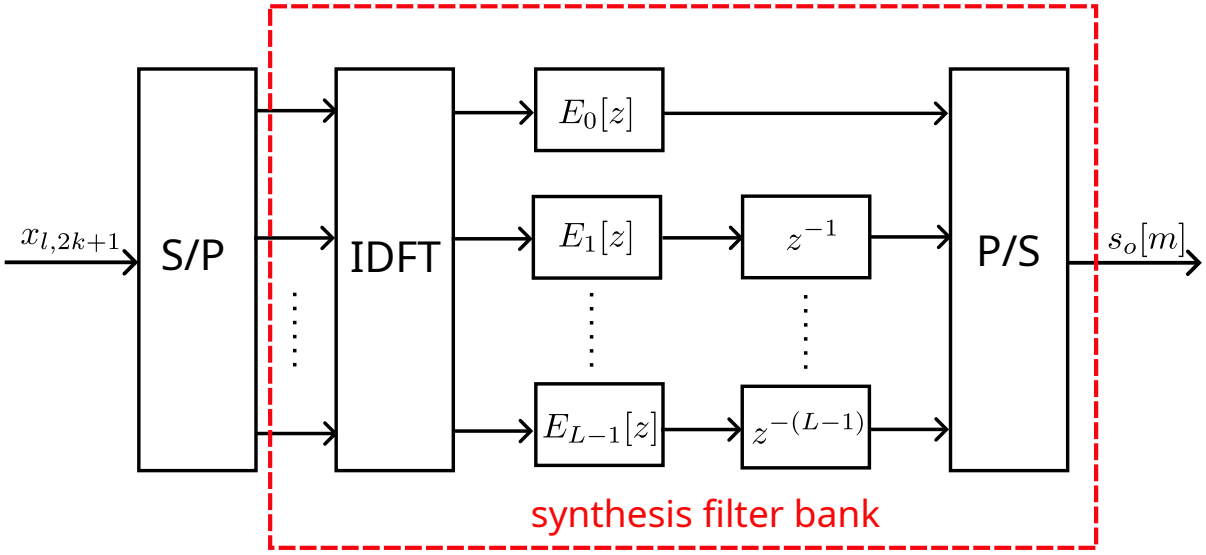

Figure 9 – Polyphase synthesis filter bank block diagram.

polyphase decomposition technique of the prototype filter allows using reduced signal processing rates during the filtering process [13]. From this technique, we can implement the FBMC modulator through an IDFT combined with a polyphase network. The same scheme applies to the filter bank on the receiver. Basically, we just need to define $G_{-d}(z)$ from $G(z)$ in the same way as it was done for $G_d(z)$. The difference will be that the frequency changes are multiples of $-1/L$, and the DFT replaces the IDFT. In fact, for each subchannel the signal of interest is shifted to the source frequency and filtered [1]. Figure 10 shows a section of the polyphase network for an overlapping factor $O = 4$ from the expression (2.44). We have that in terms of complexity, each PPN section has O multiplications while full filtering needs OL multiplications. The block diagram of the complete system is shown in the Figure 11. In fact, due to the OQAM transmission process, one must delay half the symbols by half a symbol period. For each subchannel, we alternatively use the real and imaginary part of the data symbols. From equation (2.33), it is noted that the symbol rate must be doubled. Thus, we have a single IDFT performed at double rate feeding two identical PPNs, as shown in Figure 12. The L sample sequences are processed by IDFT and directed to PPN 1 or PPN 2. Their outputs overlap over $L/2$ samples and an addition is applied. The function of the de-multiplexer (DMUX) is to switch between the odd and even multicarrier symbols (in-phase or quadrature component

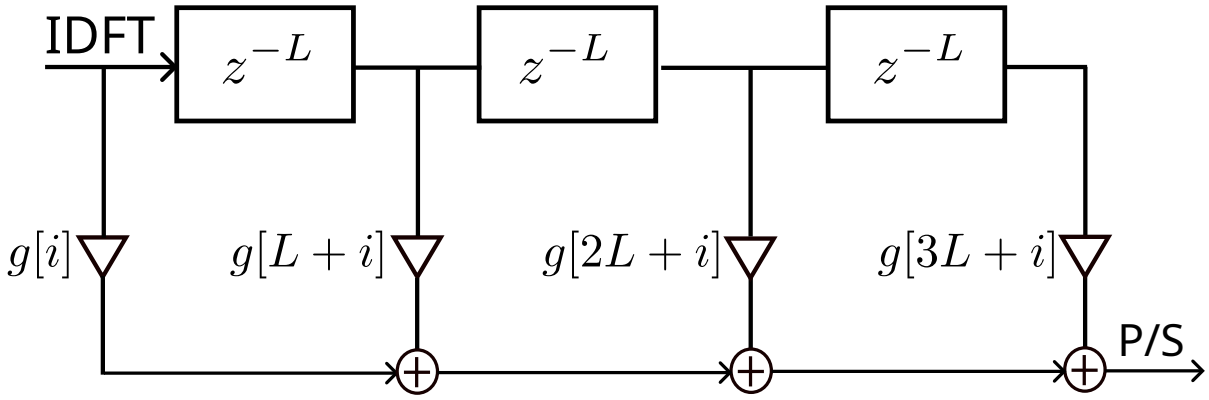

Figure 10 – PPN section with $O = 4$ [1].

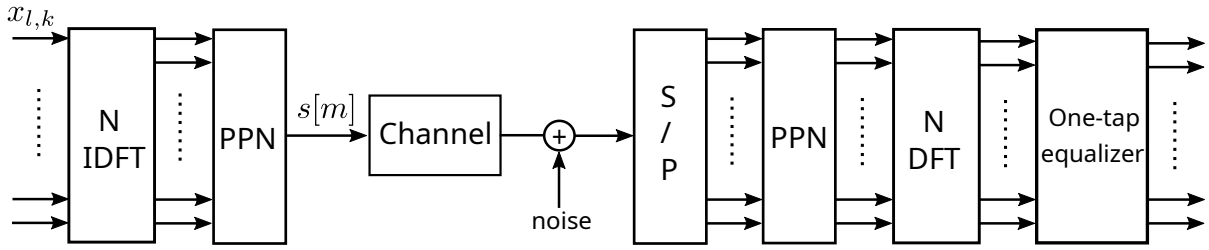

Figure 11 – Transmission and reception system using the PPN-FFT scheme.

of a QAM symbol) for its respective PPN. Thus, it can be seen that in a discrete-time implementation, it is necessary to double the number of multicarrier symbols K in order to obtain the same transmission capacity of an OFDM system. This is clear when an OFDM symbol transmits complex data every T seconds. For the same period of time in FBMC/OQAM, two FBMC symbols with real data are transmitted each $T/2$ seconds. Note the delay of $L/2$ samples in the lower block due to the use of OQAM modulation. On the receiver side the reverse process is performed. After the serial/parallel conversion process, each received symbol is destined for its PPN, half of which are delayed by $L/2$ samples. The time-frequency symbol grid is reassembled in its original structure from the even and odd symbols and the DFT is performed for each symbol [18].

2.2.3 Prototype Filters

Prototype filter design is a key point in the FBMC/OQAM system. From the specification of the base pulse, that is, $g_{0,0}[m]$ (see (2.32)), the synthesis and analysis filters are constructed by frequency shifted versions of this base pulse. In this sense, the quality of the filter for a better spectral location and robustness to the dispersive effects of the channel are directly linked to the properties of the prototype filter. In OFDM systems, the impulse response of the adopted prototype filter is the rectangular window. In ideal situations, this filter guarantees complex orthogonality by simplifying the data detection process. However, in practical situations, the orthogonality between subchannels

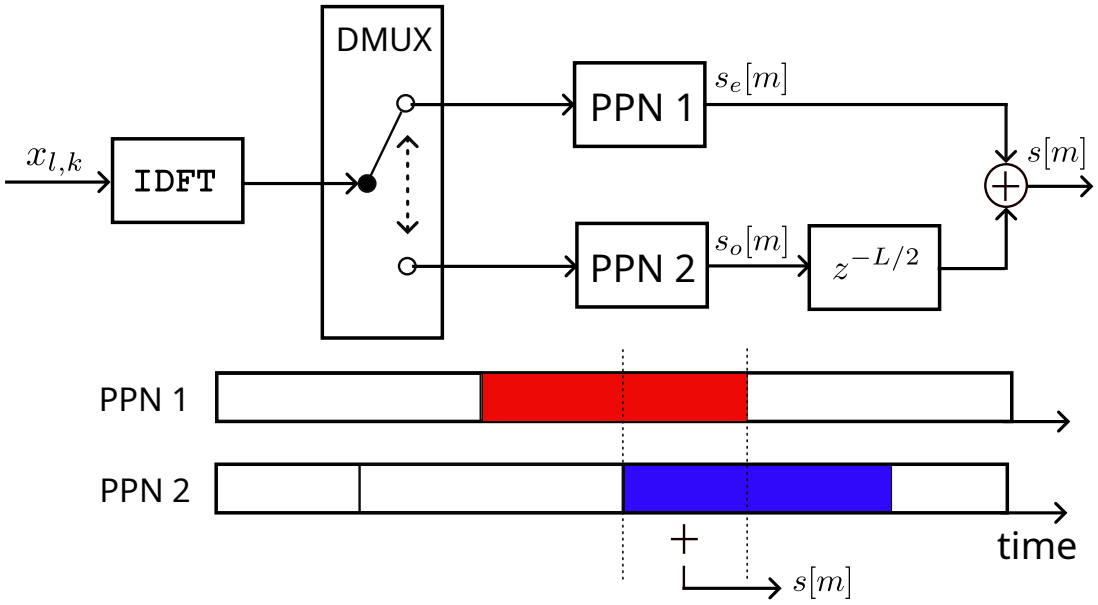

Figure 12 – FBMC/OQAM transmitter implementation scheme using one IDFT and two PPNs [2].

is compromised by the channel effects, which can cause strong ICI and OOB, as mentioned before.

The intrinsic interference of the FBMC system can be seen by the correlation between samples created by the structure of the prototype filter in the time-frequency plane. In several works [52] [54], the impulse response of the transmultiplex of the FBMC system at position (l', k') is presented in a table in order to present in the time-frequency the intrinsic interference imposed by the prototype filter. So, with equations (2.31) and (2.32) and assuming that we have only one unit impulse to be transmitted at a frequency-time position (l', k'), the impulse response of the FBMC/OQAM transmultiplex $r_{l,k} =< g_{l,k}[m]e^{j\frac{\pi}{2}(l+k)}, g^*_{l',k'}[m]e^{-j\frac{\pi}{2}(l'+k')} >$ is given by

$$\begin{aligned} r_{l,k} &= \sum_{m=-\infty}^{+\infty} g_{l,k}[m]g^*_{l',k'}[m]e^{-j\frac{\pi}{2}(l'+k')}e^{j\frac{\pi}{2}(l+k)} \\ &= \sum_{m=-\infty}^{+\infty} g[m]g[m-\Delta_k L/2]e^{j\frac{2\pi\Delta_l}{L}(P/2-m)}e^{j\pi(\Delta_l+l')\Delta_k}e^{-\frac{j\pi}{2}(\Delta_l+\Delta_k)} \end{aligned} \tag{2.49}$$

with $\Delta_l = l - l'$ and $\Delta_k = k - k'$. Note that the impulse response of the transmultiplex strongly depends on the $g[m]$ filter used. The FBMC/OQAM system uses a well-located prototype filter in both time and frequency domains. Time localization aims to limit ISI while frequency localization limits ICI. These prototype filters are based on various design criteria, such as energy concentration in the time domain and rapid decay in the frequency domain. In this section, we will present two prototype filters widely used in FBMC/OQAM systems and compare them with the rectangular window used in OFDM.

2.2.3.1 Rectangular window

The rectangular window is the prototype filter used in OFDM and perfectly separates the symbols in the time domain. The discrete impulse response of this filter is given by equation (2.50).

$$g[m] = \begin{cases} \frac{1}{\sqrt{L}}, & 0 \leq m < L-1 \\ 0, & \text{otherwise.} \end{cases} \tag{2.50}$$

Numerical calculations of equation (2.49) using the rectangular window yields the table shown below. In the frequency domain, the function becomes a sinc pulse and spreads

	$k'-3$	$k'-2$	$k'-1$	k'	$k'+1$	$k'+2$	$k'+3$
$l'-2$	0	0	0	0	0	0	0
$l'-1$	0	0	0	0	0	0	0
l'	0	0	0	1	0	0	0
$l'+1$	0	0	0	0	0	0	0
$l'+2$	0	0	0	0	0	0	0

Table 1 – Table of transmultiplex OFDM coefficients - Rectangular Filter.

across the spectrum. However, the subcarriers are orthogonal when the spectrum is sampled at frequencies $k = 0, \ldots, L-1$. Therefore, it can be noted from Table 1 that the interference in the time-frequency plane of an OFDM block for this prototype filter is completely null.

2.2.3.2 Mirabassi-Martin (PHYDYAS)

The Mirabassi-Martin function has a time-frequency response that depends on the overlapping factor used. Normally $O = 4$ is the more used resulting in a spectrum well located and has a rapid decay of side lobe energy. The researchers of the European Physical Layer for Dynamic Spectrum Access (PHYDYAS) project [16] use the prototype Mirabassi-Martin filter. The proposed filter for the PHYDYAS project has its coefficients defined as

$$g[m] = 1 + 2\sum_{i=1}^{O-1} g_i \cos\left(\frac{2\pi i m}{OL}\right) \tag{2.51}$$

where the terms g_i for $i = 0, ..., O-1$ are auxiliary coefficients in the filter design and are presented in Table 2. The response of the transmultiplex of the FBMC/OQAM system using the prototype filter PHYDYAS with the overlapping factor $O = 4$ is shown in Table 3. It is observed that there are interferences composed only of imaginary values. Note also that interferences in frequency occur only in relation to adjacent ones and in time up to the third symbol ($O = 4$). Information at the receiver is retrieved without interference just by taking the real part of the estimated symbol.

	$O=1$	$O=2$	$O=3$	$O=4$
g_0	1	1	1	1
g_1	-	$\sqrt{2}/2$	0.91143783	0.97195983
g_2	-	-	0.41143783	$\sqrt{2}/2$
g_3				0.23514695

Table 2 – Table of PHYDYAS filter coefficients for different O values.

	$k'-3$	$k'-2$	$k'-1$	k'	$k'+1$	$k'+2$	$k'+3$
$l'-2$	0	0	0	0	0	0	0
$l'-1$	$0.043j$	$-0.125j$	$-0.206j$	$0.239j$	$0.206j$	$-0.125j$	$-0.043j$
l'	$-0.067j$	0	$0.564j$	1	$0.564j$	0	$-0.067j$
$l'+1$	$-0.043j$	$-0.125j$	$0.206j$	$0.239j$	$-0.206j$	$-0.125j$	$0.043j$
$l'+2$	0	0	0	0	0	0	0

Table 3 – Table of transmultiplex FBMC/OQAM coefficients - PHYDYAS filter.

2.2.3.3 Hermite

The Hermite prototype filter was suggested in [55] and is based on Hermite polynomials $g_i\{.\}$ and can be expressed by

$$g[m] = \sqrt{F}e^{-2\pi(mF)^2} \sum_{i=\{0,4,8,12,16,20\}} \alpha_i g_i\{2\sqrt{\pi}mF\} \tag{2.52}$$

where the coefficients α_i can be found in [56]. The Hermite pulse is based on a Gaussian function and therefore has a good localization in the time-frequency plane. In fact the pulse is almost as good as the threshold reached by the Gaussian pulse and better than the PHYDYAS filter with respect to time overlapping. This feature makes the Hermite pulse robust in doubly selective channels and, in particular, in time-varying channels [57]. In terms of the overlapping factor, the maximum value that the hermite pulse can reach is $O=2$. The impulse response of the transmutiplex in the time-frequency plane using Hermite as a prototype filter is presented in Table 4. Differently from PHYDYAS, the

	$k'-3$	$l'-2$	$k'-1$	k'	$k'+1$	$k'+2$	$k'+3$
$l'-3$	0	0	$0.0373j$	$0.0561j$	$-0.0373j$	0	0
$l'-2$	0	0	$0.1197j$	0	$-0.1197j$	0	0
$l'-1$	0	0	$-0.2138j$	$0.5554j$	$-0.2138j$	0	0
l'	0	0	$0.2560j$	1	$-0.2560j$	0	0
$l'+1$	0	0	$-0.2138j$	$-0.5554j$	$-0.2138j$	0	0
$l'+2$	0	0	$0.1197j$	0	$-0.1197j$	0	0
$l'+3$	0	0	$-0.0373j$	$-0.0561j$	$-0.0373j$	0	0

Table 4 – Table of Transmutiplex FBMC/OQAM coefficients - Hermite Filter.

interferences in the Hermite filter appear more intensely only in adjacent neighbors in time, while in frequency they expand to several subcarriers. Figures 13 and 14 show the impulse

and frequency responses of the prototype filters presented in this section: rectangular window, Hermite and PHYDYAS. One can observe the influence of the side lobes in the frequency domain and the advantage, in OOB terms, of using a filter well located in the frequency. In the case of the PHYDYAS filter we have a higher overlapping factor, which consequently achieves a better spectral localization.

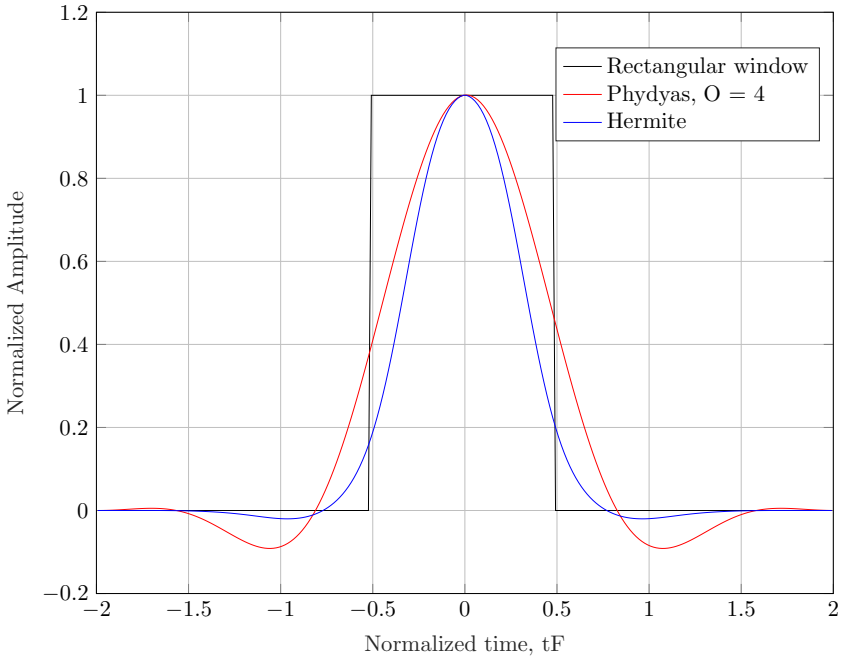

Figure 13 – Time response of the prototype filters presented.

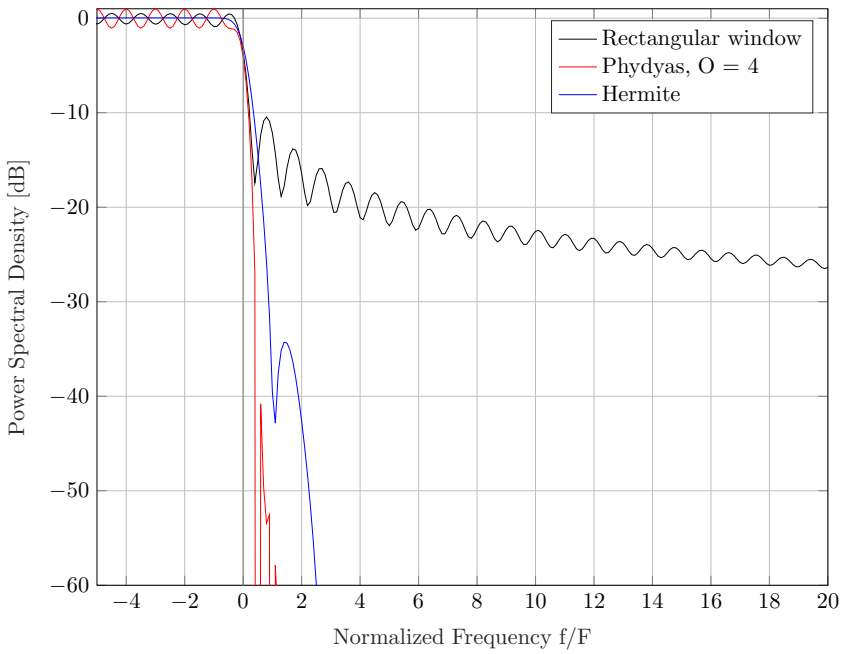

Figure 14 – Frequency response of the prototype filters presented.

From the design of the filter, we have effectively the behavior of interferences in the plane time-frequency. In the case of a filter with a more compact frequency response, each subchannel significantly interferes only with its immediate neighbors. In this type of filter, where only the spectral location is optimized, there is a bad time domain localization, causing ISI in time-dispersive channels. On the other hand, if the filter is optimized only in the time domain (like the rectangular window present in OFDM), its frequency localization will be negatively affected. Fact that generates ICI when the information is transmitted through selective channels in frequency. Since the communication channel is doubly selective, that is, both in time and in frequency, it is necessary to design a filter with good localization in both domains.

2.2.4 Matrix Description

The discrete-time representation, presented earlier, analytically describes the physical characteristics of the FBMC system. As the focus of this work will be the exclusive use of the FBMC, a new matrix description is presented from this point on. Although in practice equation (2.31) is calculated by an FFT together with the PPN and not by matrix multiplication, expressing the system in matrix form allows us to better explain some concepts that we want to highlight. This notation will have some modifications in the course of the work, adjusting to the schemes that will be proposed and studied.

As highlighted earlier and repeated here for convenience, a multicarrier transmission system can be characterized in a plane/grid structure consisting of K multicarrier symbols, where each symbol has L subcarriers. However, we will use exclusively for FBMC, $K' = 2K$ multicarrier symbols, in view of the need to keep the same OFDM data rate for later performance comparisons. As commented in the section 2.2.2, this is necessary due to double rate transmission, where in a multicarrier symbol we transmit the real part of a QAM symbol (in $T/2$ seconds) and in a second multicarrier symbol the imaginary part (in $T/2$ seconds), while in OFDM both parts are transmitted in a single symbol (in T seconds). Therefore, the k-th data symbol $\mathbf{x}_k$ to be transmitted by SFB can be written as:

$$\mathbf{x}_k = \mathbf{\Theta}_k \mathbf{a}_k \tag{2.53}$$

where $\mathbf{a}_k = [a_{0,k}, a_{1,k}, \ldots, a_{L-1,k}]^T \in \mathbb{R}^{L\times 1}$ corresponds to the real symbols belonging to a PAM constellation at the instant k and $\mathbf{\Theta}_k \in \mathbb{C}^{L\times L}$ is a diagonal matrix of the phase shift factor, whose coefficients are expressed by $(\mathbf{\Theta}_k)_l = j^{(k+l)}$. The idea of this matrix notation is to effectively use a representation of the filter bank via polyphase decomposition and not a direct implementation with a digital filter for each subchannel. First, let us consider an IDFT of N points, where $N \geq L$, which corresponds to the system without critical sampling ($N \neq L$). The interpretation of the IDFT/DFT pair size of the FBMC modulator and demodulator respectively will become clearer later in the work. For this,

let us consider the DFT spreading matrix $\tilde{\mathbf{W}}_N \in \mathbb{C}^{L\times N}$ expressed by:

$$\tilde{\mathbf{W}}_N = \begin{bmatrix} \mathbf{I}_L & \mathbf{0}_{(L\times N-L)} \end{bmatrix} \mathbf{W}_N \tag{2.54}$$

The purpose of this DFT matrix is to spread the L input data into N output samples. An alternative way to use only one $\mathbf{W}_N$ is to fill the data vector $\mathbf{x}_k$ with $N-L$ zeros. By adding zeros to the signal in time, we do not change its frequency content, but we improve the frequency resolution [40]. Considering the first option, we have that the vector in the filter input $\mathbf{d}_k \in \mathbb{C}^{N\times 1}$ can be given by

$$\mathbf{d}_k = \tilde{\mathbf{W}}_N \mathbf{x}_k \tag{2.55}$$

The convolution of the impulse response of the prototype filter with the input signal $\mathbf{d}_k$ can be implemented by multiplying this same signal by a Toeplitz matrix of the prototype filter. For this, we consider the diagonal matrix $\mathbf{G}_o$ that corresponds to the filter coefficients, that is, $\mathbf{G}_o$ =diag$(\mathbf{g}_o) \in \mathbb{R}^{N\times N}$ to $o = 0, 1, 2, ..., O-1$, where $\mathbf{g}_o = [\mathbf{g}_{oN}, \mathbf{g}_{oN+1}, \ldots, \mathbf{g}_{oN+N-1}] \in \mathbb{R}^{1\times N}$ is the vector formed by the samples of $g_{l,k}[m]$ (equation (2.32)) to k and l equal to zero and $m = oN, oN+1, \ldots, oN+N-1$. We assume that the prototype filter $g[m]$ is zero outside the time interval $0 \leq m < ON-1$. Therefore, the Toeplitz matrix $\mathbf{G} \in \mathbb{R}^{(O+K'/2-1)N\times NK'/2}$ considering $K' > 2$ FBMC symbols with size can be given as follows:

$$\mathbf{G} = \begin{bmatrix} \mathbf{G}_0 & \mathbf{0} & \ldots & \mathbf{0} \\ \mathbf{G}_1 & \mathbf{G}_0 & \ldots & \mathbf{0} \\ \vdots & \mathbf{G}_1 & \ldots & \mathbf{0} \\ \mathbf{G}_{O-1} & \vdots & \ldots & \mathbf{G}_0 \\ \mathbf{0} & \mathbf{G}_{O-1} & \ldots & \mathbf{G}_1 \\ \vdots & \vdots & \ddots & \vdots \\ \mathbf{0} & \mathbf{0} & \ldots & \mathbf{G}_{O-1} \end{bmatrix}. \tag{2.56}$$

Using the OQAM strategy in a multicarrier structure, the output vector $\mathbf{s} \in \mathbb{C}^{M\times 1}$ of length $M = (O + K'/2 - 1)N$ of the FBMC modulator is expressed by

$$\mathbf{s} = \mathbf{G}\mathbf{d}_e + \mathbf{Q}_d\mathbf{G}\mathbf{d}_o, \tag{2.57}$$

where $\mathbf{d}_e \in \mathbb{C}^{NK'/2\times 1}$ and $\mathbf{d}_o \in \mathbb{C}^{NK'/2\times 1}$ correspond respectively to the odd and even multicarrier symbols of $\mathbf{d}_k$ both already serialized, so that we have the transmission of $N/2$ samples with twice the rate of a QAM transmission with N samples. The matrix $\mathbf{Q}_d \in \mathbb{R}^{M\times M}$ represents the delay of $N/2$ in the odd symbols and is represented by

$$\mathbf{Q}_d = \begin{bmatrix} \mathbf{0}_{N/2\times M-N/2} & \mathbf{0}_{N/2} \\ \mathbf{I}_{M-N/2} & \mathbf{0}_{M-N/2\times N/2} \end{bmatrix}. \tag{2.58}$$

Note that the matrix $\mathbf{G}$ in equation (2.56) presents exactly the structure of Figure 10, while the transmitted signal of equation (2.57) corresponds to Figure 12. Also notice that the filter output has $(K'-1)N$ too many samples due to the linear convolution process. At the receiver, the reverse process of the transmitter is performed. Initially, the received signal is demodulated by the analysis filter $\mathbf{G}^T$ generating the matrix $\mathbf{Z} \in \mathbb{C}^{2\times NK/2}$ expressed by

$$\mathbf{Z} \;=\; [(\mathbf{G}^T\mathbf{s})^T; (\mathbf{G}^T\mathbf{Q}_d^T\mathbf{s})^T]. \tag{2.59}$$

Then it is necessary to reassemble the transmitted grid, organizing the even and odd symbols separated in the transmission. Considering each position in time-frequency, we have $z_{n,k} = [\mathbf{z}]_{i,n+\frac{N}{2}(k-i)}$ for $n = 1, 2, \ldots, N$ and i is given by

$$i = \begin{cases} 2, & \text{for } \mathrm{mod}(k,2) = 0 \\ \mathrm{mod}(k,2), & \text{otherwise} \end{cases} \tag{2.60}$$

where mod(x,y) returns the remainder after dividing x by y. Such process is necessary to adjust the time-instants in their respective positions, since they were separated in the transmission. Then, through the DFT matrix $\tilde{\mathbf{W}}_N$, we obtain the vector $\mathbf{y}_k \in \mathbb{C}^{L\times 1}$, expressed as:

$$\mathbf{y}_k = \tilde{\mathbf{W}}_N\mathbf{z}_k, \tag{2.61}$$

where $\mathbf{z}_k = [z_{1,k}, z_{2,k}, \ldots, z_{N,k}] \in \mathbb{C}^{N\times 1}$. Finally, knowing that FBMC/OQAM induces imaginary interference, we recover the transmitted symbol $\mathbf{a}_k$ by compensating the phase and imposing the real orthogonality condition, that is,

$$\hat{\mathbf{a}}_k = \Re\{\mathbf{\Theta}_k^H\mathbf{y}_k\} \tag{2.62}$$

The central concept of the FBMC technique is to combine the frequency division principle with a subcarrier filtering functionality. The filter bank is efficiently implemented using the polyphase decomposition resulting in a structure based on the Fourier transform. The prototype filter must have an impulse response that is well localized in both time and frequency. Thus, interference between adjacent symbols is minimized without the need to use the cyclic prefix and, consequently, achieving better spectral efficiency. The use of these filters does not guarantee complex orthogonality and high spectral efficiency simultaneously. The solution is to relax one of the properties using FBMC/OQAM which depends only on the real orthogonality. However, the loss of complex orthogonality causes problems in adapting the system to MIMO transmissions. In addition, the sensitivity problems in high mobility and high PAPR scenarios remain similar to those present in OFDM.

2.3 OTFS System

The OTFS modulation has been introduced by Hadani et al. [24] as a promising technique to combat the Doppler effect produced by doubly dispersive time-varying multipath channels. Using a pre-processing via sympletic finite Fourier transform (SFFT), which is a two-dimensional FFT, OTFS converts time-varying channels into invariant channels in a domain called delay-Doppler (also known as the Zak domain). Through the OTFS waveform, it is assume that all symbols in a transmission block experience the same channel gain, providing a high order of diversity. This is true if the delays and Doppler are fixed within an OTFS frame. In this way, OTFS is more robust to the carrier frequency shift, being more suitable for use in high mobility scenarios and millimeter wave systems. Also, depending on the block size to be transmitted, the PAPR of OTFS is much smaller than the one from OFDM and FBMC. In terms of OOB emission, OTFS maintains the same problem that exists in OFDM, as it uses the same formatting filter. At the transmitter, the symbols of a QAM constellation positioned on a delay-Doppler (DD) grid are mapped to symbols of a time-frequency grid by the inverse SFFT (ISFFT) and transmitted over the channel using the OFDM multicarrier technique [25]. Basically, it can be seen as a pre-coding via SFFT in a system that uses an OFDM transceiver as its core. Such a technique converts the time-dispersive channel into an invariant channel within the delay-Doppler domain. Thus, combined with a sophisticated equalization scheme in this delay-Doppler domain the information symbols inside the block undergo almost constant attenuation [26].

We have seen that a multicarrier system that operates with symbols in the time-frequency domain can be characterized as a block structure composed of K symbols with a duration of T seconds, where each symbol has L subcarriers spaced between them by F Hz. Thus, in the time-frequency domain we obtain a grid with L points spaced by F Hz along the frequency axis and K points along the time axis with a space of T seconds. Considering the critical sampling process, that is, $TF = 1$, this grid in the TF domain can be expressed by [24]

$$\mathbf{\Lambda} = \{(iF, nT),\ \ i = 0, \ldots, L-1; n = 0, \ldots, K-1\}, \tag{2.63}$$

In this sense, we can define the total bandwidth as $B = LF$ Hz and the total transmission time interval as KT seconds. Such representation is the one we have at the input of an OFDM modulator. However, in OTFS, we first have pre-processing done by ISFFT so that our data symbols come from a grid in the delay-Doppler domain. This grid consists of L points (number of subcarriers) along the delay domain spaced $\Delta\tau = \frac{1}{LF}$ and K points (number of symbols) along the Doppler domain spaced $\Delta\nu = \frac{1}{KT}$ [26]. Its representation can be expressed by

$$\mathbf{\Gamma} = \left\{\left(\frac{l}{LF}, \frac{k}{KT}\right),\ \ l = 0, \ldots, L-1; k = 0, \ldots, K-1\right\}. \tag{2.64}$$

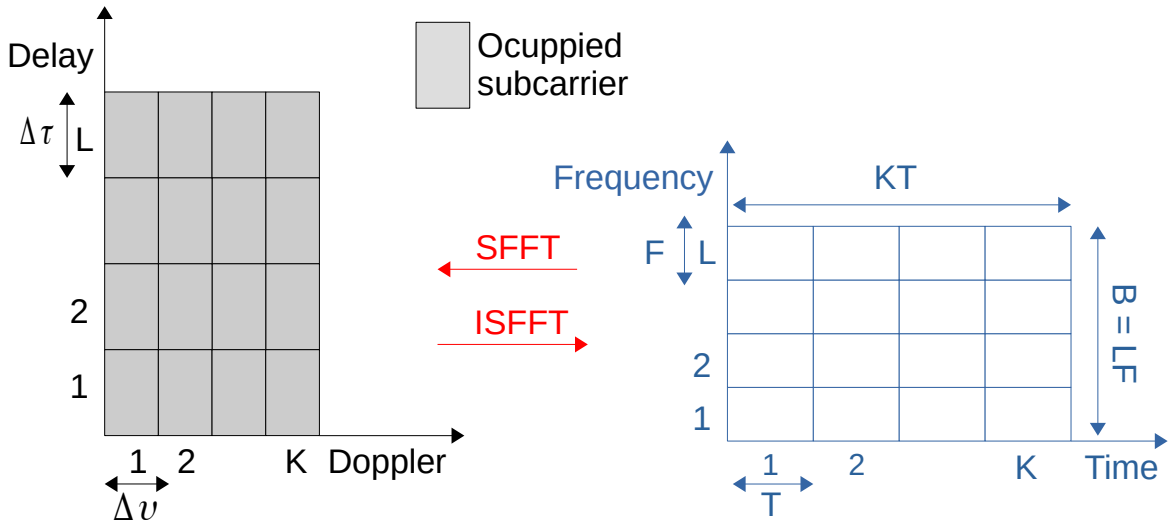

Figure 15 – Symplectic Fourier Duality - Analysis of time-frequency and delay-Doppler grids.

Consequently, the transmission bandwidth B is the inverse of the delay resolution and the total transmission duration KT is the inverse of the Doppler resolution. Figure 15 presents the respective grids from the perspective of the SFFT and the ISFFT. Therefore, while in a conventional OFDM or FBMC system the information data is represented from a time-frequency grid, in OTFS the data initially comes from a delay-Doppler grid. Thus, through the ISFFT we retrieve these data in the time-frequency grid for its eventual transmission by the specific multicarrier technique.

The key point of the OTFS technique is the pre and post processing via ISFFT/SFFT respectively. It can be noted that SFFT is a two-dimensional Fourier transform, in this sense, it is equivalent to implement a K-point IDFT followed by an L-point DFT. Based on these definitions, first, after a serial-to-parallel data stream converter L blocks of K-point IDFT are fed by QAM symbols, yielding $\bar{a}_{l,k}$ which is given by

$$\bar{a}_{l,k} = \sum_{n=0}^{K-1} a_{l,n} e^{j\frac{2\pi kn}{K}} \tag{2.65}$$

where $a_{l,n}$ denotes the n-th complex symbol to be transmitted in the l-th subcarrier in DD domain. Then, time-domain spreading is performed from the L-point DFT. Thus, we have a sequence of complex numbers $x_{l,k}$ mapped to the Λ grid in the TF domain, as follows:

$$x_{l,k} = \sum_{i=0}^{L-1} \bar{a}_{i,k} e^{-j\frac{2\pi il}{L}}. \tag{2.66}$$

Replacing (2.65) into (2.66) the signal at the input of the OFDM modulator can be expressed by

$$x_{l,k} = \sum_{i=0}^{L-1} \sum_{n=0}^{K-1} a_{i,n} e^{j2\pi(\frac{nk}{K} - \frac{il}{L})}. \tag{2.67}$$

In continuous time, the signal to be transmitted via the OFDM modulator is described by equation (2.1) and repeated here for convenience

$$s(t) = \sum_{l=0}^{L-1} \sum_{k} x_{l,k} g(t - kT) e^{j2\pi lF(t-kT)} \tag{2.68}$$

Linear time-varying wireless communication channels can be represented in different ways. In addition to the time-frequency domain, the channel representation in the delay-Doppler domain can be characterized. In this domain, one can better analyze the effects of delay spreading and Doppler spreading. This channel can be described for V independent paths by

$$h(\tau, \nu) = \sum_{p=0}^{V-1} h_p \delta(\tau - \tau_p) \delta(\nu - \nu_p) \tag{2.69}$$

where h_p , τ_p, and ν_p denote the complex path gain, delay, and Doppler shift associated with the p-th path, respectively. The term $h(\tau, \nu)$ is called the Doppler variant impulse response [58]. Basically it represents the doubly selective channel through the delay-Doppler domain. Thus, disregarding the noise, the received signal $r(t)$ can be given by

$$r(t) = \int_{\tau} \int_{\nu} h(\tau, \nu) s(t - \tau) e^{j2\pi\nu(t-\tau)} d\tau d\nu \tag{2.70}$$

For scenarios with high Doppler spreading, symbols coming from the DD domain experience a slowly varying channel compared to symbols coming from the TF domain [26]. Basically, the channel model in OTFS is sparse so that only a drastic change in path sizes or velocitys can cause channel variations in the DD domain. In this way, the channel persists longer than transmissions in time or frequency [59].

Using a matrix notation to formulate the system model, the signal at the input of the OFDM modulator $\mathbf{X}_{\text{OTFS}} \in \mathbb{C}^{L \times K}$ is given by

$$\mathbf{X}_{\text{OTFS}} = \mathbf{W}_L \mathbf{A} \mathbf{W}_K^H, \tag{2.71}$$

where $\mathbf{A} \in \mathbb{C}^{L \times K}$ represents the transmitted complex data symbols in the delay-Doppler domain. After the pre-coding process, we implement the conventional OFDM modulation through an L-point IDFT. Thus, disregarding the cyclic prefix the transmitted signal can be expressed by:

$$\mathbf{S}_{\text{OTFS}} = \mathbf{W}_L^H \mathbf{X}_{\text{OTFS}} = \mathbf{A} \mathbf{W}_K^H \tag{2.72}$$

The column vectorization of $\mathbf{S}_{\text{OTFS}} \in \mathbb{C}^{L \times K}$ in (2.72) yields $\mathbf{s} = \text{vec}(\mathbf{S}_{\text{OTFS}}) = (\mathbf{W}_K^H \otimes \mathbf{I}_L)\mathbf{a} \in \mathbb{C}^{LK \times 1}$, where $\mathbf{a} = \text{vec}(\mathbf{A}) \in \mathbb{C}^{LK \times 1}$ and $\otimes$ refers to the Kronecker product. At the receiver the inverse process is applied. First, OFDM demodulation is performed through the DFT returning the signal to the TF domain. Finally, through a SFFT we resume the

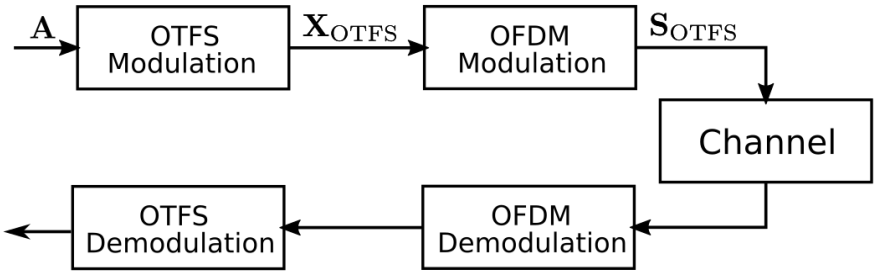

Figure 16 – Block diagram of an OTFS scheme.

symbols transmitted in the delay-Doppler domain for detection. Figure 16 illustrates the complete OTFS system.

The main idea of OTFS is to convert the time-varying channels into time invariant channels in the Doppler-delay domain. It is noticeable that OTFS can be easily implemented by applying pre- and post-coding on the K transmitted OFDM symbols, but this implies a big change in terms of pilot allocation, channel estimation, and equalization. Combined with a specific data detection process in the delay-Doppler domain, the scheme proves to be highly effective at applications that require high data rate and mobility. However, the complexity in the process of compensation of interferences coming from the channel is more complex than the simple equalizer in the TF domain of conventional OFDM.

2.4 Comparative Analysis

In the previous sections we described the transmission process of OFDM, FBMC and OTFS multicarrier systems. In this section we will make a comparative analysis between these three techniques, in addition to the inclusion of the SC-FDMA system in this analysis. The SC-FDMA system is obtained by applying the DFT spreading matrix $\mathbf{W}_L$ to the input of the OFDM modulator and consequently applying the matrix $\mathbf{W}_L^H$ to the receiver after equalization in the frequency domain [60]. The metrics that will be addressed are PAPR and error performance through bit error rate (BER). In terms of OOB emissions, Figure 14 presented in section 2.2.3 makes clear the advantage of FBMC for the other mentioned systems. The filtering process makes us have a better location in the spectrum, significantly reducing OOB emissions.

We begin by analyzing PAPR, whose high value is usually a problem in multicarrier systems. Usually, the evaluation of PAPR is obtained through curves of CCDF (complementary cumulative distribution function). The CCDF curve demonstrates the probability of a signal being above or below a certain power level. Figure 17 presents the CCDF curve for the mentioned systems for $L = 128$, $K = 8$ and 4-QAM/OQAM modulation. Note that for FBMC/OQAM and OFDM the results are practically the same.

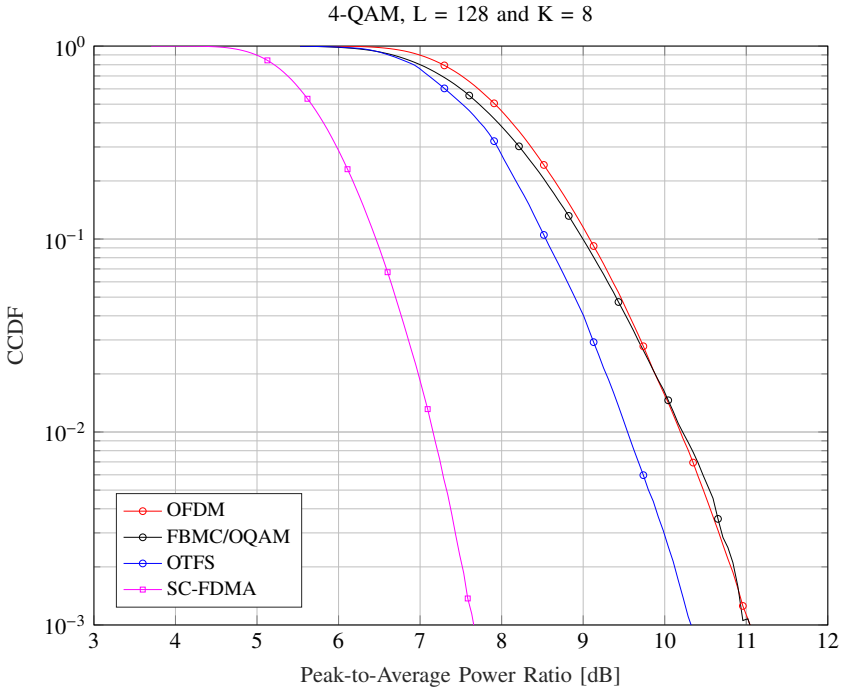

Figure 17 – PAPR comparison between the different systems.

This is expected by the multicarrier nature of these systems, dividing the total bandwidth into $L = 128$ subchannels. However, for OTFS, we see from equation (2.72) that the multicarrier nature remains, but the spectrum is divided only into K sub-channels so that we have a reduction in PAPR. That is, PAPR does not depend on the number of subcarriers (L), but on the number of multicarrier symbols (K) that will be transmitted. Finally, the SC-FDMA technique obtains a low PAPR due to the frequency spreading obtained by the DFT. There is practically the cancellation between this precoding DFT with the IDFT of the OFDM modulator in such a way that a single carrier system is emulated. Thus, it is plausible to obtain this low PAPR.

The performance in terms of BER will be analyzed using the Monte Carlo simulation [61] and consider that the transmitted signal is affected by a Rayleigh fading channel using the ITU-T Vehicular A model described in [62]. Perfect channel estimation is also assumed at the receiver and equalization is based on the minimum mean square error (MMSE) criterion. For all systems this equalizer will be used in the time-frequency domain with only one coefficient per sub-channel which we call MMSE-TF. However, for the OTFS system, the equalizer will be included with the same MMSE criterion, but in the delay-Doppler domain, which we will call MMSE-DD. A more detailed analysis of the equalizers and the structure of the channel used will be carried out in the next chapter. Regarding the modulation used, a QAM constellation is applied for the OFDM, OTFS and SC-FDMA systems, while for the FBMC/OQAM the same constellation, but in the OQAM format, is considered. The summary of the data used for these simulations are presented in the

table 5. Figure 18 shows the BER for 16QAM/OQAM in a non-mobility scenario ($\vartheta = 0$

General parameters			
Total subcarriers (L)	128		
Subcarrier spacing (F)	15 kHz		
Modulation	4-QAM/OQAM and 16-QAM/OQAM		
Channel Model	ITU-T Vehicular A		
Velocity (ϑ)	0 and 300 km/h		
Carrier frequency	2.5 GHz		
Specific parameters			
OFDM, OTFS and SC-FDMA		FBMC/OQAM	
Multicarrier symbols (K)	8	Multicarrier symbols (K')	16
Cyclic prefix length	16		
OFDM FFT size (N)	256	Filter bank FFT size (N)	256

Table 5 – Simulation parameters.

km/h). The performance is practically the same between the OFDM and FBMC/OQAM systems. OTFS and SC-FDMA systems show superior performance due to the spreading of data symbols before transmission. However, it is important to note that OTFS with the MMSE-DD equalizer does not get additional performance in this non-mobility scenario. This is already expected given that the main objective of OTFS is to combat time-varying channels. Figure 19 presents the BER for the same configurations, but now for a scenario with a velocity of 300 km/h. The sensitivity of OFDM, FBMC/OQAM and SC-FDMA systems is effectively observed in this type of scenario. It is also worth mentioning the

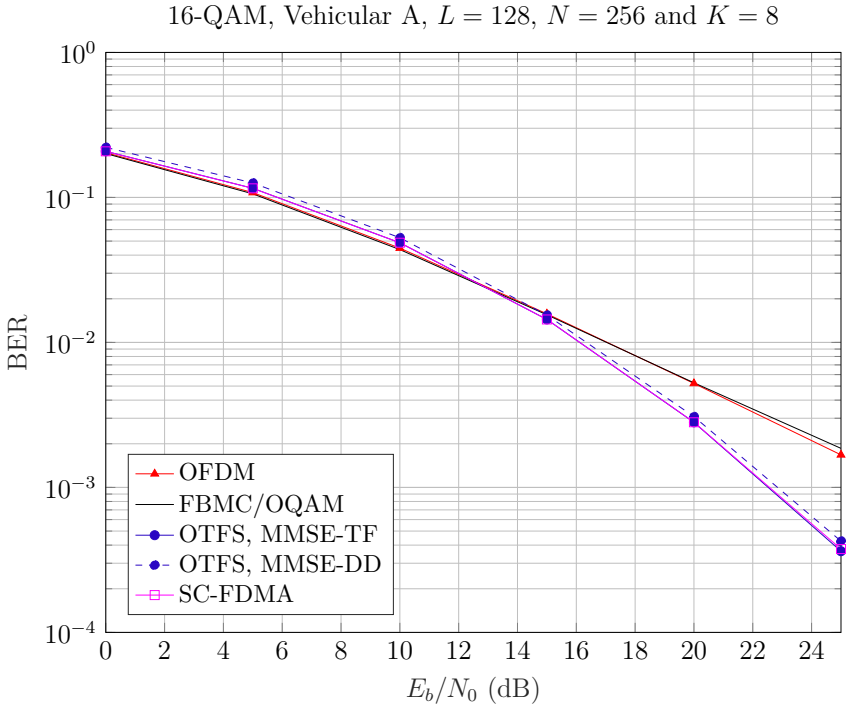

Figure 18 – BER for 16-QAM and a velocity of 0 km/h.

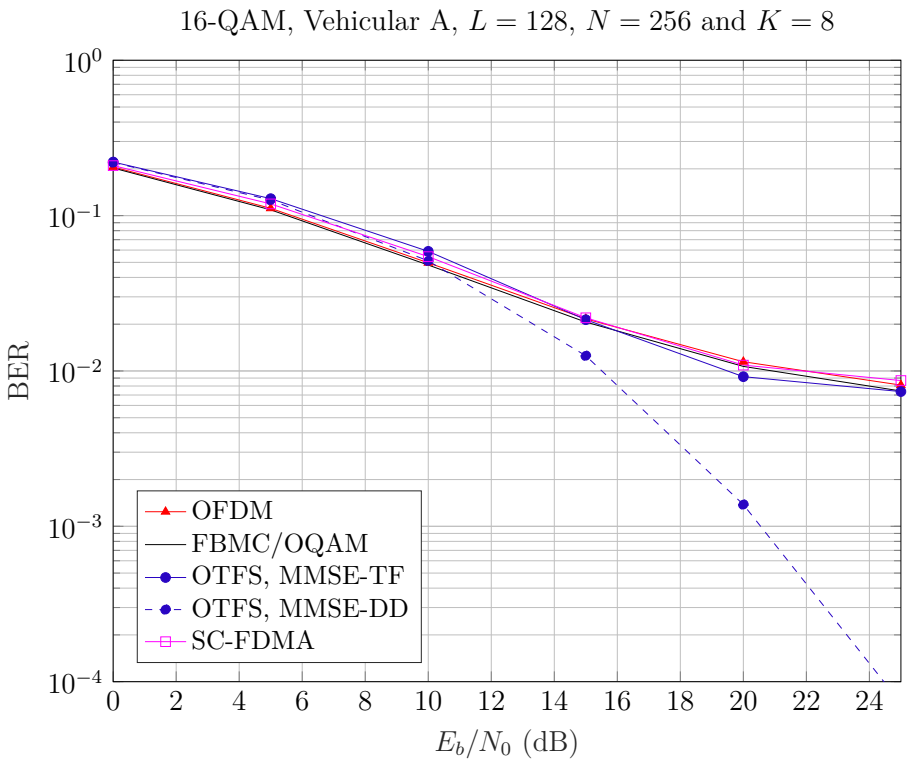

Figure 19 – BER for 16-QAM and a velocity of 300 km/h.

poor performance even for the OTFS in the case of using the MMSE-TF equalizer where the full diversity obtained in the DD domain is not used. Finally, as mentioned, the use of detection techniques in the DD domain such as the MMSE equalizer, brings a high gain in error performance, providing this robustness of OTFS to Doppler spreading. The biggest problem in this type of detection is the complexity of the receivers that are well above the simple MMSE-TF equalizer of OFDM and FBMC/OQAM systems. The discussion of the complexity of the receivers, as well as the systems as a whole, will be addressed in later chapters, since new techniques of transmission and detection of data will be proposed. Figures 20 and 21 present the same scenarios as Figures 18 and 19, however for 4-QAM modulation. The vast majority of conclusions seen for 16QAM have been maintained. The only difference is in the better performance for SC-FDMA and OTFS systems in the high mobility scenario, as illustrated in Figure 21. As expected, the channel interference compensation in the DD domain is more effective.

2.5 Conclusion

OFDM systems aim to combat channel selectivities in order to maintain a high data rate. However, the various new services such as autonomous vehicles, health monitoring, online games and the Internet of Things (IoT) will demand, in addition to very high data rates, very low latency, energy efficiency, better spectrum allocation and robustness to

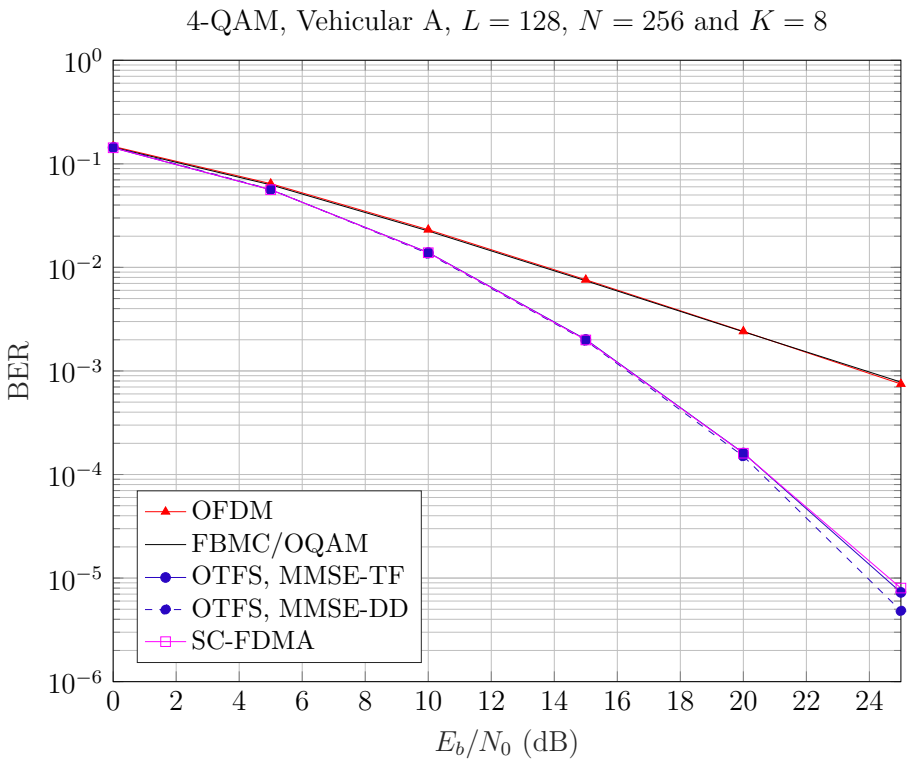

Figure 20 – BER for 4-QAM and a velocity of 0 km/h.

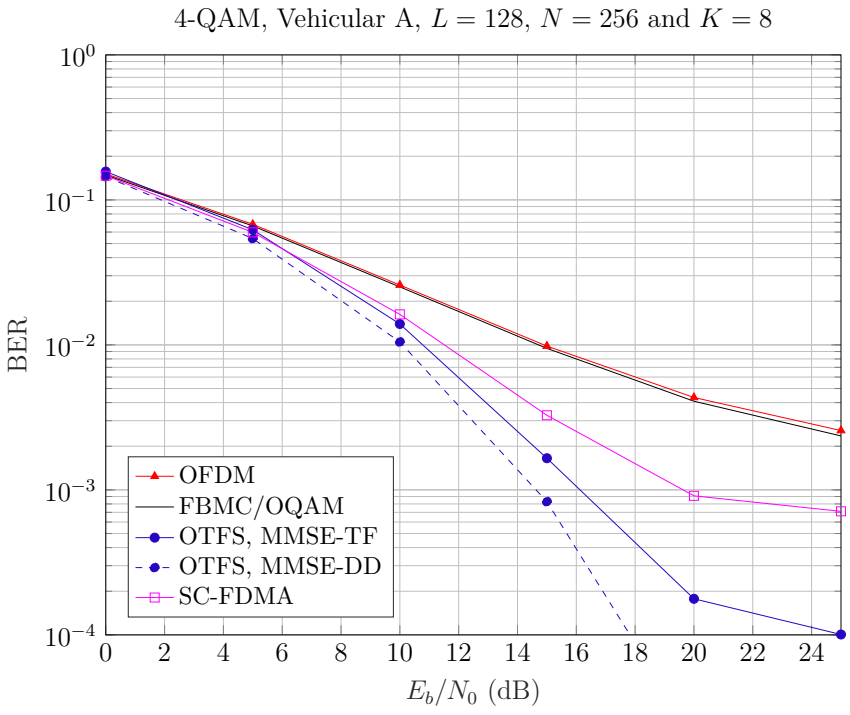

Figure 21 – BER for 4-QAM and a velocity of 300 km/h.

interference. As OFDM is may not be the best choice to satisfy all these physical layer requirements, several waveforms have been introduced as a potential replacement. While the FBMC technique is concerned with improving the spectral localization at the expense

of the loss of complex orthogonality, the OTFS system does not change its spectrum, however, combats time-varying channel interference and maintains lower PAPR than seen in OFDM. A waveform that can encompass most of these features without a considerable increase in computational complexity is needed. We will see in the following chapters some alternative schemes that move in this direction.

3 DFT precoded Filter Bank Scheme

The FBMC/OQAM system provides an improvement in spectral localization over conventional OFDM through the filtering process on each subcarrier. However, this filtering generates imaginary interference and consequently the loss of complex orthogonality. The transmitted symbols are accompanied by interference terms caused by the transmitted data around their neighbors in both the time domain and the frequency domain. For the SISO case, we saw that this can be circumvented by adopting OQAM modulation and restricting the orthogonality to the real field. However, for the MIMO scenario this is not possible, mainly in the channel estimation process. Thus, the biggest challenge for the application of FBMC systems is the restoration of complex orthogonality. Spreading the data symbols over the entire time band or all subcarriers can be used for this purpose. That way, MIMO techniques can be applied directly in FBMC as in OFDM. Recently, a new precoding method based on spreading by a pruned DFT in combination with a scaling operation to compensate for interference imposed by filters was proposed in [38]. This scheme, called Pruned DFT Spread FBMC, presents the advantages of FBMC modulation and SC-FDMA, such as well-located spectrum reducing OOB emissions, PAPR and low latency, in addition to partially restoring complex orthogonality.

In this chapter, we introduce a novel scheme based on the pruned DFT spread FBMC system which does not rely on OQAM modulation, decreasing the system complexity, while maintaining its good PAPR characteristics. The technique called DFT precoded filter bank is developed by spreading symbols in the frequency domain and a data allocation strategy. The main aim is to obtain a filter bank-based waveform with complex orthogonality. We describe the necessary steps for its design as well as possibilities that arise from a more elaborate analysis of the filter bank. Using the matrix notation previously presented with some specific adjustments, we derive the filter interference compensation coefficients, in addition to understanding other details of the system.

3.1 Principles

Figure 22 shows a precoding method to restore the complex orthogonality. It consists in spreading the transmitted symbols in the frequency domain through a Fourier transform and an one-tap scaling stage. The principle of this scheme can be summarized as follows. First, $L/2$ complex symbols are pre-compensated by a scale factor and then pass through an DFT of length L, forming the precoding process to be transmitted by the filter bank. The $L/2$ data symbols are inserted in the first and last $L/4$ positions of the DFT whereas the intermediate values are set to zero. As we will see later, this strategy

is necessary to avoid filter interference in the frequency domain, while the compensation stage avoids filter interference in the time domain. The idea here is now to transmit $L/2$ complex symbols at double rate in order to obtain the maximum transmission capacity as the OFDM and FBMC/OQAM system. In other words, while the FBMC/OQAM system transmits L real data symbols every $T/2$ seconds, in the proposed system the transmission of complex symbols, is made over $L/2$ subcarriers transmitted also every $T/2$ seconds. In conventional FBMC-OQAM, two time-frequency positions are required to transmit a complex-valued data symbol. In the proposed technique, on the other hand, the now complex data symbols no longer belong to a specific time-frequency position, but are spread over several subcarriers (frequency axis). Considering our matrix notation and the representation of symbols in a time-frequency grid, the symbols $\mathbf{x}_k \in \mathbb{C}^{L\times 1}$ transmitted at the k-th time instant via the filter bank are given by

$$\mathbf{x}_k = \mathbf{C}_f \mathbf{a}_k, \tag{3.1}$$

where $\mathbf{a}_k \in \mathbb{C}^{L\times 1}$ now, is the k-th multicarrier symbol containing $L/2$ complex data with unit power derived from a QAM constellation. Such data symbols are positioned according to the previously defined strategy, i.e, $\mathbf{a}_k = [a_{0,k} \ldots, a_{L/4-1,k}, 0, \ldots, 0, a_{L/4,k} \ldots, a_{L/2-1,k}]^T$. The matrix $\mathbf{C}_f \in \mathbb{C}^{L\times L}$ represents the precoding containing the DFT and the filter compensation stage which will be defined next. Note that there is no longer a need for the $\pi/2$ phase rotation factor which is used in the scheme with OQAM modulation, thus removing L real multiplications from both the transmitter and the receiver. As has been said, complex symbols are transmitted and no longer real symbols as in conventional FBMC. For these reasons, there is no longer a need to separate even and odd symbols for transmission via polyphase decomposition. In this way, we will update our $\mathbf{G}$ transmission filter matrix in order to facilitate the analysis in the proposed waveform. Taking into account the transmission of K' multicarrier symbols, we can define the global IDFT matrix $\tilde{\mathbf{W}}^H \in \mathbb{C}^{NK'\times LK'}$ as

$$\tilde{\mathbf{W}}^H = \mathbf{I}_{K'} \otimes \tilde{\mathbf{W}}_N^H, \tag{3.2}$$

where $\otimes$ refers to the Kronecker product which maps $\tilde{\mathbf{W}}_N$ (see equation (2.54)) to the correct K' time positions. Then, the transmitted data is obtained by convolving the IDFT output by the prototype filter impulse response through a Toeplitz filter

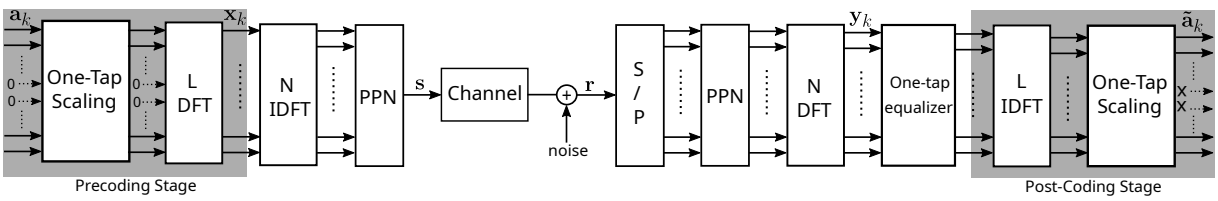

Figure 22 – Block scheme of the DFT precoded filter bank system.

matrix. Let us consider the diagonal matrix $\mathbf{G}_o$ corresponding to the filter coefficients, that is, $\mathbf{G}_o = \text{diag}(\mathbf{g}_o) \in \mathbb{R}^{N/2\times N/2}$ for $o = 0, 1, 2, ..., 2O-1$, where $\mathbf{g}_o$ is given by $\mathbf{g}_o = [g[oN/2], g[oN/2+1], \ldots, g[oN/2+N/2-1]]$. First, let us define the matrix $\dot{\mathbf{G}}_o \in \mathbb{R}^{N/2\times N}$ as follows

$$\dot{\mathbf{G}}_o = \Big[\underbrace{\mathbf{0} \ \ldots \ \mathbf{0}}_{(o \bmod 2) \text{ times}} \quad \mathbf{G}_o \quad \underbrace{\mathbf{0} \ \ldots \ \mathbf{0}}_{1-(o \bmod 2) \text{ times}} \Big] \tag{3.3}$$

where the number of zeros arrays of size $N/2 \times N/2$ around the coefficients array of the filter $\mathbf{G}_o$ depends on the value of o. Thus, the new Toeplitz matrix of the filter $\mathbf{G} \in \mathbb{R}^{ON+(K'-1)N/2\times NK'}$ can be expressed as:

$$\mathbf{G} = \begin{bmatrix} \dot{\mathbf{G}}_0 & \mathbf{0} & \mathbf{0} & \ldots & \mathbf{0} \\ \dot{\mathbf{G}}_1 & \dot{\mathbf{G}}_0 & \mathbf{0} & \ldots & \mathbf{0} \\ \dot{\mathbf{G}}_2 & \dot{\mathbf{G}}_1 & \dot{\mathbf{G}}_0 & \ddots & \vdots \\ \vdots & \dot{\mathbf{G}}_2 & \dot{\mathbf{G}}_1 & \ddots & \mathbf{0} \\ \vdots & \vdots & \dot{\mathbf{G}}_2 & \ddots & \dot{\mathbf{G}}_0 \\ \dot{\mathbf{G}}_{2O-1} & \vdots & \vdots & \ddots & \dot{\mathbf{G}}_1 \\ \mathbf{0} & \dot{\mathbf{G}}_{2O-1} & \ldots & \ddots & \dot{\mathbf{G}}_2 \\ \vdots & \mathbf{0} & \dot{\mathbf{G}}_{2O-1} & \ddots & \vdots \\ \vdots & \vdots & \vdots & \ddots & \vdots \\ \mathbf{0} & \mathbf{0} & \mathbf{0} & \ldots & \dot{\mathbf{G}}_{2O-1} \end{bmatrix}. \tag{3.4}$$

Once the transmission matrix to the precoded symbols has been defined, the output data vector $\mathbf{s}$ of length $M = ON + \frac{N}{2}(K-1)$ from the filter bank is given by

$$\mathbf{s} = \mathbf{G}\tilde{\mathbf{W}}^H\mathbf{x} = \bar{\mathbf{G}}\mathbf{x}, \tag{3.5}$$

where $\bar{\mathbf{G}} = \mathbf{G}\tilde{\mathbf{W}}^H \in \mathbb{C}^{M\times LK'}$ and $\mathbf{x} = \text{vec}([\mathbf{x}_0, \mathbf{x}_1, \ldots, \mathbf{x}_{K'-1}]) \in \mathbb{C}^{LK'\times 1}$. In contrast to the array $\mathbf{G}$ defined in equation (2.56), the structure of the new array $\mathbf{G}$ generates the delay in the symbols every $N/2$ sample transparently. While the first notation is interesting for understanding the process of double rate transmission, the more current description will be more useful for derivations of equalizer, SIR, and SINR expressions.

The transmission of vector $\mathbf{s}$ is affected by AWGN and a doubly-selective channel. This channel can be modeled by a time-variant impulse response $h[\tau, t]$, where τ represents the delay and t the time instant [63]. The time-varying multipath channel is characterized by $h[\tau, t_1] \neq h[\tau, t_2]$ for $t_1 \neq t_2$. Thus, we represent the impulse response of this channel in a time-variant convolution matrix $\mathbf{H} \in \mathbb{C}^{M\times M}$, defined as [56]

$$[\mathbf{H}]_{i,j} = h[i-j, i]. \tag{3.6}$$

Given the transmitted signal $\mathbf{s}$, the received signal $\mathbf{r} \in \mathbb{C}^{M\times 1}$ can be described by

$$\mathbf{r} = \mathbf{H}\mathbf{s} + \mathbf{n}, \tag{3.7}$$

where $\mathbf{n}$ are the AWGN samples with zero mean and power σ_n^2. Similarly, in the receiver the reverse process of the transmitter is done. Initially, the received signal is demodulated by the analysis filter $\mathbf{G}^T$. The demodulated signal $\mathbf{z} \in \mathbb{C}^{NK' \times 1}$ can be expressed as follows:

$$\mathbf{z} = \mathbf{G}^T \mathbf{r} \tag{3.8}$$

To each position in time and frequency, we have $z_{n,k} = [\mathbf{z}]_{n+Nk}$ for $n = 0, 1 \ldots, N-1$. The detected vector $\mathbf{y}_k \in \mathbb{C}^{L \times 1}$ is obtained after the spreading DFT $\tilde{\mathbf{W}}_N$ as

$$\mathbf{y}_k = \tilde{\mathbf{W}}_N \mathbf{z}_k, \tag{3.9}$$

where $\mathbf{z}_k = [z_{0,k}, z_{1,k}, \ldots, z_{N-1,k}] \in \mathbb{C}^{N \times 1}$. To compensate for interferences coming from the channel, a one-tap frequency domain equalization process is performed by $\mathbf{e}_k \in \mathbb{C}^{L \times 1}$, originating $\tilde{\mathbf{x}}_k \in \mathbb{C}^{L \times 1}$ which is expressed as

$$\tilde{\mathbf{x}}_k = \text{diag}\{\mathbf{e}_k\} \mathbf{y}_k. \tag{3.10}$$

Thus, the symbol estimated $\tilde{\mathbf{a}}_k \in \mathbb{C}^{L \times 1}$ is obtained after the post-coding or despreading operation expressed as follows

$$\tilde{\mathbf{a}}_k = \mathbf{C}_f^H \tilde{\mathbf{x}}_k. \tag{3.11}$$

Finally, to obtain the estimated symbols, the $L/2$ intermediate values between the $L/4$ initial and final symbols are discarded, since no data was transmitted at these positions in $\mathbf{a}_k$.

The phase shift component, which guarantees the real orthogonality, is used in FBMC/OQAM (see (2.53)). As mentioned earlier, this is not the case with the proposed transmission structure. Our system simply transmits complex symbols at a data rate that is twice that of an OFDM system during half of the time. In short, while in OFDM L complex symbols are transmitted every T seconds, the proposed technique transmits $L/2$ complex symbols every $T/2$ seconds, totaling L complex symbols in the same period of time than an OFDM system. The idea is to add a pre and post processing in the FBMC system to eliminate the interference from the filter in the time domain and, through a strategy of transmitting the information symbols, eliminate the interference of the filter in the frequency domain. As the filter bank is implemented by a combination of an IFFT and a PPN, in the case of a precoding based on an FFT of the same order as the IFFT of the filter bank, the two would cancel each other out. From these operations, we only have multiplications of the filter coefficients with the data symbols. So, the key point here is to look at the filter coefficients as a flat channel and have a compensation stage of these coefficients similar to an equalizer.

3.2 Restoration of Complex Orthogonality

Bailan-Low's theorem is quite clear about the criteria needed to obtain complex orthogonality. It is impossible to use well-localized band-limited filters in both the time and frequency domains. In this sense, the filtering process will introduce an interference in both domains that need to be eliminated. This is the role of the transmission strategy adopted in conjunction with the precoding matrix $\mathbf{C}_f$ that will be derived in this section. Before that, we will analyze some important issues regarding the prototype filter that can be used so that the proposed technique restores the complex orthogonality

The compensation stage is a multiplicative factor based on the filter-bank structure in order to eliminate interference coefficients. As it is a factor of only one-tap, it is necessary that the interference contribution due to the overlapping of the filter in its neighboring pulses is also of only one coefficient. From (2.32) it is noted that the pulse duration and consequently its number of coefficients is controlled by the overlapping factor O. The term O indicates the number of neighboring symbols the filter will overlapping and cause interference. We can find the optimal value from the analysis of 3 base pulses. Considering $N = L$ without loss of generality, initially we consider that OL is the pulse width and $L/2$ is the pulse width selected for transmission. The idea is to avoid replicas with in 2 consecutive pulses since we transmit every $L/2$. Since the selected pulse starts at a time $OL/2 - L/4$, the complete pulse ends at OL; since we spread the symbols on a L-point DFT, we must have

$$\begin{aligned} OL - \left(\frac{OL}{2} - \frac{L}{4}\right) &\leq L \\ O + \frac{1}{2} &\leq 2 \\ O &\leq \frac{3}{2} \end{aligned} \tag{3.12}$$

Therefore, we deduce that the overlapping factor should not be greater than $O = 1.5$ to avoid a large interference between the symbols in time. Thus, the interference induced by the filter is only one coefficient per subcarrier. In this way, each symbol transmitted within a window of length $L/2$ will be multiplied by the sample value of a single pulse at each time instant. Figure 23 illustrates this approach.

Note that for $O = 1.5$, the start of the third adjacent pulse is at the limit position, so it is interfering with only one pulse and, consequently, such interference is of only one coefficient. However, for $O = 2$, it can be seen that the third pulse starts to interfere with the first pulse, giving rise to an interference of more than one coefficient. At first this limitation may seem like a problem. However, with current concerns on systems with low latencies, a smaller filter is of paramount importance. There are also several studies on precoded and conventional FBMC versions applying filters with $O = 1$. Considering then

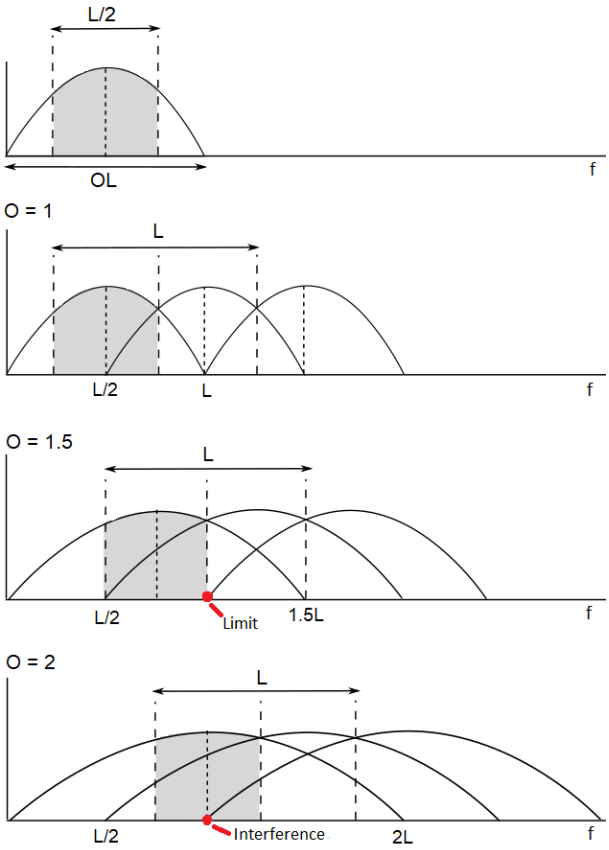

Figure 23 – Limitation of the overlap factor to 1.5.

the use of a prototype filter within this reality, the objective now is to find the coefficients of the compensation stage that eliminates such interference.

To obtain the derivation of the precoding operation performed by the matrix $\mathbf{C}_f$, let us consider the definition of $\tilde{\mathbf{G}}$, which corresponds to the transmission of a single FBMC symbol ($K' = 1$), expressed by $\tilde{\mathbf{G}} = [\mathbf{G}_0; \mathbf{G}_1; ....; \mathbf{G}_{2O-1}] \in \mathbb{R}^{ON \times N}$. In order to cancel the imaginary interference, the precoding matrix must be chosen so that the following condition is attended:

$$\mathbf{C}_f^H \tilde{\mathbf{W}}_N \tilde{\mathbf{G}}^T \tilde{\mathbf{G}} \tilde{\mathbf{W}}_N^H \mathbf{C}_f = \mathbf{F}, \tag{3.13}$$

where $\mathbf{F} \in \mathbb{R}^{L \times L}$ is a matrix with unit values in the first and last $L/4$ positions of its main diagonal and zeros elsewhere. We recall that the goal of this precoding operation is to restore complex orthogonality. From the matrix notation of the filter bank presented, we can now define $\mathbf{C}_f$ to eliminate interference from the filtering process. The idea is that this $\mathbf{C}_f$ matrix represents a spreading in frequency, combined with a filter compensation stage in order to eliminate the interference caused by the filter overlapping on adjacent pulses. So, to restore complex orthogonality, $\mathbf{C}_f$ can be expressed as follows

$$\mathbf{C}_f = \mathbf{W}_L \text{diag}\{\tilde{\mathbf{b}}\}, \tag{3.14}$$

where $\tilde{\mathbf{b}} \in \mathbb{R}^{L\times 1}$ is the scale factor with $L/2$ compensation coefficients in the positions according to the transmission strategy defined for $\mathbf{a}_k$; its $L/2$ intermediate samples are equal to zero. Replacing (3.14) in (3.13), the $\tilde{l}$-th position of the vector $\tilde{\mathbf{b}}$ can be expressed by

$$[\tilde{\mathbf{b}}]_{\tilde{l}} = \begin{cases} \sqrt{\frac{1}{[\tilde{\mathbf{c}}]_{\tilde{l}}}}, & \text{for } \tilde{l} = \left[0, \ldots, \frac{L}{4}-1; L-\frac{L}{4}-1, \ldots, L-1\right] \\ 0, & \text{otherwise} \end{cases} \tag{3.15}$$

with

$$\tilde{\mathbf{c}} \;=\; \text{diag}\{\mathbf{W}_L^H \tilde{\mathbf{W}}_N \tilde{\mathbf{G}}^T \tilde{\mathbf{G}} \tilde{\mathbf{W}}_N^H \mathbf{W}_L\}. \tag{3.16}$$

Due to the product $\tilde{\mathbf{G}}^T\tilde{\mathbf{G}}$, it can be seen that this compensation coefficient depends only on the filter response and is constant over time. Thus, this coefficient can be applied by a point-to-point multiplication on all active subcarriers. As the filtering process is done at both the transmitter and the receiver, the compensation must be done on both sides. This eliminates the intrinsic interference of the filter in the time domain. In the frequency domain, interference is eliminated through the imposed transmission strategy. Figure 24 shows the reason for the transmission strategy used and how $[\tilde{\mathbf{c}}]_{\tilde{l}}$ depends on the position $\tilde{l}$. Note that half of the symbols in each subcarrier are amplified ($[\tilde{\mathbf{c}}]_{\tilde{l}} > 1$), while the rest are attenuated. Thus, the proposed solution is to transmit where $[\tilde{\mathbf{c}}]_{\tilde{l}} > 1$. Consequently, the data symbols are inserted in the corresponding first and last $L/4$ positions of the DFT. The transmission rate L is maintained by doubling the rate. Therefore, this strategy combined with precoding allows us to use QAM modulation. We will see later in this work that this allows to relax the restrictions of the filter to obtain several advantages. On the

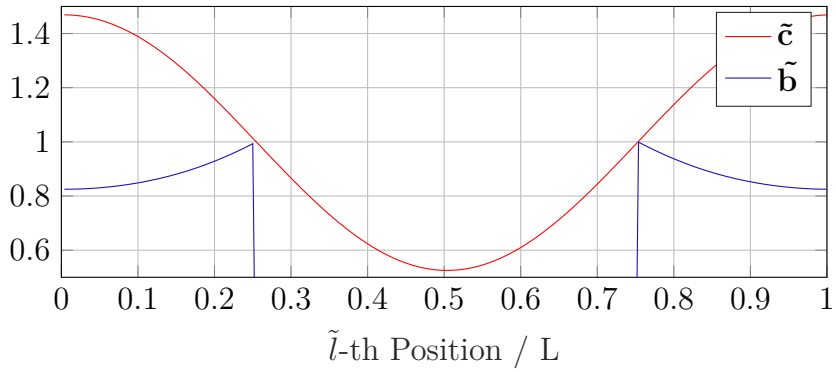

Figure 24 – The proposed transmission idea is to transmit in the $L/2$ larger elements of $\tilde{\mathbf{c}}$.

receiver side we only consider the positions in which the transmitted symbol is retrieved.

The idea of precoding is to obtain $[\text{diag}\{\mathbf{C}_f^H \tilde{\mathbf{W}}_N \tilde{\mathbf{G}}^T \tilde{\mathbf{G}} \tilde{\mathbf{W}}_N^H \mathbf{C}_f\}]_{\tilde{l}} \approx 1$, that is, to restore the complex orthogonality, differently from regular FBMC where only real orthogonality is present. From our matrix notation, we can clearly observe the cancellation of filter interference by the matrix of pre- and post-coding $\mathbf{C}_f$. Note that if the system is

sampled critically, i.e. $L = N$, and the overlapping factor is 1.5, we would have cancellation between the precoding DFT and the filter bank IDFT, that is, $\mathbf{W}_L^H \mathbf{W}_L = \mathbf{I}_L$. Thus, the equation (3.16) could be rewritten by $\tilde{\mathbf{c}} = \text{diag}\{\tilde{\mathbf{G}}^T \tilde{\mathbf{G}}\}$. Basically, we would have a single-carrier system with $\mathbf{a}_k = \mathbf{y}_k$ and no spectral localization advantages due to filter loss, as the precoding perfectly equalizes the prototype filter. For example, we consider $N = L = 4$ and $K' = 1$ where we can exchange $\mathbf{a}_k$ for just $\mathbf{a}$. Initially we set $O = 2$ so the base filter with length $OL = 8$, $\mathbf{g}_o = [g_0, g_1, \ldots, g_7]$. Truncating this pulse to get $O = 1.5$, we zero the first and last sample of the filter. From this we calculate the compensation vector $\tilde{\mathbf{c}}$ as follows

$$\begin{aligned} \tilde{\mathbf{c}} &= \text{diag}\{\tilde{\mathbf{G}}^T \tilde{\mathbf{G}}\} \\ &= [g_4^2, g_1^2 + g_5^2, g_2^2 + g_6^2, g_3^2] \end{aligned} \tag{3.17}$$

Using the transmission strategy, the vector of transmitted symbols is given by $\mathbf{a} = [a_0, 0, 0, a_1]$. Thus, applying the IDFT that composes the filter bank to the already pre-coded data, we have the vector $\mathbf{d} \in \mathbb{C}^{N \times 1}$ expressed by

$$\begin{aligned} \mathbf{d} &= \mathbf{W}_N^H \mathbf{x}_k \\ &= \mathbf{W}_N^H \mathbf{C}_f \mathbf{a} \\ &= \text{diag}\{\tilde{\mathbf{b}}\}\mathbf{a} \\ &= \left[\frac{a_o}{g_4}, 0, 0, \frac{a_1}{g_3}\right] \end{aligned} \tag{3.18}$$

Finally, passing the sequence through the filter through the array $\tilde{\mathbf{G}}$ we get

$$\mathbf{s} = \tilde{\mathbf{G}}\mathbf{d} \tag{3.19}$$

$$= \begin{bmatrix} 0 & 0 & 0 & 0 \\ 0 & g_1 & 0 & 0 \\ 0 & 0 & g_2 & 0 \\ 0 & 0 & 0 & g_3 \\ g_4 & 0 & 0 & 0 \\ 0 & g_5 & 0 & 0 \\ 0 & 0 & g_6 & 0 \\ 0 & 0 & 0 & 0 \end{bmatrix} \left[\frac{a_o}{g_4}, 0, 0, \frac{a_1}{g_3}\right] = \begin{bmatrix} 0 \\ 0 \\ 0 \\ \frac{a_1 g_3}{g_3} \\ \frac{a_0 g_4}{g_4} \\ 0 \\ 0 \\ 0 \end{bmatrix}. \tag{3.20}$$

At the input of the FBMC demodulator at the receiver (based on that we have an ideal channel), we would have the QAM constellation of the transmitted symbols. In this sense, it is necessary that the system does not operate critically sampled ($L = N$) for the filtering process to be applied. Therefore, the IDFT length, N, must be $N > L$ so that the precoding stage DFT does not cancel out with the filter bank IDFT. However, in practice the systems never operate at a critical sampling rate ($N = L$), that is, the size of the DFT will always be greater than the number of active subcarriers [56]. The remaining

DFT points are set to zero. This has many important implications, especially for channel estimation.

For an overlapping factor equal to 1.5, that is, only one filter coefficient contributes to the interference, it is possible to compensate for this filter interference and recover the transmitted complex signal. Thus, equalization becomes simpler, as the symbols are now free from filter interference and one can focus on minimizing the effects introduced by the communication channel.

3.3 One-tap Equalizer in Frequency Domain

Generally, the equalization performed by $\mathbf{e}_k = [e_{0,k}, \ldots, e_{L-1,k}]$ (as detailed in (5.3)) uses criteria such as MMSE or zero forcing (ZF) to compensate for channel interference. Despite its simplicity, the ZF equalizer can present a very deteriorated performance due to the noise amplification effect. Unlike the ZF, the equalizer based on the MSE criterion takes into account channel and noise statistics. In this way, noise amplification is reduced. To find the equalizer coefficients, we first define the channel coefficients. One can represent such coefficients in the frequency domain from the matrix product $\bar{\mathbf{G}}^H \mathbf{H} \bar{\mathbf{G}}$. In many practical scenarios, the off-diagonal elements of $\bar{\mathbf{G}}^H \mathbf{H} \bar{\mathbf{G}}$ are so small that they are dominated by noise [38]. In this way, it is possible to represent the one-tap channel $\mathbf{h} \in \mathbb{C}^{LK' \times 1}$ by

$$\mathbf{h} = \operatorname{diag}\left\{\bar{\mathbf{G}}^H \mathbf{H} \bar{\mathbf{G}}\right\}. \tag{3.21}$$

Considering each position in time and frequency, we have $h_{l,k}$ by

$$h_{l,k} = [\mathbf{h}]_{l+L(k-1)}. \tag{3.22}$$

From this definition, a simple one-tap ZF equalizer is provided by $(1/h_{l,k})$. To obtain a balanced solution between noise and channel interference, we employ a MMSE equalizer, which can be expressed as follows:

$$e_{l,k} = \frac{h_{l,k}^*}{|h_{l,k}|^2 + \sigma_n^2} \frac{1}{\frac{1}{L}\sum_{l=0}^{L-1} \frac{1}{1+\frac{\sigma_n^2}{|h_{l,k}|^2}}}. \tag{3.23}$$

The first term of the expression (3.23) represents the conventional one-tap MMSE equalizer while the second term is a normalization factor that guarantees the unbiased of the estimated symbols. If delay spread and Doppler spread are low enough, this one-tap equalizer is sufficient to compensate for channel interference.

3.4 System Evaluation

Even though OFDM has all the restrictions mentioned in this work, its design is simple via Fourier transform. It is necessary to obtain a waveform that solves the

problems inherent to the OFDM system, however, without much higher complexity. Table 8 presents a comparison of transmission schemes in terms of computational complexity of the transmitter. For the OFDM and SC-FDMA technique, the cyclic prefix was disregarded. If we ignore the channel equalization process, the table also represents the complexity of the receiver. We consider the calculations for transmitting a block consisting of K

Scheme	Complexity
OFDM	$KL\log L$
FBMC/OQAM	$K'\left(L+N\log N+ON\right)$
SC-FDMA	$K\left(L\log L+N\log N\right)$
DFT Precoded FB	$K'\left(\frac{L}{2}+L\log(L/2)+N\log N+ON\right)$
OTFS	$KL\log(L)+LK\log(K)+KL\log L$

Table 6 – Computational complexity of transmission scheme.

(OFDM kernel) or $K'=2K$ (FBMC kernel) multicarrier symbols each consisting of L subcarriers. As mentioned in the section 2.1.1, the DFT can be implemented efficiently by an FFT, where the number of complex multiplications for an n-point FFT is $n\log n$. Thus, for OFDM we have $L\log L$ multiplications referring to the IFFT that performs the modulation. For K multicarrier symbols, then we have $KL\log L$ multiplications. In the FBMC/OQAM the term $N\log N$ corresponds to the IFFT of the filter bank and ON is the number of multiplications with respect to the prototype filter. The term L represents the phase factor that generates the rotation of $\pi/2$ in real data symbols. By double rate transmission, twice as many symbols are needed in time to maintain the same OFDM baud rate, so each term specified above is multiplied by K'. For SC-FDMA, the IFFT of $N>L$ points is maintained in order to avoid critical sampling. Add to this IFFT, the FFT of L points from the precoding (spreading) which requires $KL\log L$ multiplications. For the case of DFT Precoded system we have K' multicarrier symbols each with $L/2$ subcarriers. Thus, for each symbol, $K'(L/2)$ multiplications referring to the compensation stage are required. The filter bank is implemented via IFFT combined with PPN from $K'(N\log N+ON)$ multiplications. Additionally we have $K'(L\log(L/2))$ multiplications referring to the spread of the $L/2$ complex data symbols in the frequency from an FFT. For the OTFS, the ISFFT can be implemented from the set of an IFFT of K points and an FFT of L points, then applying $KL\log L+LK\log K$ multiplications. Finally, the term $KL\log K$ represents the transmission of data symbols already encoded by the OFDM modulator.

By comparing the complexity described in Table 8, the computational complexity of our transmission scheme is approximately two times greater than in SC-FDMA considering $O=1.5$ and $N=2L$. Basically, the computational complexity of the proposed technique

concerning the SC-FDMA at the transmitter can be approximated by

$$\frac{K'(\frac{L}{2} + L\log\frac{L}{2} + N\log N + ON)}{K(L\log L + N\log N)} \approx 2 \tag{3.24}$$

One of the benefits of frequency spreading via DFT in a multicarrier system is the effective reduction of PAPR. Figure 25 shows the CCDF of the PAPR for transmitted symbols using 4-QAM. Note that the DFT precoded has the same PAPR characteristics

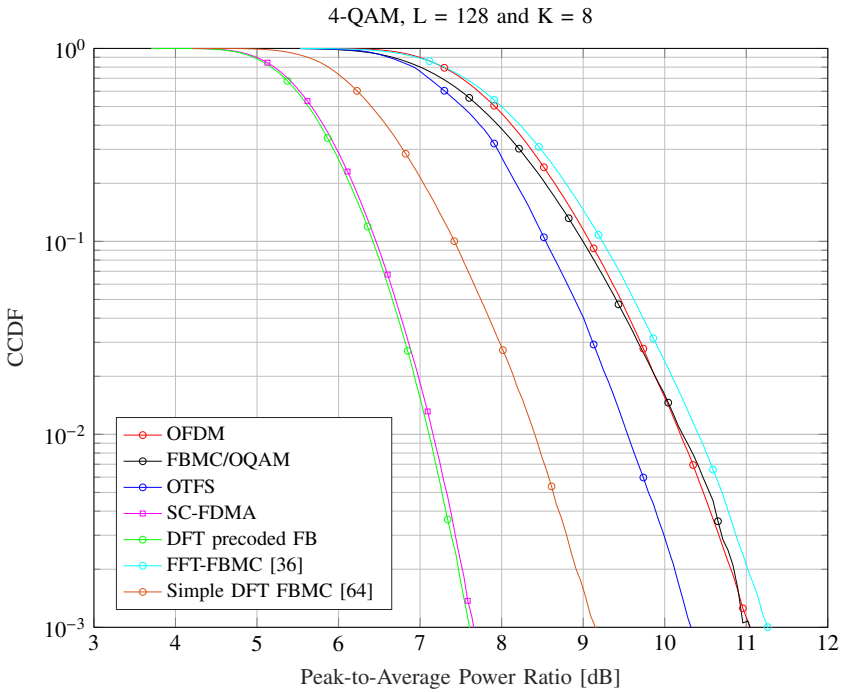

Figure 25 – CCDF from PAPR for the schemes discussed.

obtained by the SC-FDMA system. This result is intuitive, since the scheme uses frequency spreading via DFT. Thus, it is expected that some PAPR reduction is intrinsically achieved in comparison with schemes that do not use such precoding. The proposed scheme also outperforms other frequency spreading techniques for FBMC. Compared with the scheme proposed by Na and Choi in [64] where frequency spreading with an optimal phase pattern is employed, it can be seen that the proposed scheme obtains better performance.

The inclusion of the filtering process, which improves the spectral confinement as shown in Figure 26, is one of the great advantages of the proposed system. The influence of the side lobes can easily be observed in the frequency domain, as well as the advantage, in OOB terms, of using a filter well located in the frequency. For the correct detection of transmitted symbols, we saw that a prototype filter with $O \leq 1.5$ is necessary. In this sense, it is interesting to design a filter with this feature that adds good location in time and frequency. We use a truncated version of the Hermite prototype filter to obtain a pulse with the characteristic of $O = 1.5$. However, it is worth mentioning that it is possible to optimize the prototype filter instead of using a truncated version. It should

also be noted that the higher the overlapping factor, the better the spectral location. For FBMC/OQAM, the overlapping factor value of the prototype filter can be less constrained. The PHYDYAS filter proposed in [16] has a higher overlapping factor ($O = 4$), which consequently achieves a better spectral localization. However, even using a filter within the complex orthogonality limit, it is noted that the OOB emissions of the proposed scheme are comparable to FBMC/OQAM transmissions and much better than those of OFDM and OTFS.

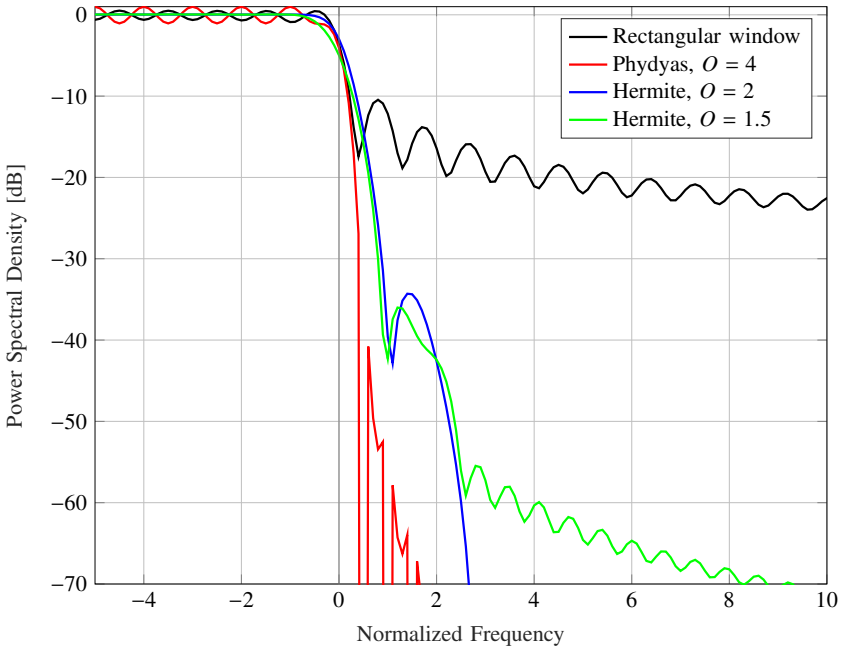

Figure 26 – Power Spectral Density comparison between filters.

The proposed system was also evaluated in terms of bit error rate in scenarios with and without mobility. For situations with mobility, the delay taps experiences a Doppler-shift. Each delay tap is generated based on the Jakes model, using the formula $\upsilon_i = f_d \cos(\theta_i)$ [65]. The term υ_i is the Doppler-shift tap for i-th path, while θ_i is uniformly distributed from 0 to 2π and f_d is the maximum Doppler-shift given by.

$$f_d = \frac{f_c \vartheta}{c}, \tag{3.25}$$

where f_c is the carrier frequency, ϑ is the specified velocity, and c is the velocity of light. For the simulations, the same parameters indicated in the Table 5 of the section 2.4 were used. Again, we consider the transmission is affected by a Rayleigh fading channel using the ITU-T Vehicular A model and perfect channel estimation is assumed at the receiver. The MMSE-TF one-tap equalizer is considered for all schemes. For OTFS the MMSE-DD equalizer is also illustrated. Figures 27 and 28 illustrate the error performance of the proposed system for 16-QAM modulation without and with mobility respectively. For the mobility situation, a velocity of 300 km/h was considered. Note that in the

scenario without mobility, the proposed system presents the same performance seen in the SC-FDMA and OTFS systems. Such performance is superior to that seen by the

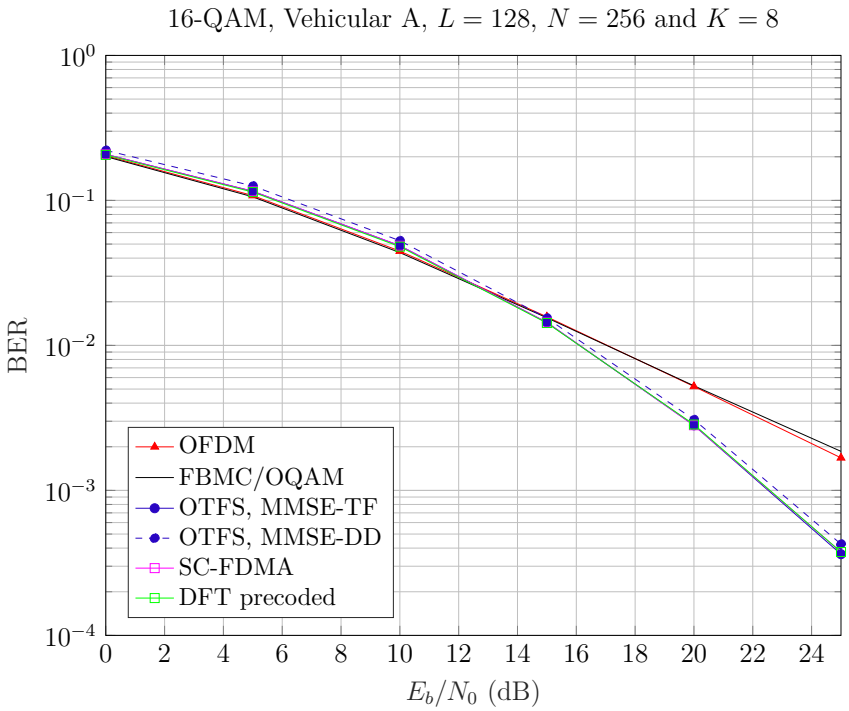

Figure 27 – BER for 16-QAM and a velocity of 0 km/h.

OFDM and FBMC/OQAM techniques in the described scenario. In the situation where there is mobility, it is observed that the proposed system obtains a slight robustness in order to obtain a slightly higher error performance than that seen in SC-FDMA. Another important point is that this performance is also superior to that seen in OTFS with the MMSE-TF equalizer. The main objective of OTFS is to minimize the effects of Doppler spreading, however, for this it is necessary to peform a detection in the DD domain to obtain the maximum possible diversity. Figures 29 and 30 present the same scenarios seen in the last two figures, however, now for a 4-QAM modulation. The BER results for this situation remain unchanged, except in the case of mobility where the OTFS with the MMSE-TF equalizer has better performance.

3.5 Conclusion

The loss of complex orthogonality is the main challenge to be overcome in FBMC/OQAM. The imaginary interference, inherent in the system itself, is approximately nullified by the condition imposed by equation (3.13), restoring the complex orthogonality. Therefore, the proposed system allows the transmission of complex symbols together with MIMO techniques, which are not feasible using conventional FBMC/OQAM. The proposed system combines the filtering characteristics of FBMC with the frequency

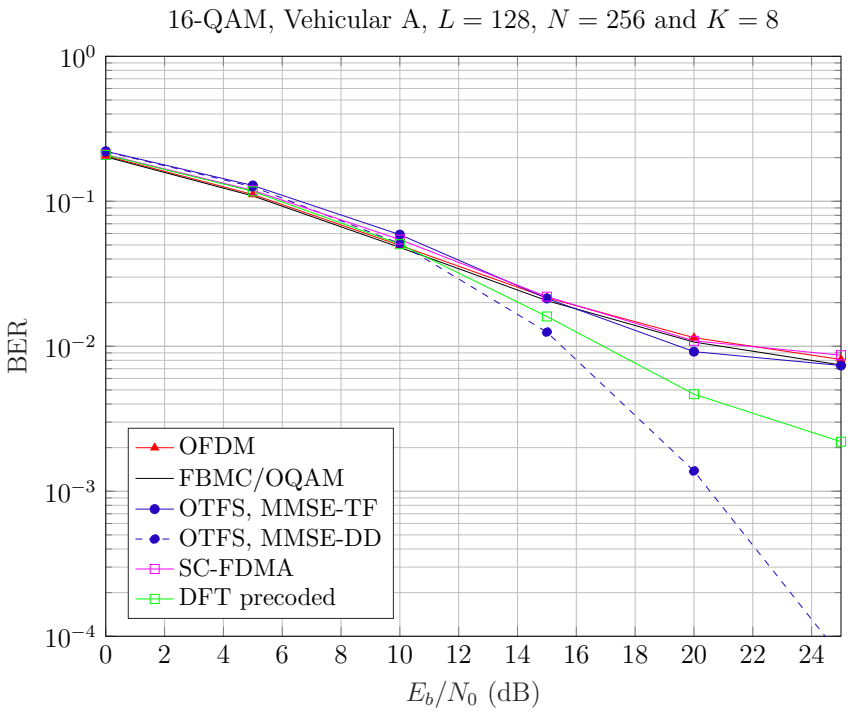

Figure 28 – BER for 16-QAM and a velocity of 300 km/h.

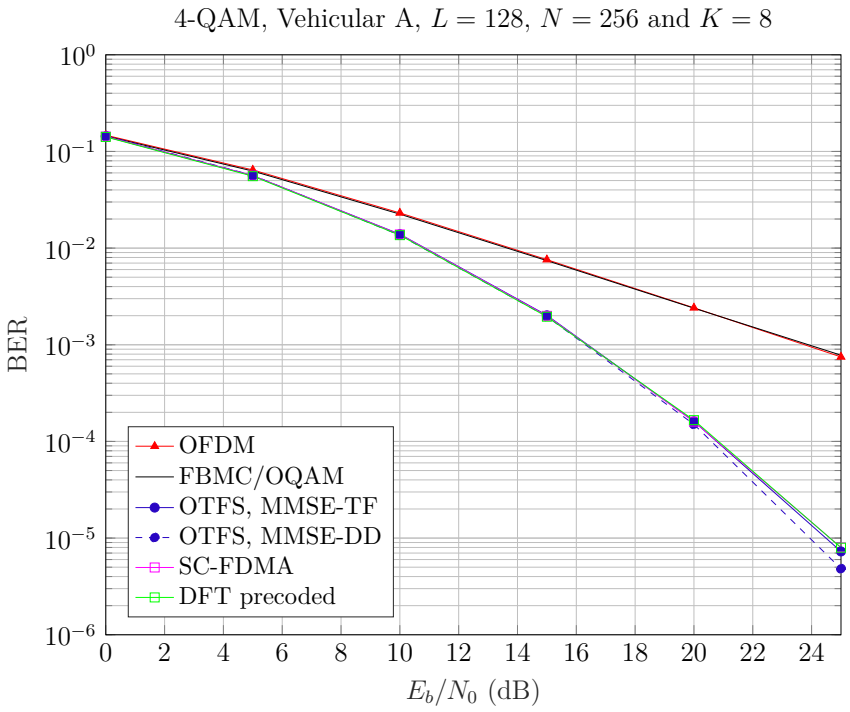

Figure 29 – BER for 4-QAM and a velocity of 0 km/h.

spreading characteristic of SC-FDMA. Thus, a waveform without CP is obtained, with complex orthogonality, low PAPR and good spectral localization. Furthermore, a slight robustness to doubly dispersive channels is perceived. This is all possible from symbol spreading via DFT combined with a filter compensation stage to eliminate imaginary

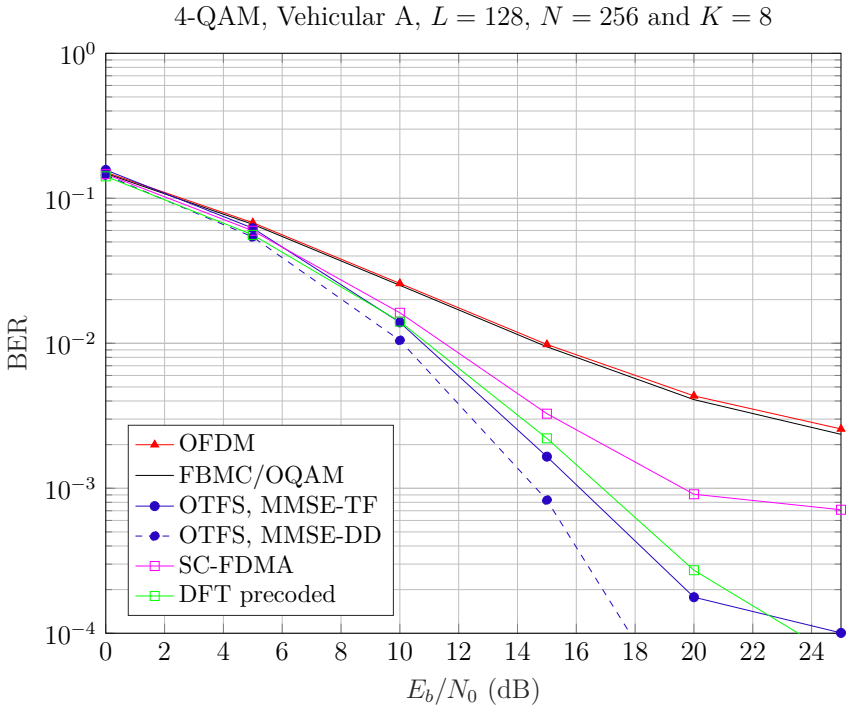

Figure 30 – BER for 4-QAM and a velocity of 300 km/h.

interference in the time domain. Parallel to this, data is introduced at specific positions on the DFT in order to eliminate imaginary interference in the frequency domain. It applies complex data symbols to half of the bins of this DFT and transmits them via a filter bank operating at double rate. For all this to be possible, it is necessary to use a prototype filter with an overlapping factor less than or equal to 1.5. If the overlapping value is greater than 1.5, interference will appear and the precoding can no longer eliminate it and more robust reception techniques are needed for better symbol detection. From the simulation results, it can be seen that a one-tap equalizer presents a good performance in compensating the channel interference, if the delay propagation and Dopler spreading are sufficiently low. In practice this type of scenario is quite common so that the interference induced by the channel is dominated by noise [57]. However, situations with high velocity can significantly decrease performance and more robust receivers are also required. It is worth mentioning that in the transmission structure shown in Figure 22 the symbols are detected in the time domain, in exactly the same way as in SC-FDMA systems. An important feature in SC-FDMA systems is that equalizers can be implemented via decision feedback in an iterative way. In the next chapter, we discuss the design of these equalizers and their impact on the performance of the proposed system. The readjustment and structuring of this equalizer to the precoded scheme can be extremely useful and give an additional performance gain in the system. We will also discuss another type of iterative receiver that aims to cancel out interference from both the channel and the filter. We will analyze both receivers in different scenarios even using multiple antennas in reception.

4 Iterative receivers for interference cancellation

The effect of channel interference can be reduced by proper signal processing methods on the receiver side. When the channels are well behaved and do not have deep spectral attenuation, the performance of the one-tap linear equalizers presented above is satisfactory. On the other hand, channels that induce severe ISI, such as those with deep spectral attenuation, have a frequency response that cannot be inverted in any way. Added to this is the fact that the filter bank based system does not use cyclic prefix, so that in highly dispersive channels, the system will not work properly with the one-tap equalizer, especially at high SNR values. Thus, in general, it can be said that linear equalization techniques are not suitable to compensate for channels that cause strong frequency-selective fading in the transmitted signal. To combat the distortions caused by this type of channel, non-linear equalizers/receivers are often used. Among the non-linear equalization techniques, the most used is decision feedback equalizer (DFE), as it is simple to implement and has a good performance [66]. The main disadvantage of DFE is the error propagation effect for channels with low SNR. Another type of receiver to combat such interference are those based on interference canceling [67]. In this chapter we will see these two types of receivers in iterative format in order to obtain better performance in highly dispersive scenarios and also propose the use of filter overlapping factors above 1.5 to obtain better spectral localization.

4.1 Iterative-Block Decision Feedback Equalizer

Linear equalization based on the MMSE criterion was considered in the DFT precoded system, where we observed that, with this equalization scheme, the error performance of this system presents only a slight robustness to highly time-dispersive channels. Decision feedback equalizers are a better performing alternative to linear equalizers. They are composed of two filters: a feedforward (FF) filter and a feedback filter. In general, the feedforward filter is a linear equalizer that allows for the compensation of the ISI caused by the pre-cursor components of the channel impulse response. On the other hand, the feedback filter compensates for the ISI caused by the post-cursor components [54]. Thus, its performance becomes superior to that obtained with linear techniques due to its ability to cancel the post-cursor ISI using previously detected symbols. However, unlike a linear equalizer, if a decision error occurs, the DFE equalizer initiates an error propagation event, leading to unreliable detections and error bursts. The error propagation event ends when the decisions that are fed to the FB filter become correct. Thus, an effective channel

interference compensation by the forward filter is important to obtain reliable estimates so that the feedback can eliminate the residual ISI.

The structure of the DFE equalizer can be hybrid, using the FF in the frequency domain and the feedback filter in the time domain or both filters can be carried out in the frequency domain. This last structure can be implemented iteratively and efficiently, leading to the well-known iterative block decision feedback equalizer (IB-DFE) scheme. As this equalizer strongly compensates for channel interference, it is possible to increase the filter overlapping factor in some situations without significant performance loss, even if it does not resolve filter interference. Figure 31 presents the IB-DFE adapted for the DFT precoded system. In a first moment, the symbols received in the serial format,

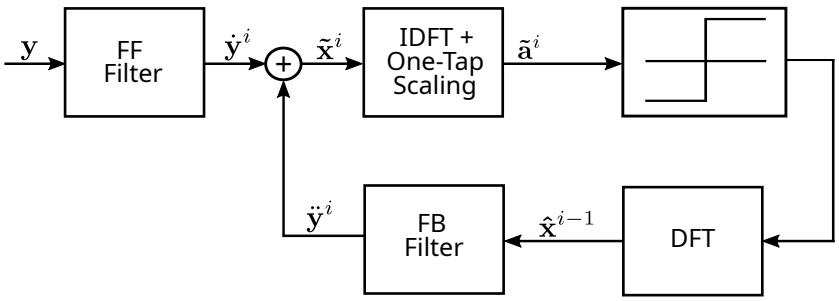

Figure 31 – Block scheme of the IB-DFE receiver.

that is, $\mathbf{y} = \text{vec}([\mathbf{y}_0, \mathbf{y}_1, \ldots, \mathbf{y}_{K'-1}]) \in \mathbb{C}^{LK' \times 1}$, pass through the MMSE equalizer and the post-coding process (IDFT + compensation stage) of the system is carried out. After post-coding, the symbols are detected and returned to the frequency domain by an DFT in an iterative process. In this process, the symbols are filtered by a feedback filter in order to eliminate residual interference. Thus, the symbol estimate $\tilde{\mathbf{x}}^i$ for the i-th iteration is formed by

$$\tilde{\mathbf{x}}^i = \dot{\mathbf{y}}^i + \ddot{\mathbf{y}}^i, \tag{4.1}$$

where $\dot{\mathbf{y}}^i \in \mathbb{C}^{LK' \times 1}$ is the output of the feedforward filter in the i-th iteration and is given by

$$\dot{\mathbf{y}}^i = \mathbf{P}^{i,H}\mathbf{y}, \tag{4.2}$$

with $\mathbf{P}^{i,H} \in \mathbb{C}^{LK' \times LK'}$ corresponding to the feedforward filter that aims to maximize the SINR of the detected symbols at each iteration. The vector $\ddot{\mathbf{y}}^i \in \mathbb{C}^{LK' \times 1}$ is the output of the feedback filter, and it can be expressed as

$$\ddot{\mathbf{y}}^i = \mathbf{Q}^{i,H}\hat{\mathbf{x}}^{i-1}, \tag{4.3}$$

where $\mathbf{Q}^{i,H} \in \mathbb{C}^{LK' \times LK'}$ is the matrix corresponding to the feedback filter and $\hat{\mathbf{x}}^{i-1} \in \mathbb{C}^{LK' \times 1}$ is the frequency domain estimated vector after symbol decision. The role of this feedback

filter is the removal of the residual ISI. Basically, estimated symbols are applied as feedback to improve reliability at each iteration. Let us define a matrix for the one-tap channel coefficients $\mathbf{h}$ as $\overline{\mathbf{H}} = \text{diag}\{\mathbf{h}\} \in \mathbb{C}^{LK' \times LK'}$. Thus, to obtain the optimal coefficients of both filters for each iteration, we minimize the mean squared error (MSE) conditioned to $\overline{\mathbf{H}}$, as follows:

$$\text{MSE}^i = \quad E[||\mathbf{P}^i\mathbf{y} + \mathbf{Q}^i\hat{\mathbf{x}}^{i-1} - \mathbf{a}||^2], \tag{4.4}$$

where $\mathbf{a} = \text{vec}([\mathbf{a}_1, \mathbf{a}_2, \ldots, \mathbf{a}_{K'-1}]) \in \mathbb{C}^{LK' \times 1}$. Note that in the first iteration, when $\mathbf{Q}^1 = 0$, the FF equalizer coefficients, $\mathbf{P}^1$, are independent of decisions. Considering that at the receiver the channel is estimated correctly, the probability of the decisions being correct are high, as long as the SNR is not low. In other words, the error propagation effect will be mainly due to noise and not to ISI. As the iteration is performed, the equalizer should perform better. As an accurate estimation of the correlation matrices is a complex process [66] and considering a good performance of the FF filter, it is considered, from now on as in [68], that the feedback decisions are correct. With this assumption, we have optimal feedback after the first iteration and the FF filter becomes a matched filter with the channel [69]. Thus, by imposing the constraint that the feedback filter removes the ISI but not the desired symbol, by minimizing the MSE expressed by (4.4) we obtain the coefficients of the filters $\mathbf{P}^i$ and $\mathbf{Q}^i$, which are given by [70]:

$$\mathbf{P}^i = \mathbf{R}_{\mathbf{yy}}^{-\mathbf{1}}(\mathbf{I}_{LK'} - \mathbf{Q}^i)\mathbf{R}_{\mathbf{ya}}, \tag{4.5}$$

and

$$\mathbf{Q}^{i+1} = -[\mathbf{R}_{\mathbf{ay}}\mathbf{P}^i - \rho\mathbf{I}_{LK'}], \tag{4.6}$$

where ρ is given by

$$\rho = \frac{\text{Tr}[\mathbf{R}_{\mathbf{ay}}\mathbf{P}^i]}{LK'}. \tag{4.7}$$

$\mathbf{R}_{\mathbf{yy}}, \mathbf{R}_{\mathbf{ya}}$ and $\mathbf{R}_{\mathbf{ay}}$ (all of size $LK' \times LK'$) are expressed by

$$\mathbf{R}_{\mathbf{yy}} = \overline{\mathbf{H}}\overline{\mathbf{H}}^H + \sigma_n^2\mathbf{I}_{LK'}, \tag{4.8}$$

$$\mathbf{R}_{\mathbf{ya}} = \overline{\mathbf{H}}, \tag{4.9}$$

and

$$\mathbf{R}_{\mathbf{ay}} = \overline{\mathbf{H}}^H \tag{4.10}$$

and are respectively the correlation matrices between the received symbols themselves, between the received and transmitted symbols and vice versa. Due to the accurate estimation of the symbol correlation matrices, ($\hat{\mathbf{x}}^{i-1}$) being a complex process and considering

that the feedforward filter will perform well in the first iteration, such an assumption that the feedback decisions will be correct is feasible. We remind that at the first iteration ($i = 1$) $\mathbf{Q}^1 = 0$, due to the lack of previous decisions. $\mathbf{P}^1$ is also reduced to

$$\mathbf{P}^1 = \mathbf{R}_{\mathbf{yy}}^{-\mathbf{1}}\mathbf{R}_{\mathbf{ya}}, \tag{4.11}$$

i.e., the MMSE-TF equalizer. It can be seen from this description and from Figure 31 that the proposed equalizer is a modified version of the classic IB-DFE, now taking into account the characteristics of the proposed pre-coded filter bank system. The main differences are the inclusion of the filter compensation process and the different structure of the data in the DFT input, which must follow the same structure of the transmission symbol, i.e. the symbols decided in the first and last $L/4$ positions with zeros in the intermediate values. Better error performance is expected especially in high mobility scenarios.

The IB-DFE design is based only on channel knowledge, thus, the performance gain in terms of BER decreases significantly when overlapping factors of order of four (case of the PHYDYAS filter) are used, since in this case, large interferences arise from the filter. In the case of using filters with overlapping factors greater than 1.5, more robust receivers that handle both channel and filter interference are needed to minimize this problem. The use of techniques based on interference cancellation can be an alternative approach.

4.2 Iterative Interference Cancellation Receiver

The iterative DFE equalizer is obtained using only the channel information, its performance declines rapidly as the overlapping factor increases. Thus, more robust receivers are needed to minimize this problem. The use of techniques based on interference cancellation can be an alternative approach. In [71] and [72] the authors propose interference cancellation techniques for the FBMC system in order to mitigate intrinsic interference and also the interference that appears in high mobility scenarios. In order to handle more efficiently interferences stemming from the doubly-selective channel, Figure 32 presents a simple but effective interference cancellation scheme in an iterative format (IIC). For a very aggressive channel the first estimate may not be very accurate, so,

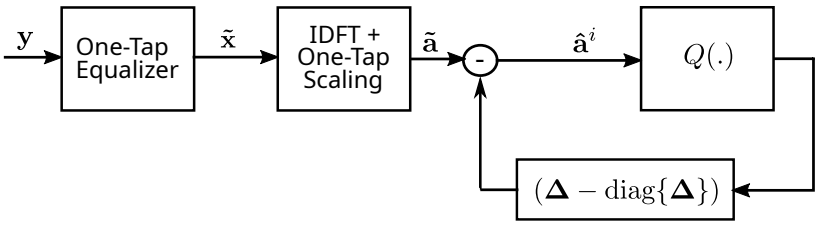

Figure 32 – Block scheme of the IIC receiver.

detection schemes with interference estimation and cancellation are not always effective

due to error propagation. Therefore, the challenge is to mitigate the error propagation through iterations, i.e., to improve the reliability of the symbols detected at each iteration. Performing a parallel-serial conversion to $\tilde{\mathbf{a}}_k$ in (3.11), the input-output ratio of the entire transmission system $\tilde{\mathbf{a}} \in \mathbb{C}^{LK' \times 1}$ can be modeled by

$$\tilde{\mathbf{a}} = \underbrace{\mathbf{C}^H \text{diag}\{\mathbf{e}\} \bar{\mathbf{G}}^H \mathbf{H} \bar{\mathbf{G}} \mathbf{C}}_{\boldsymbol{\Delta}} \mathbf{a} + \underbrace{\mathbf{C}^H \text{diag}\{\mathbf{e}\} \bar{\mathbf{G}}^H}_{\boldsymbol{\Upsilon}} \mathbf{n}. \tag{4.12}$$

where $\mathbf{C} \in \mathbb{C}^{LK' \times LK'}$ corresponds to the system precoding process for all transmitted blocks and is given by

$$\mathbf{C} = (\mathbf{I}_{K'} \otimes \mathbf{C}_f) \tag{4.13}$$

The off-diagonal values of $\boldsymbol{\Delta} \in \mathbb{C}^{LK \times LK}$ and $\boldsymbol{\Upsilon} \in \mathbb{C}^{LK \times M}$ represent the contribution of the interference coming from the filter and the channel, respectively. Finally, $\mathbf{e} \in \mathbb{C}^{LK \times 1}$ is the column vectorization of all elements of $\mathbf{e}_k$, that is, $\mathbf{e} = \text{vec}([\mathbf{e}_0, \mathbf{e}_1, \ldots, \mathbf{e}_{K'-1}])$.

The focus of the IIC is on channel and filter interference described by the elements outside the main diagonal of $\boldsymbol{\Delta}$. For $O > 1.5$, the received symbols are corrupted by prototype filter interference terms, that is, some values outside the main diagonal of $\boldsymbol{\Delta}$ become significant. The basic idea of the proposed scheme is to first pass the symbols through a ZF or MMSE equalizer, followed by post-coding, which provides provisional estimates of the data vectors. Based on these estimates, the level of interference will be minimized and performance improved by removing unwanted (off-main diagonal) terms in $\boldsymbol{\Delta}$. Thus, similarly to the approaches suggested in [67] for OFDM, we can cancel the interference at the quantizer input considering the i-th iteration by

$$\hat{\mathbf{a}}^{i+1} = \tilde{\mathbf{a}} - (\boldsymbol{\Delta} - \text{diag}\{\boldsymbol{\Delta}\}) Q(\hat{\mathbf{a}}^i) \tag{4.14}$$

where $Q(.)$ denotes the quantization operator. The algorithm is initialized with $\hat{\mathbf{a}}^0 = \tilde{\mathbf{a}}$, representing the system output using only the conventional one-tap equalizer of equation (3.23). It should be noted that $L/2$ data symbols are quantized, so it is necessary to generate the data allocation strategy in the transmission to pass $\tilde{\mathbf{a}}$ through the interference canceller. Moreover, $(\boldsymbol{\Delta} - \text{diag}\{\boldsymbol{\Delta}\})$ are the interference terms which are subtracted through iterative process, bringing greater reliability to the detected symbols. That is, the receiver subtracts the interference terms from the data symbols and the process is repeated until a given number of iterations are completed.

The interferences can come from the time-varying channel or through the transmission filter with an overlapping factor above the limit imposed by the technique. Considering only the filter interference, that is, $\mathbf{H} = \mathbf{I}_M$, Figure 33 shows the representation of the interference in and off-main diagonal interference terms for overlapping factors 1.5 and 4. Note that for the higher overlapping factor off-diagonal interference terms are significant, whereas in the case of $O = 1.5$, off-main diagonal interference is almost suppressed by

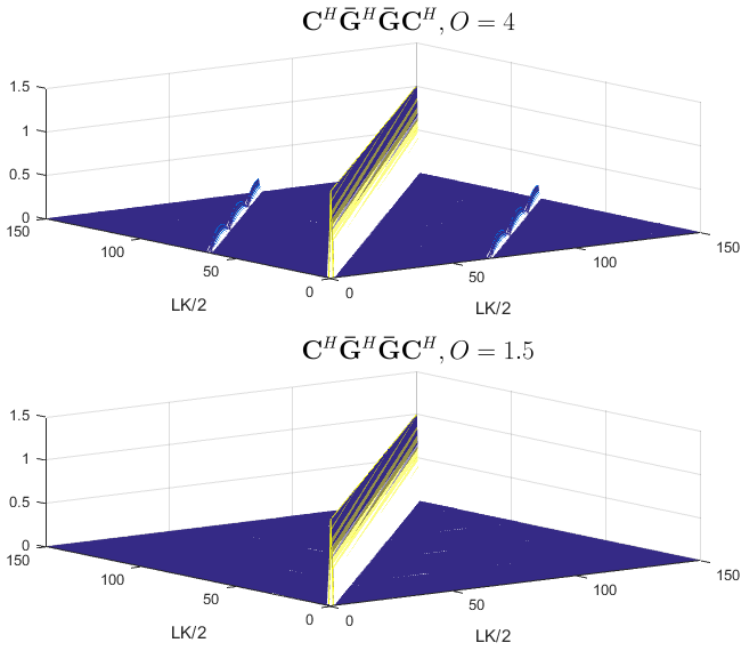

Figure 33 – Representation of the interference terms in $\mathbf{C}^H\bar{\mathbf{G}}^H\bar{\mathbf{G}}\mathbf{C}^H$.

precoding via DFT plus the scaling factor. For the scenario where the fading channel is present, Figure 34 shows the symbol estimates before and after one iteration of interference cancellation, for a Vehicular A channel, $O = 4$, velocity of 500 km/h and a SNR of 20 dB. By using the interference canceller to remove the off-main diagonal interferences we have a more reliable estimate, as illustrated in Figure 34. Results for more than one iteration of interference cancellation were not shown because further gains are difficult to be noticed in the Figure.

To summarize, the idea of the IIC is to further reduce the influence of residual filter interference and increase robustness in high mobility scenarios. The removal of these interferences may allow the application of some conventional MIMO techniques using longer filters in the DFT precoded filter bank system. It should also be noted that the IIC is suitable for the uplink scenario, since the complexity of the receiver is concentrated in the base station. Furthermore, the low PAPR characteristics of the transmitted signal, due to its DFT precoding, also make it attractive for the uplink scenario. Because of the low OOB emission, this application in the uplink in multiuser systems becomes simple. In the cases of the receivers proposed in [71] and [72], the transmission was changed from OQAM to QAM. In this way, the real orthogonality condition of the FBMC with OQAM is no longer satisfied. Therefore, in these proposed receivers even in the SISO system interference cancellation methods must be applied at the receiver.

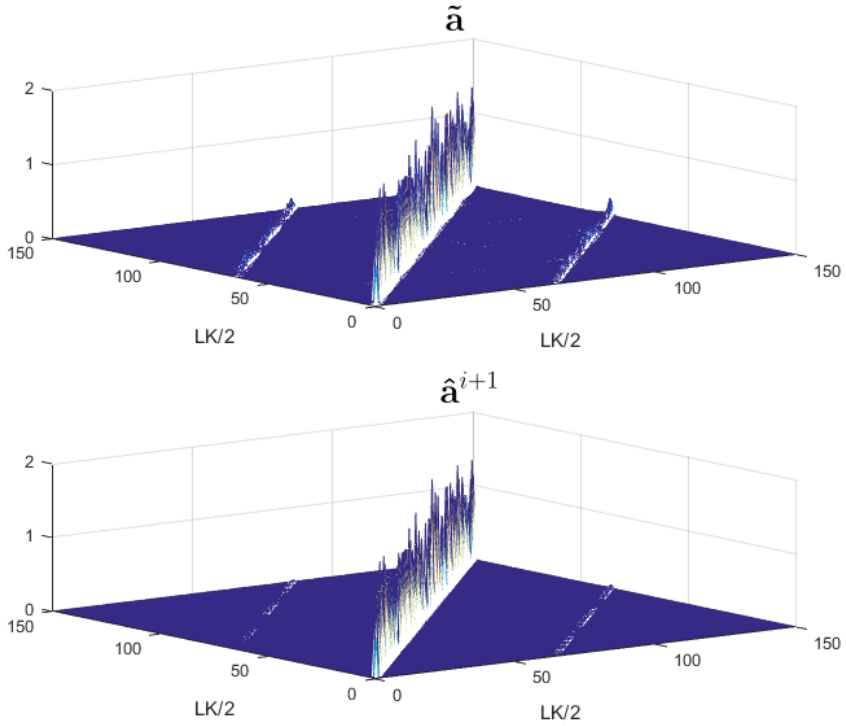

Figure 34 – Symbol received for $O = 4$ and in a 20 dB SNR using the MMSE equalizer ($\tilde{\mathbf{a}}$) and using the proposed receiver ($\hat{\mathbf{a}}^{i+1}$).

4.3 Comparative Analysis Between Receivers

In order to validate the use of iterative receivers, we will present some BER curves using different filter overlapping factors and in scenarios with and without mobility. We used the truncated Hermite filter as well as the conventional Hermite ($O = 2$) and the PHYDYAS filter with $O = 4$. The Tapped Delay Line (TDL) - A model is added to the Vehicular A model, considering a delay spread of 300 ns [73]. The rest of the parameters are presented in Table 7. Note that we used 3 different values of the number of subcarriers L. The idea is to evaluate and verify the data symbol spreading process in the frequency and how this spreading impacts the error performance. We also describe the system

General parameters	
Total subcarriers (L)	32, 128 and 256
Multicarrier symbols (K')	16
Filter bank FFT size (N)	256 and 512
Subcarrier spacing (F)	15 kHz
Modulation	4-QAM and 16-QAM
Channel Model	ITU-T Vehicular A and TDL-A 300ns
Velocity (ϑ)	0 and 300 Km/h
Carrier frequency	2.5 GHz

Table 7 – Parameters of the simulations in Chapter 4.

performance with the Genie-Aided version of the receivers. The term Genie-Aided is defined as the performance obtained by assuming a perfect interference estimate, that is, the exact transmitted symbols are involved to estimate the interference ($\tilde{\mathbf{a}} = \mathbf{a}$). Thus, we have the maximum performance that the iterative equalizer can obtain. First, the Figure 35 shows the evolution of the equalizer as we increase the number of iterations using 16-QAM modulation, $L = 128$ and the Hermite filter truncating in order to obtain $O = 1.5$. Note that between the first two iterations there is a significant gain in performance, while

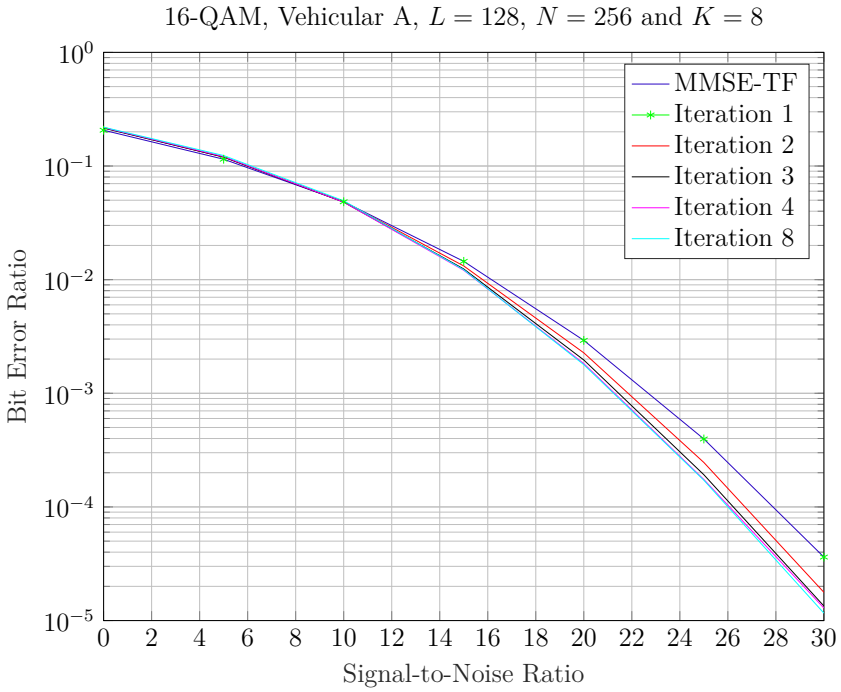

Figure 35 – Evolution of the IB-DFE equalizer.

the gain of the others iterations is reduced. For values above 4 iterations, it can be seen that the gain is insignificant compared to the fourth iteration. In this way, we will consider 4 iterations for the next curves, since there is no significant performance gain with more iterations. Figure 36 presents the BER curve for the DFT precoded system for a 16-QAM constellation with $L = 256$ using the Vehicular A channel model without mobility. First, note that in normal scenarios ($O = 1.5$) the IB-DFE equalizer has a better error performance compared to the MMSE-TF equalizer. Another important point to highlight is the validity of our assumption to consider correct decisions in the process of derivation of coefficients, since the performance is similar to the maximum gain of the equalizer as shown in the Genie-Aided curve. Finally, the filter overlapping factor can be raised to 2 and the error performance with the iterative equalizer will still be better than when using the MMSE equalizer on the previous limit of $O = 1.5$. In the scenario with mobility, the results remain similar as shown in Figure 37 for a situation with a velocity of 300km/h. As expected, due to Doppler spreading, the BER suffers a noticeable degradation. However, the iterative equalizer does provide a significant performance improvement, especially if

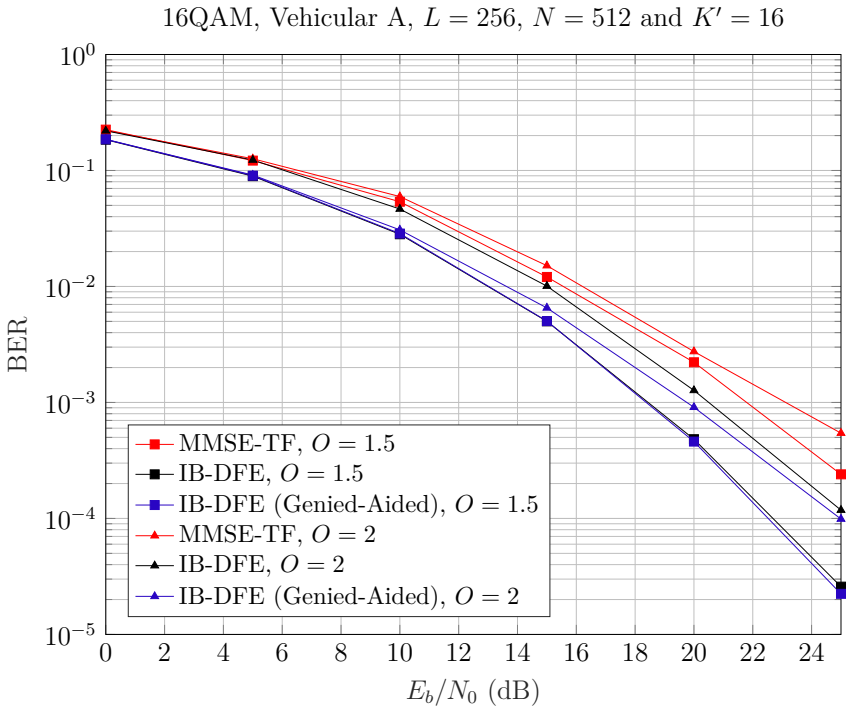

Figure 36 – BER for IB-DFE with 16-QAM, vehicular A channel and $\vartheta = 0$km/h.

we consider the maximum performance the equalizer can achieve. For a BER of 2×10^{-3} the difference at high SNRs between the iterative equalizer and the MMSE-TF both with $O = 1.5$ is almost 4 dB. It is worth mentioning that the performance with overlapping

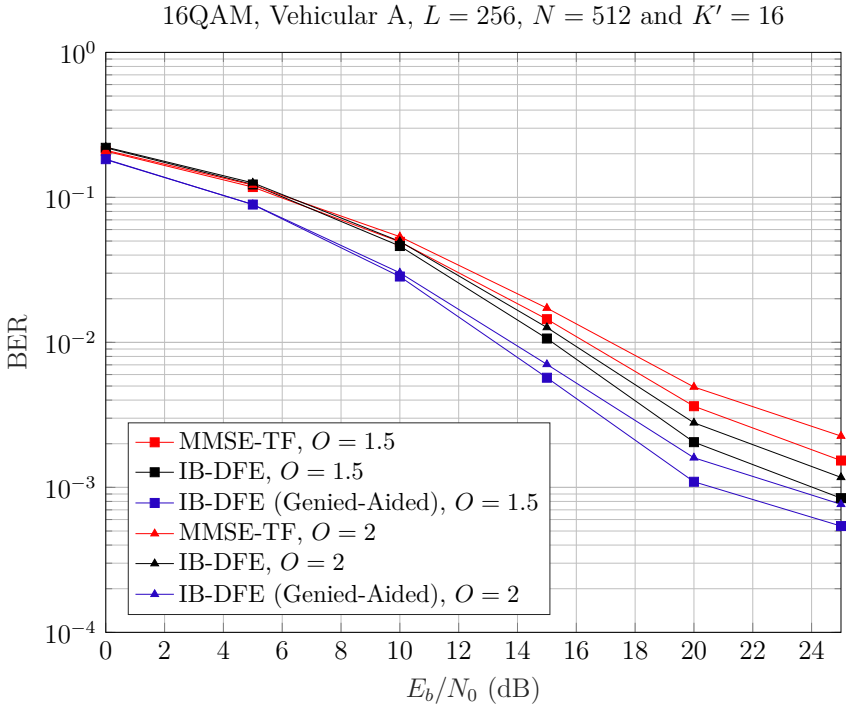

Figure 37 – BER for IB-DFE with 16-QAM, vehicular A channel and $\vartheta = 300$km/h.

factors greater than 1.5 will depend on the filter used. The performance using, for example, the PHYDYAS filter truncated in $O = 2$ can present different performance from that presented by the Hermite filter. Each prototype filter has its characteristics in time and frequency that even modify the performance due to the used channel. In Figure 38, we present the BER for 4-QAM modulation without mobility. It is possible now for this scenario with the iterative receiver to increase the overlapping factor from 1.5 to 4 and still obtain a superior error performance than the one obtained when using the linear MMSE equalizer, even when an overlapping factor of 1.5 is considered for the linear structure. Considering systems with the same overlapping factor, the error performance for a BER of 10^{-4} is increased by at least 2.5 dB with the iterative structure. For a scenario with

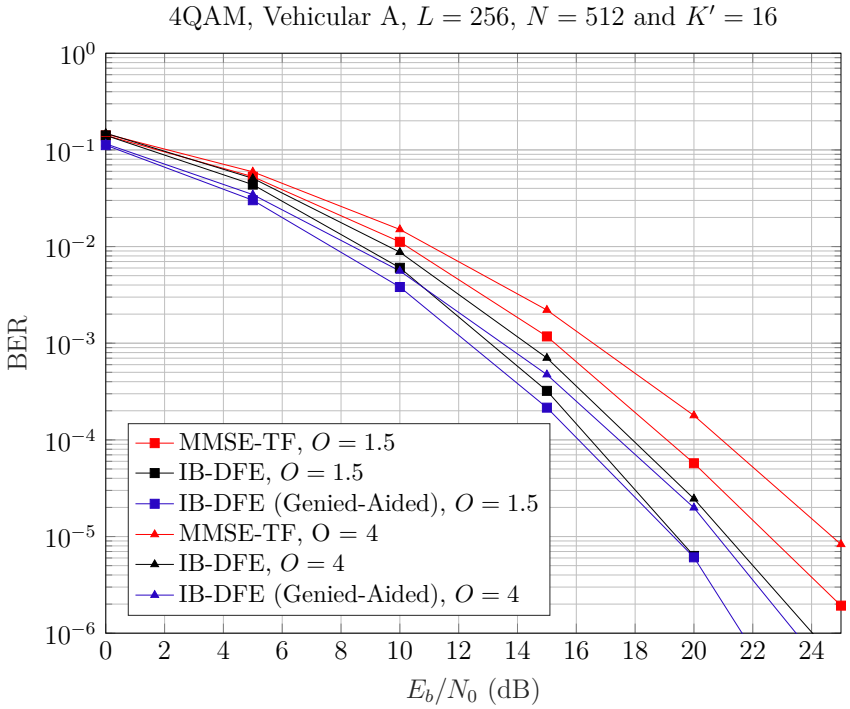

Figure 38 – BER for IB-DFE with 4-QAM, vehicular A channel model and $\vartheta = 0$km/h.

mobility as illustrated in Figure 39, the performance improvement by the iterative equalizer is even more evident. The performance in genie-aided is highlighted, showing that the IB-DFE can obtain high gains in smaller constellations, even in a scenario with high Doppler spreading.

In relation to the IIC the Figure 40 presents the BER curves for 16-QAM and a velocity of 0 km/h. As we can see, IIC's performance using 10 or 4 iterations is similar. Thus, due to reducing computational complexity, we will only use 4 iterations. It is now possible for this scenario with the IIC to increase the overlapping factor from 1.5 to 4 (improving the spectral confinement) and still obtain a better error performance than the one obtained with the conventional MMSE equalizer even when the system with this equalizer uses a filter with $O = 1.5$. It should be noted that for this scenario without

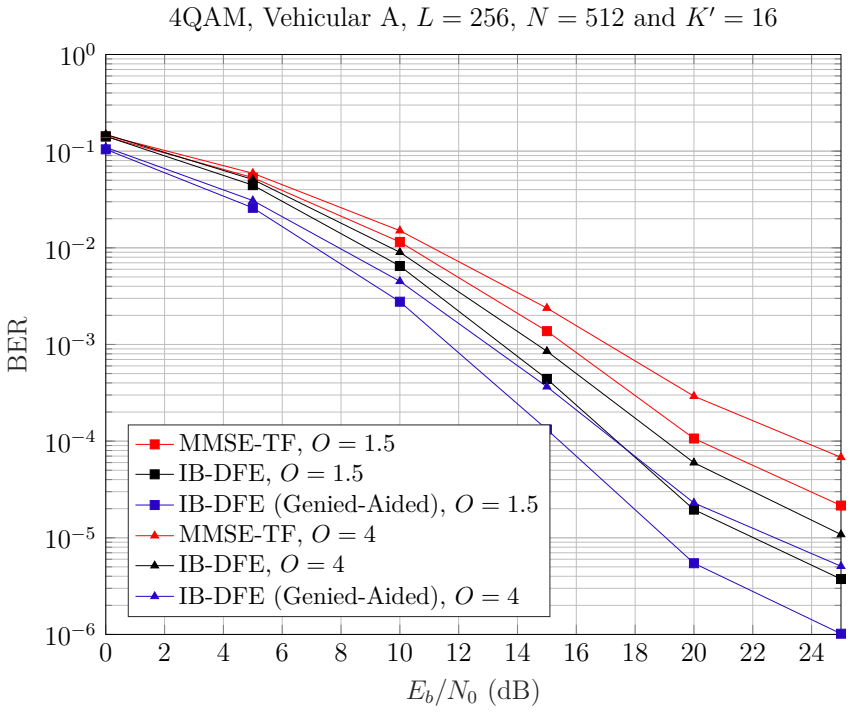

Figure 39 – BER for IB-DFE with 4-QAM, vehicular A channel model and $\vartheta = 300$km/h.

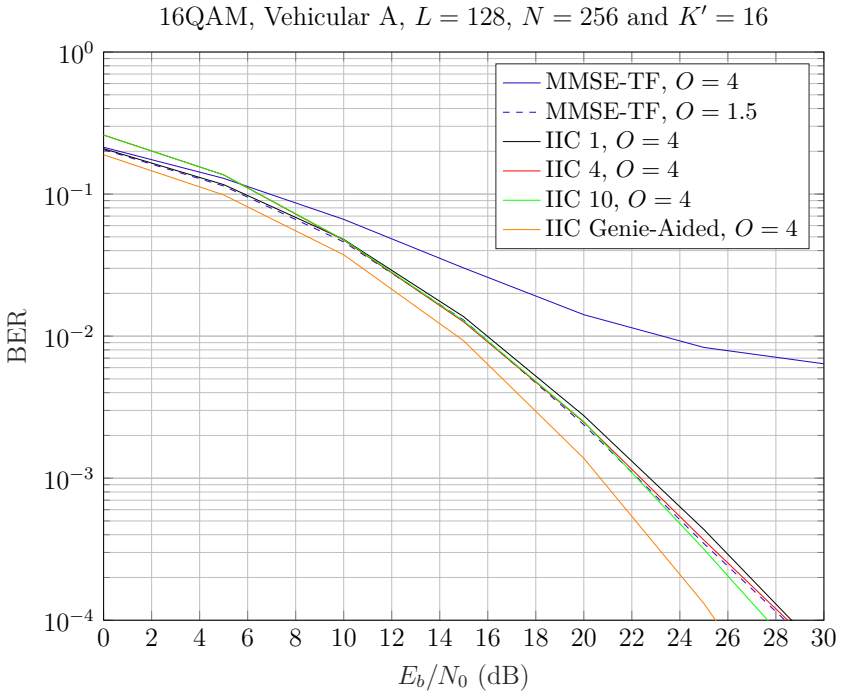

Figure 40 – BER for ICC with 16-QAM, vehicular A channel and $\vartheta = 0$km/h.

mobility, the one-tap equalizer is sufficient and the interference is only induced by the filter. Thus, when we have the proposed receiver with an overlapping factor equal to 1.5, there is no performance improvement, since there is almost no off-diagonal interference (the filter interference is correctly compensated by the system). Finally, when the feedback

with perfect detection of the symbols is considered, the performance of the interference canceller with $O = 4$ exceeds considerably the MMSE equalizer with the $O = 1.5$. Figure 41 presents the results considering the same scenario, but now with a velocity of 300 km/h. As in this case, the channel has high mobility, the transmultiplexer matrix not

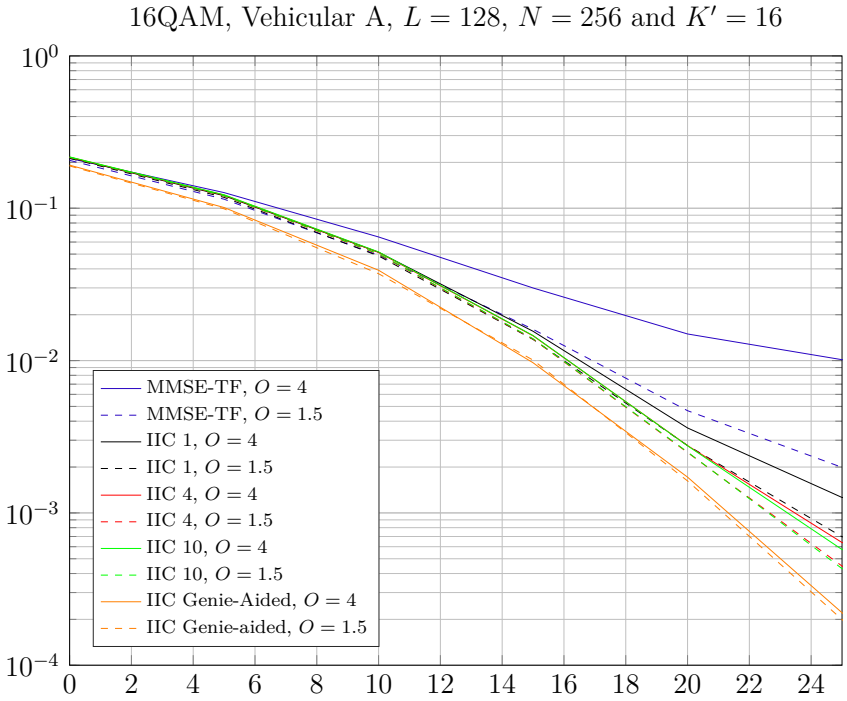

Figure 41 – BER for ICC with 16-QAM, vehicular A channel and $\vartheta = 300$km/h.

only has off-diagonal components related to the filter but also to the time-variant channel response. First, note whether it is $O = 1.5$ or 4, the performance improvement that the receiver provides so that with just one iteration we have a BER lower than that seen in the MMSE-TF. It is also noted that again the performance for 4 and 10 iterations are identical with no need to use more than 4 iterations even with mobility. In this scenario, the errors on the decided symbols have a strong impact on the reception quality, as seen in the large performance disparity with respect to the genie-aided results.

Performing a comparative analysis between the two receivers, the Figure 42 presents the BER for 16-QAM modulation, $L = 32$ and velocity of 0 km/h for the TDL-A channel model. Only 1 and 4 iterations were used for the IIC receiver. The performance gain of the IIC is clearly observed when compared to the MMSE case with $O = 4$. Note that the curves obtained with one and four iterations of the IIC with $O = 4$ are similar to those obtained with $O = 1.5$ and genie-aided, indicating that interference (elements off the main diagonal of the matrix $\mathbf{\Delta}$) is not high. It is worth mentioning that by spreading more symbols in the frequency, that is, increasing the value of L, we have a slight improvement in error performance. However, even reducing the value of L to 32, again the one-tap equalizer is sufficient and effective to cancel the channel-induced interference in this static

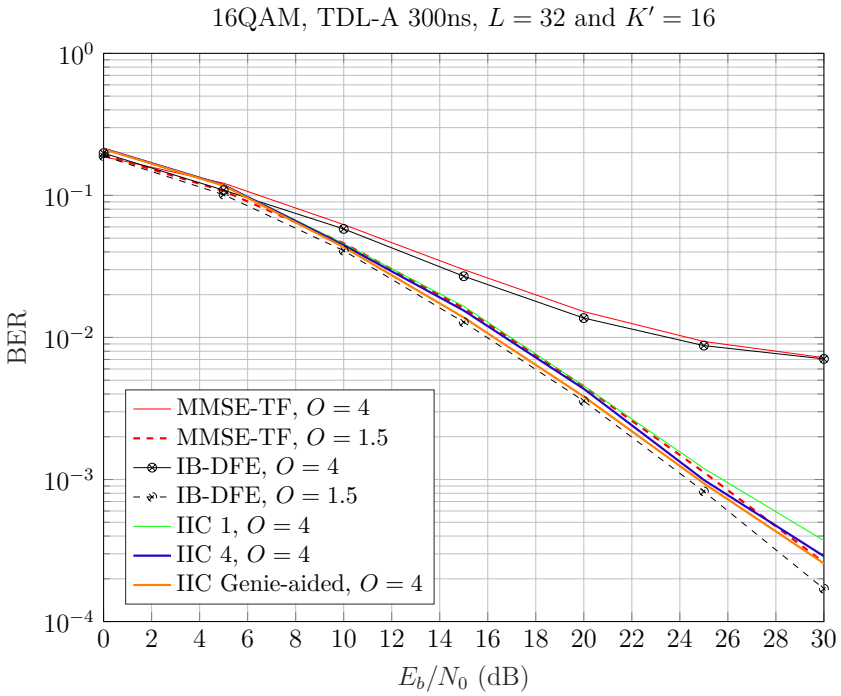

Figure 42 – BER for iterative receivers with 16-QAM, TDL-A channel and $\vartheta = 0$km/h.

scenario to $O = 1.5$. When compared to the IB-DFE equalizer, the IIC scheme performs much better for $O = 4$, due to the iterative removal of interference from not only the channel but also from the filter. On the other hand, the IB-DFE presents a slightly superior performance in normal situations ($O = 1.5$). The results presented in Figure 43 consider the same scenario, but now with a velocity of 300 km/h. In this case, the channel is highly mobile and the error performance is affected, as now the interferences come not only from the filter but also from the time-varying channel. Note again that the IIC manages to achieve good performance even using a longer filter, with similar performance to the $O = 1.5$ case. Furthermore, in the high mobility scenario the performance gain is even more considerable and again, in the Genie-Aided mode a high gain is obtained compared to the same receiver in the non-mobility case.

Note that, in this case, the IIC receiver performs better at high SNRs, even for $O = 1.5$. For the genie-aided case, notice that unlike the case without mobility, a high gain is presented showing the robustness that this receiver can reach. In this scenario, the IB-DFE with $O = 4$ has its performance severely affected by interference, thus making the IIC an alternative with better performance. In the normal situation without the presence of filter interference, both performances are pretty even with a small advantage of the IIC.

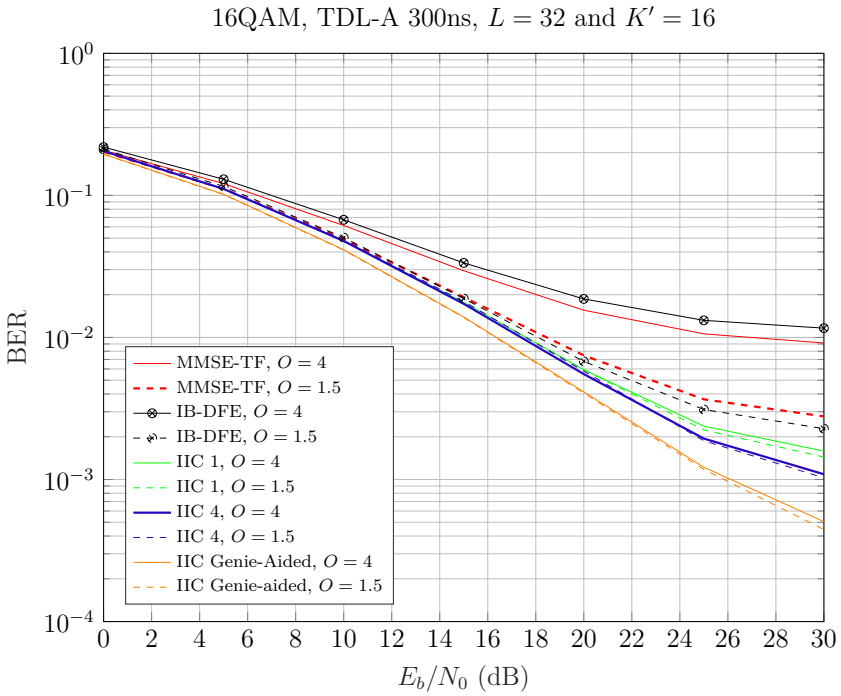

Figure 43 – BER for iterative receivers with 16-QAM, TDL-A channel and $\vartheta = 300$km/h.

4.4 Conclusion

The iterative receivers introduced in this chapter are an alternative for extreme cases where one operates in a highly dispersive environment or where a better spectral localization is needed. The IB-DFE does not deal with filter interference; however, it eliminates residual channel interference allowing to increase the filter overlap factor (interference is generated) and keep gains at the same levels as the MMSE equalizer. On the other hand, the IIC receiver aims to minimize both channel and filter interference. All of this is achieved at the cost of increasing receiver complexity. For the IB-DFE equalizer it was noted that 4 iterations are enough, while for the IIC 10 iterations were used. In terms of increasing the overlapping factor, the IIC performed better to the point of maintaining the same BER of $O = 1.5$, using the PHYDYAS filter ($O = 4$). In terms of mobility, both receivers show a improvement compared to the MMSE equalizer. In view of the recovery of complex orthogonality by the DFT precoded scheme, we will see in the next chapters that we can improve even more the performance in this type of scenario by modifying the transmission format through the filter bank and also the precoding.

5 Two-Dimensional FFT Precoded Filter Bank

The OTFS technique applies the OFDM multicarrier system as the core for data transmission. However, other multicarrier techniques can also be used as a kernel to implement this transmission, as long as complex orthogonality between the pulses of the transmitter/receiver is guaranteed [26]. Thus, to use OTFS with a FBMC transceiver as its core it is necessary to eliminate the interference coming from the filters in order to recover complex orthogonality. As previously reported, this objective can be achieved using pre-coding via DFT. We will see below that this can be done using a part of the OTFS itself with the addition of the multiplicative compensation factor. Therefore, we propose a system called 2D-FFT filter bank, which combines the main advantages of FBMC and OTFS systems.

5.1 2D-FFT Filter Bank Principles

Figure 44 shows the block diagram of the 2D-FFT scheme and its respective signal domains. Basically, we reused the pre- and post-coding process of the pre-coded DFT system along with the data transmission strategy and added an IDFT performed on the multicarrier symbols. Thus, there is an IFFT performed in the Doppler domain and an FFT in the delay domain, generating a time-frequency spreading via ISFFT as in OTFS. The difference lies in the addition of a compensatory multiplicative factor and in the data structure. Furthermore, after mapping the symbols on the time-frequency grid, symbols will now be transmitted by a filter bank.

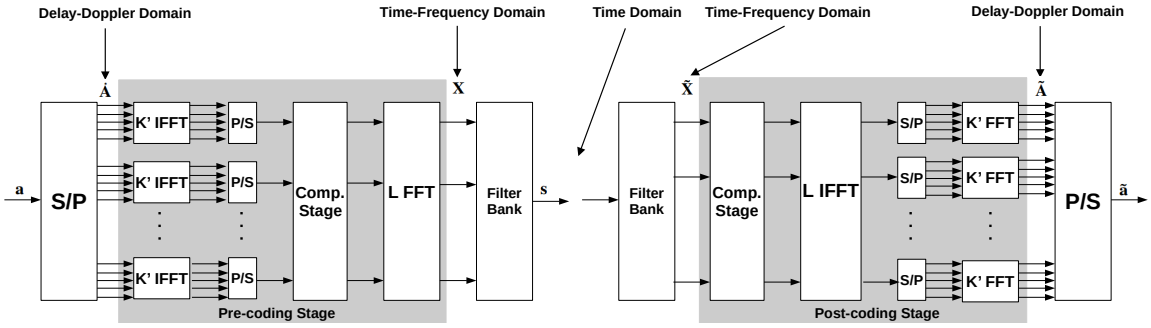

Figure 44 – Block scheme of the 2D FFT-FB system.

Initially the data symbols are in the delay-Doppler domain. After a serial to parallel data stream converter $L/2$ blocks of K'-point IDFT are fed by QAM symbols, producing their mapping to the delay-frequency domain. Then the encoding process is added that

restores the complex orthogonality. First the compensation stage is applied and then the data are allocated in the first and last L/4 positions of a L-point DFT generating the final mapping for the time-frequency domain. Thus, data symbols no longer belong to one position on a specific frequency, but are spread across multiple subcarriers. In this way, it is clear that one can apply the ISFFT and restore the complex orthogonality at the same time. Using matrix notation, the signal at the filterbank input can be expressed by

$$\mathbf{X} = \underbrace{\mathbf{W}_L \text{diag}\{\tilde{\mathbf{b}}\}}_{\mathbf{C}_f} \dot{\mathbf{A}} \mathbf{W}_{K'}^H \tag{5.1}$$

where $\dot{\mathbf{A}} \in \mathbb{C}^{L \times K'}$ contains K' symbols, each with $L/2$ complex data symbols from a QAM constellation. These symbols are placed on the first and last $L/4$ positions of the L-point DFT ($\mathbf{W}_L$) with zeros in the remaining ones. Realizing the similarity between equations (5.1) and (2.71), matrices $\dot{\mathbf{A}}$ and $\mathbf{A}$ (OTFS transmitted data) can be direct related. Considering each position, that is, $[\mathbf{A}]_{l,k} = a_{l,k}$ for $k = 0, 1, ..., K-1$, an example of the QAM-symbols mapping from $\mathbf{A}$ to $\dot{\mathbf{A}}$ for $L = 4$ and $K = 2$ is given as follows

$$\mathbf{A} = \begin{bmatrix} a_{0,0} & a_{0,1} \\ a_{1,0} & a_{1,1} \\ a_{2,0} & a_{2,1} \\ a_{3,0} & a_{3,1} \end{bmatrix} \rightarrow \dot{\mathbf{A}} = \begin{bmatrix} a_{0,0} & a_{2,0} & a_{0,1} & a_{2,1} \\ 0 & 0 & 0 & 0 \\ 0 & 0 & 0 & 0 \\ a_{1,0} & a_{3,0} & a_{1,1} & a_{3,1} \end{bmatrix} \tag{5.2}$$

Basically, in the DFT entry present at ISFFT the data symbols are placed in the first and last $L/4$ bins of the DFT with the intermediate values being zeros. Note that, a double-rate transmission with respect to the conventional OTFS is required to obtain the maximum data transmission capacity. However, as we will see, this has no impact on a better discrimination in the delay-Doppler domain. The transmission process through the channel is done in the same way as seen for the DFT precoded in Chapter 3. At the receiver, after the synthesis filter we have three alternatives. The first is to run the simple one-tap equalizer in the TF domain or leave to minimize channel-related problems in the delay-Doppler domain after the post-coding process. Alternatively, a third option would be to use the iterative receivers seen in Chapter 4 where they operate in both domains. We saw that for OTFS the MMSE-TF equalizer did not perform so well that it was necessary to handle detection effectively in the DD domain. For the 2D-FFT case this is changed due to the filtering process. Thus, initially we will keep the equalization process in the TF domain. Therefore, to compensate for interferences coming from the channel, a one-tap equalization process is performed by $\mathbf{e}_k$, originating $\tilde{\mathbf{x}}_k \in \mathbb{C}^{L \times 1}$ which is expressed as Therefore, to compensate for interferences coming from the channel, a one-tap equalization process is performed by $\mathbf{e}_k$, originating $\tilde{\mathbf{x}}_k \in \mathbb{C}^{L \times 1}$ which is expressed as

$$\tilde{\mathbf{x}}_k = \text{diag}\{\mathbf{e}_k\}\mathbf{y}_k. \tag{5.3}$$

The one-tap equalizer applied in this work was based on the MMSE criterion, which we commonly call MMSE-TF. Such equalizer for the proposed system remains the same as was derived in equation (3.23). If delay propagation and Doppler effect are low enough, an one-tap equalizer is sufficient to compensate channel interference. Finally and considering all time instants, the detected symbols represented by $\tilde{\mathbf{A}} \in \mathbb{C}^{L \times K'}$ are obtained through the SFFT combined with the compensation stage:

$$\tilde{\mathbf{A}} = \underbrace{\mathbf{W}_L^H \text{diag}\{\tilde{\mathbf{b}}\}}_{\mathbf{C}_f^H} \tilde{\mathbf{X}} \mathbf{W}_{K'} \tag{5.4}$$

where $\tilde{\mathbf{X}} = [\tilde{\mathbf{x}}_0; \tilde{\mathbf{x}}_1; \ldots; \tilde{\mathbf{x}}_{K'-1}] \in \mathbb{C}^{L \times K'}$. The estimated symbols are obtained taking the first and the last $L/4$ symbols and discarded the intermadiate values, since no data was transmitted in those positions of $\dot{\mathbf{A}}$. As with DFT precoded, we have a time-frequency spacing (density) equal to $TF = 0.5$, however, only complex symbols $L/2$ are transmitted, leading to an equivalent time-frequency spacing of $TF = 1$ for L complex symbols. We can see that while OTFS looks like a generalization of SC-FDMA, the 2D-FFT is a generalization of DFT precoded filter bank. There is a certain similarity between equations (2.71) and (5.1), since they represent the samples that will be transmitted by the specific multicarrier modulator. While (2.71) uses the OFDM technique, in (5.1) a filter bank system will be used. The addition of the compensation stage, as well as the structure of symbols from the QAM constellation, are also noteworthy. In general, it is possible to see in both cases a coding based on a ISFFT on the data symbols whereas the difference lises in the multicarrier transmission scheme, i.e., OFDM vs filter bank.

Frequency-Time spreading is an interesting technique to filter bank systems because it is the basis for solving the problem of complex orthogonality loss. Through spreading, we have an additional code dimension (in addition to time and frequency) that allows us to eliminate the interference imposed by the filter at the time of transmission and reception. By recovering complex orthogonality, equalization becomes simpler as the symbols are now free from filter interference. Furthermore, it is possible to see from the signal (5.1) at the input of the filter bank that OTFS can naturally be used, since the orthogonality recovery process is a part of the OTFS. The novelty of our proposal to implement an OTFS-based data transmission can be summarized, for now, as: the transmission of $L/2$ information symbols at a doubled rate using a filter bank, assure the complex orthogonality through DFT spreading and a filter compensation stage and to use this DFT block as part of the OTFS transmission. It is interesting to note that in a conventional OTFS transmission a delay-Doppler grid ($L \times K$) is transformed into a time-frequency grid ($K \times L$) through the inverse symplectic transform (Figure 15). In our proposed technique, a grid ($L \times K'$) in the delay-Doppler domain, with only $L/2$ active subcarriers, is transformed into a time-frequency domain grid ($K' \times L$), as shown in Figure 45. To maintain the same symbol density of a ($K \times L$) conventional OTFS (for comparison

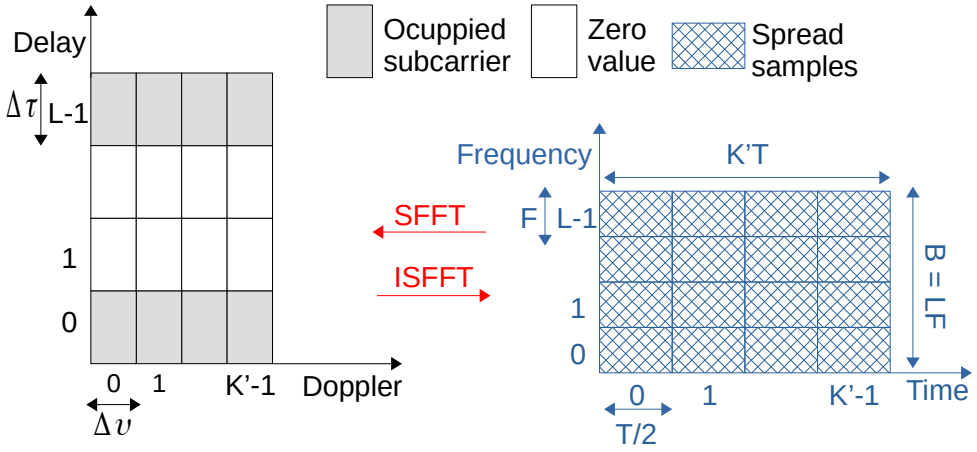

Figure 45 – Analysis of time-frequency and delay-Doppler grids in the proposed scheme.

purposes), we must have $K' = 2K$. So, the grid $(2K \times L)$ is divided in two grids $(K \times L)$ where each will be filtered by a PPN as seen in Figure 12. Finally, one of the grids is delayed by $N/2$ samples and both streams are summed, generating the transmission at doubled rate. This transmission technique leads our technique to have the same Doppler spread discrimination as a $(K \times L)$ conventional OTFS. Due to its similarity to OTFS, the same detection techniques proposed and implemented in the OTFS technique can be applied to the 2D-FFT FB one. However, the use of frequency domain equalizers, such as the one-tap used in OFDM systems, have much better performance in 2D-FFT FB.

5.2 Delay-Doppler Domain Equalizer

Frequency domain equalization is very useful in multicarrier systems, such as OFDM and FBMC, because of its simplicity. However, an OTFS system combined with an equalizer in the delay-Doppler domain is able to explore the full channel diversity both in time and frequency. Let us consider $\mathbf{H}_{ef} \in \mathbb{C}^{LK' \times LK'}$ as the effective channel matrix, that encompasses the entire transmission (filter bank) and coding process. So, unlike the frequency domain equalizer $\mathbf{e}_k$ which only considers the multicarrier modulation stage, from now on both the pre- and post-coding processes are also considered. Thus, $\mathbf{H}_{ef}$ can be written as:

$$\mathbf{H}_{ef} = \mathbf{C}^H \bar{\mathbf{G}}^H \mathbf{H} \bar{\mathbf{G}} \mathbf{C}, \tag{5.5}$$

where $\mathbf{C} \in \mathbb{C}^{LK' \times LK'}$ is rewritten by adding the K IDFTs that constitute the 2D-FFT pre-coding process and is given by

$$\mathbf{C} = (\mathbf{I}_{K'} \otimes \mathbf{C}_f)(\mathbf{W}_{K'} \otimes \mathbf{I}_L). \tag{5.6}$$

The MMSE equalizer in the delay-Doppler domain $\mathbf{E}_{dd} \in \mathbb{C}^{LK' \times LK'}$ can be expressed by

$$\mathbf{E}_{dd} = \mathbf{H}_{ef}^H (\mathbf{H}_{ef} \mathbf{H}_{ef}^H + \sigma_n^2 \mathbf{I}_{LK'})^{-1}. \tag{5.7}$$

Thus, the estimated symbols are given by

$$\hat{\mathbf{a}} = \mathbf{E}_{dd}\tilde{\mathbf{a}}, \tag{5.8}$$

where $\tilde{\mathbf{a}} = \text{vec}(\tilde{\mathbf{A}}) \in \mathbb{C}^{LK' \times 1}$. Note that for the equalization process in the DD domain, all the values of the $\mathbf{E}_{dd}$ matrix are necessary and not just the main diagonal like the MMSE-TF equalizer. As we have seen in Chapter 1, OTFS technique combined with this delay-Doppler domain equalizer proves to be more robust in high mobility scenarios than when using a frequency domain equalizer. However, its complexity is significantly higher, mainly due to the need to invert an matrix of size $LK' \times LK'$.

In order to deal more efficiently with interference from the doubly selective channel, the iterative receivers introduced in Chapter 4 can also be applied in the 2D-FFT system. In reality, they can even be applied to OTFS, however, such receivers are based on a good first estimate of an MMSE-TF equalizer. This estimate is not as good in OTFS as seen in Figure 19 in Chapter 1. Its robustness to Doppler appears especially when transmitting the data in the delay-Doppler domain, where the maximum of the available diversity is exploited. In this way, it is imagined that the same happens with the 2D-FFT FB, a fact that does not occur, as we will see later. It should be noted that readjustments are necessary in the iterative receivers due to ISFFT. For the IB-DFE, in the feedback process the ISFFT replaces the DFT, while for the calculation of the IIC (see (4.14)) the new matrix $\mathbf{C}$, defined in equation (5.6), is used. Both receivers upgraded to 2D-FFT are illustrated in Figure 46.

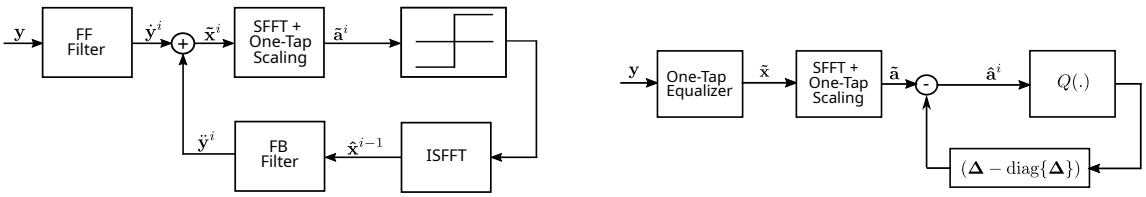

(a) IB-DFE (b) IIC

Figure 46 – Updated iterative receivers for the 2D-FFT system.

Note that the iterative schemes are a kind of hybrid receivers in domain terms with two stages. In the first step, the conventional one-tap MMSE equalizer in the frequency domain is used, bringing reliable estimates that will be fed to some processing in the delay-Doppler domain, obtaining a good final estimate of the symbols.

The OFDM transceiver is the simplest way to implement the OTFS transmission, since the condition of complex orthogonality between the transmitter/receiver pulses is implicitly guaranteed [24]. For regular FBMC systems, the loss of complex orthogonality makes the use of OTFS unfeasible. However, as previously seen complex orthogonality is guaranteed in the proposed scheme through pre-coding techniques defined by $\mathbf{C}_f$ and by

adjusting the overlap factor of the prototype filter to $O \leq 1.5$. The implementation of SFFT is easily performed by adding IDFT/DFT blocks in the pre-coding process ($\mathbf{C}_f$). We call this new transmission technique that generalizes SC-FDMA and FBMC systems as 2D-FFT-FB. The main objective of the proposed system is to improve the performance in high mobility scenarios and to minimize OOB emissions. Moreover, as it will be shown in the following sections 2D-FFT-FB has good performance with low complexity frequency domain equalizers.

5.3 Comparisons and Analysis

To show the benefits of the proposed system and validate the work, this section present several simulation results. The simulation method chosen for this chapter as well as for the previous and subsequent ones is Monte Carlo because it has a simple and very flexible structure. We start by comparing the PAPR and computacional complexity to other different techniques. Finally, we evaluated the error performance in terms of BER in scenarios with medium delay spread and high mobility. The filter bank modulator (see Figure 3) used for the simulations was implemented using the Hermite filter detailed in [55] which is based on a Gaussian function and therefore has a good location in the time-frequency plane. Again, we truncated the pulse to obtain $O = 1.5$ to avoid filter bank interference. The multicarrier symbol duration of both systems is approximately the same.

5.3.1 PAPR

Although OTFS is a multicarrier system by nature, its PAPR is much smaller than OFDM and FBMC [74]. That is because, as shown in (2.72), the PAPR does not depend on the number of subcarriers (L), but on the size transmitted block (K) [24]. In this sense, it is interesting to obtain a good trade-off between complexity and performance, to choose a smaller K with a larger number of subcarriers. The 2D-FFT FB system has similar behavior; however, the PAPR still depends on the number of subcarriers due to the DFT spread from L to N to avoid critical sampling. However, such dependence is low, resulting in a PAPR similar to that obtained in OTFS as shown in Figure 47 using $L = 128$, $K' = 16$ and a 4-QAM.

5.3.2 Computational Complexity

Table 8 presents the computational complexity of the 2D FFT-FB transmitter scheme, and also to OTFS and DFT Precoded FB. We recall that the DFT can be implemented efficiently by an FFT, where the number of complex multiplications for an L-point FFT is $L \log L$. For 2D-FFT, due to the ISFFT the term $(K'L/2)\log(K')$ is the additional complexity when compared to DFT Precoded system. In numerical terms, the

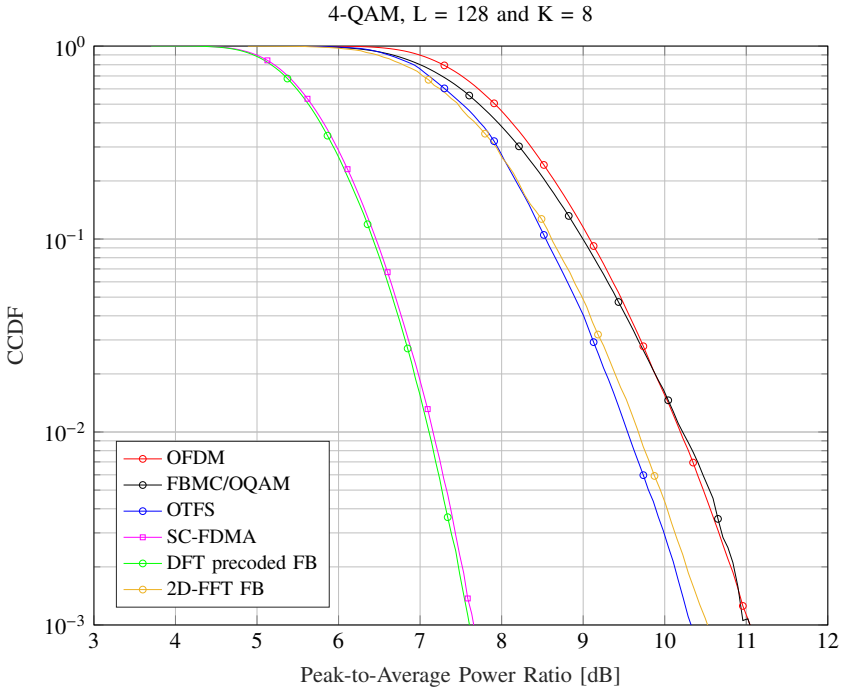

Figure 47 – PAPR analysis between waveforms.

complexity between the two is practically the same. In relation to the OTFS technique,

Scheme	Complexity
DFT Precoded FB	$K'\left(\frac{L}{2} + L\log(L/2) + N\log N + ON\right)$
OTFS	$LK\log(L) + LK\log(K) + KL\log L$
2D FFT-FB	$K'\left(\frac{L}{2} + L\log(L/2) + (L/2)\log(K') + N\log N + ON\right)$

Table 8 – Computational complexity of transmission scheme.

the computational complexity of our transmission scheme again considering $O = 1.5$ and $N = 2L$ is approximately three times greater. To be specific, the ratio between the computational complexity of the proposed technique and the OTFS at the transmitter can be approximated by

$$\frac{K'(\frac{L}{2} + L\log\frac{L}{2} + \frac{L}{2}\log(K') + N\log N + ON)}{LK\log(L) + LK\log(K) + KL\log L} \approx 3 \tag{5.9}$$

As we will see below, considering simpler receivers in the time-frequency domain one can arrive to a global complexity close to the OTFS in our proposal, achieving similar error performance.

5.3.3 Performance in Doubly-Selective Channels

Finally, we will analyze the robustness of the 2D-FFT system in a high mobility scenario using both the MMSE-TF and the MMSE-DD and the IIC receiver. The

communication channel specifications are the same as discussed in the previous simulations. For comparison with our proposed system, we also present the performance of the OTFS and DFT precoded filter bank system. The remaining simulation parameters are shown in Table 9. Note that the FFT used in the proposed systems (DFT precoded and 2D-FFT) is twice the size ($N = 2L$) of that used in OTFS. Note also that we need to use $N > L$ for the filtering process to be carried out, as explained previously. However, we could choose to use $N = 256$ also for OTFS because in terms of BER results the performance is equivalent.

Figure 48 shows the uncoded BER for the three systems using a time-frequency domain equalizer and for a velocity of 300 km/h. As we can see our system has superior performance for both 4-QAM and 16-QAM modulation. Note that the OTFS system presents a considerable performance loss when increasing the modulation order, having an error floor beginning at 25 dB. This behavior of the OTFS system is due to the fact that the frequency domain equalizer does not allow the system to extract all channel diversity, which normally occurs when equalization is performed in the delay-Doppler domain. On the other hand, the filtering process makes the performance superior in the 2D-FFT system, enabling the use of simpler equalizers in the time-frequency domain. Figure 49 presents the MMSE equalizer in both the time-frequency domain (represented by MMSE-TF) and the delay-Doppler domain (represented by MMSE-DD) for the proposed system compared to the OTFS for 4-QAM and a velocity of 400 km/h. We added a curve referring to the FBMC/OQAM system with the same defined settings. Note that the performance is not good when compared to other techniques, showing the sensitivity of the system to this type of scenario. As we can see, the performance in the delay-Doppler domain of OTFS and 2D-FFT systems is practically the same. However, this result for OTFS-MMSE-DD is obtained at the expense of greater computational complexity. Moreover, at this velocity the OTFS system with a frequency domain equalizer has even greater performance loss

General parameters			
Total subcarriers (L)		128	
Subcarrier spacing (F)		15 kHz	
Modulation		4-QAM and 16-QAM	
Channel Model		ITU-T Vehicular A	
Velocity (ϑ)		0, 300 and 400 Km/h	
Carrier frequency		2.5 GHz	
Specific parameters			
OTFS		2D-FFT and DFT Precoded	
Multicarrier symbols (K)	8	Multicarrier symbols (K')	16
Cyclic prefix length	8		
OFDM FFT size (N)	128	Filter bank FFT size (N)	256

Table 9 – Simulation parameters for the BER simulations from Chapter 5.

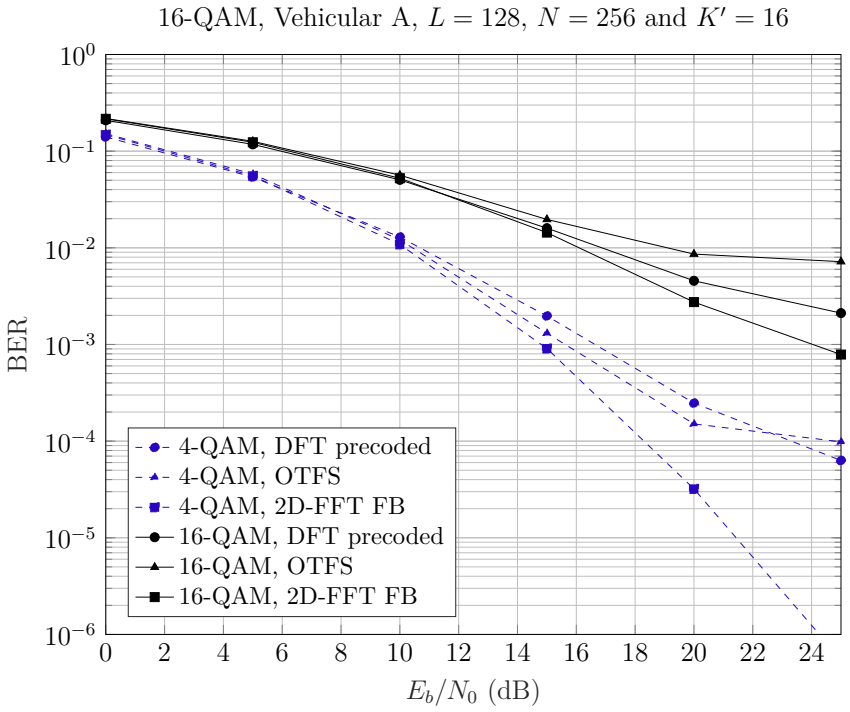

Figure 48 – Error performance comparison using time-frequency domain equalizer for a velocity of 300 km/h.

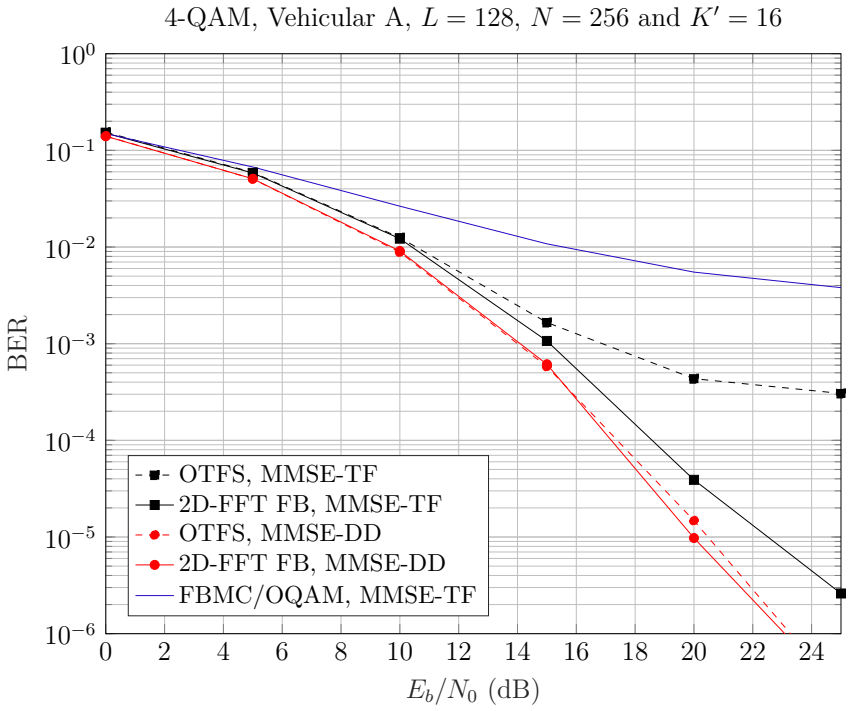

Figure 49 – Error performance comparison using time-frequency domain equalizer (MMSE-TF) and delay-Doppler domain equalizer (MMSE-DD) for 4-QAM and velocity of 400 km/h.

when compared to the proposed system with the same equalizer.

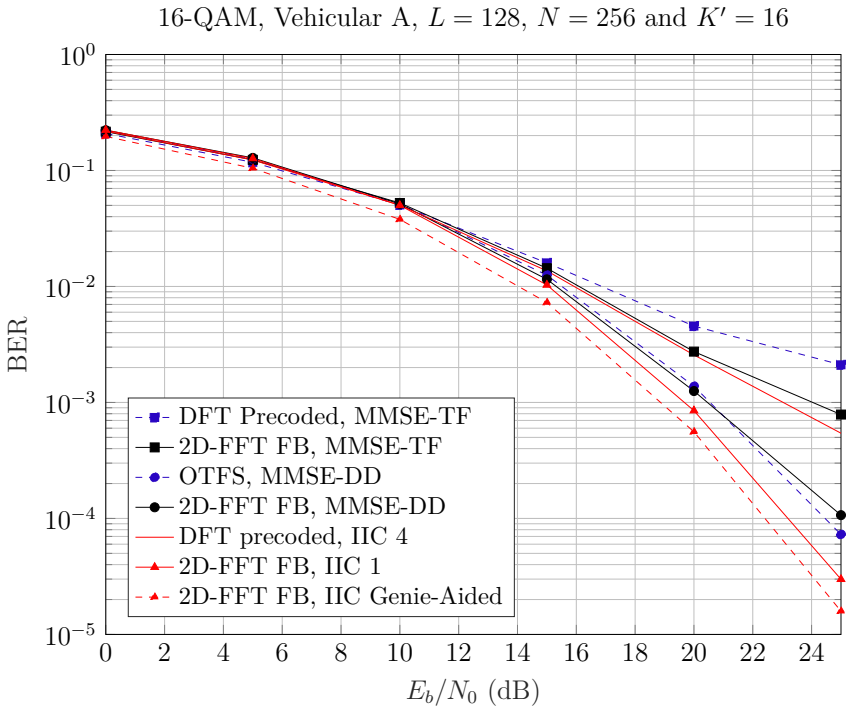

Figure 50 – Error performance using different receivers for 16-QAM and a velocity of 300 km/h.

Figure 50 presents the results using the proposed IIC receiver for a velocity of 300 km/h and a 16-QAM modulation. Note that the IIC receiver has less computational complexity than the full delay Doppler one applied to OTFS and still has superior performance with just one iteration. It should also be noted that even with one iteration, the receiver approaches the maximum performance that can be obtained as shown by the Genied-Aided curve. It is worth to note that this hybrid receiver cannot be used with a OTFS transmission, due to the error propagation phenomenon caused by the use of frequency domain equalization (which is the first stage of the proposed IIC equalizer). For the DFT precoded scheme, even with 4 iterations the performance of the IIC receiver is not significantly improved when compared to its use in the proposed system. Moreover, for the MMSE-DD receiver OTFS and 2D-FFT achieve similar performances. The difference will be on account of the computational complexity, PAPR and OOB emissions.

Observing the system as a whole in its final version, it can be seen that its structure has some similarities with that of the OTFS system. However, this structure was obtained at with an inside-out approach - from the filter bank to pre- and post-processing. Initially, it is concerned with recovering complex orthogonality, eliminating interference from the filter in the time domain (spreading via DFT combined with the compensation factor) and in the frequency domain (data transmission strategy). From this stage, analyzes were started in order to obtain a novel waveform that adds robustness in high mobility scenarios, preserving this complex orthogonality and maintaining a low PAPR. The crucial

point here is to see that the restoration of complex orthogonality can be done using part of the ISFFT (with strategic changes). From a direct analysis of the OTFS system, it seems to us that the use of the FBMC technique is not evident due to the loss of complex orthogonality. In short, our proposal does not require a cyclic prefix and, in the multiuser context, it provides a high level of spectral separation between users. In addition, through the filtering process the frequency domain onte-tap equalizer present in the OFDM can be implemented in the receiver in a simple way, obtaining good results. This allowed to introduce a hybrid receiver that uses a frequency-domain equalization stage combined with a delay-Doppler domain interference canceller. Such a receiver presents good error performance even in comparison with more complex receivers applied in OTFS exclusively in the delay-Doppler domain.

The precoded systems via filter bank presented in this work, have complex orthogonality. In this sense, the use of OQAM modulation is avoided, but the transmission of complex data in half of the subcarriers of a multicarrier symbol at a doubled rate. One issue that has not been explored is the requirement to keep transmitting every $T/2$ seconds from the FBMC/OQAM, a fact that is no longer needed in the studied systems. In the next chapter we will see that we can change the waveform design in terms of transmission through the filter bank and obtain some significant characteristics for the system.

6 Generalized version of precoded filter bank systems via rate factor

The precoding method introduced in this work allows recovering complex orthogonality. This fact allows the transmission of complex QAM symbols and no longer OQAM symbols using the concept of double rate transmission through two transmission chains via polyphase networks. However, this type of double rate transmission is specific to OQAM modulation, where it is no longer needed. In this context, it is possible to modify the structure of the signal transmitted via the filter bank, making the waveform project more flexible and exploring some characteristics. In this chapter we will generalize the proposed precoded filter bank systems to obtain significant advantages in terms of PAPR and robustness in high mobility scenarios. Through the proposed matrix structure, a performance analysis of the SINR, SIR and BER is performed.

6.1 Rate Factor

As was seen, the symbol transmission in the TF domain $x_{l,k}$ through multicarrier system can be expressed by equation (2.31) and repeated here by convenience

$$s[m] = \sum_{l=0}^{L-1} \sum_{k=0}^{K'-1} x_{l,k} g_{l,k}[m] \tag{6.1}$$

Note that the version shifted in time and frequency of the filter $g_{l,k}[m]$ as well as the prototype filter $g[m]$ used define the used transmission scheme, either OFDM or FBMC. In FBMC/OQAM systems, symbols are transmitted every $L/2$ sample with the same transmission capacity as in OFDM system. Now, we propose to generalize the transmission rate for L/β and adopt the QAM modulation. Basically, β is what we call a rate factor - it must necessarily be a power of two and will be the term that will produce the modified structure of the waveform. Applying the rate factor, (see (2.32)) can be generalized as

$$g_{l,k}[m] = g[m - kL/\beta] e^{j\frac{2\pi l}{L}(m - kL/\beta)}. \tag{6.2}$$

The term β determines the interval of samples in which the symbol transmission is performed. For example, (2.31) can represent a symbol transmission $x_{l,k}$ by an OFDM modulator if $\beta = 1$ and $g_{l,k}[m]$ is a rectangular filter with $O = 1$. In this case, symbols are transmitted every L samples. For the case where the prototype filter is not a rectangular window with a longer length, interference is generated due to the superposition of the pulses, breaking the complex orthogonality between them. This way enters our pre-coding whether based on the ISFFT (2D-FFT FB) or just on the frequency spreading (DFT

precoded FB). The data stream itself must also be modified to avoid filter interference in the frequency domain. The vector $\mathbf{a}_k$ for DFT precoded filter bank or the matrix $\dot{\mathbf{A}}$ now has L/β complex symbols that are compensated by the filter compensation factor ($\tilde{\mathbf{b}}$) and are inserted into the $L/2\beta$ first and last DFT positions of L points. Note that by increasing β from 2 to 4 or 8, for example, we transmit fewer data. However, these L/β data will be spread over L subcarriers and transmitted by the filter bank operating with a rate factor β, guaranteeing the maximum transmission capacity.

Finally, our transmission matrix must be modified in order to support such a generalization. Thus, let us consider the diagonal matrix $\mathbf{G}_o$ corresponding to the filter coefficients, that is, $\mathbf{G}_o = \text{diag}(\mathbf{g}_o) \in \mathbb{R}^{N/\beta \times N/\beta}$ for $o = 0, 1, 2, ..., \beta O - 1$, where $\mathbf{g}_o$ is given by $\mathbf{g}_o = [g[oN/\beta], g[oN/\beta + 1], \ldots, g[oN/\beta + N/\beta - 1]]$. Then, we define the matrix $\tilde{\mathbf{G}}_o \in \mathbb{R}^{N/\beta \times N}$ as follows

$$\tilde{\mathbf{G}}_o = \Big[\underbrace{\mathbf{0} \;\; \mathbf{0} \;\; \ldots}_{(o \bmod \beta) \text{ times}} \quad \mathbf{G}_o \quad \underbrace{\mathbf{0} \;\; \ldots \;\; \mathbf{0}}_{\beta - 1 - (o \bmod \beta) \text{ times}} \Big] \tag{6.3}$$

where the number of arrays of zeros of size $N/\beta \times N/\beta$ around the coefficients array of the filter $\mathbf{G}_o$ depends on the value of o and β. Thus, the Toeplitz matrix of the filter $\mathbf{G} \in \mathbb{R}^{ON + (K-1)N/\beta \times NK}$ can be expressed as:

$$\mathbf{G} = \begin{bmatrix} \tilde{\mathbf{G}}_0 & \mathbf{0} & \mathbf{0} & \ldots & \mathbf{0} \\ \tilde{\mathbf{G}}_1 & \tilde{\mathbf{G}}_0 & \mathbf{0} & \ldots & \mathbf{0} \\ \tilde{\mathbf{G}}_2 & \tilde{\mathbf{G}}_1 & \tilde{\mathbf{G}}_0 & \ddots & \vdots \\ \vdots & \tilde{\mathbf{G}}_2 & \tilde{\mathbf{G}}_1 & \ddots & \mathbf{0} \\ \vdots & \vdots & \tilde{\mathbf{G}}_2 & \ddots & \tilde{\mathbf{G}}_0 \\ \tilde{\mathbf{G}}_{O\beta-1} & \vdots & \vdots & \ddots & \tilde{\mathbf{G}}_1 \\ \mathbf{0} & \tilde{\mathbf{G}}_{O\beta-1} & \ldots & \ddots & \tilde{\mathbf{G}}_2 \\ \vdots & \mathbf{0} & \tilde{\mathbf{G}}_{O\beta-1} & \ddots & \vdots \\ \vdots & \vdots & \vdots & \ddots & \vdots \\ \mathbf{0} & \mathbf{0} & \mathbf{0} & \ldots & \tilde{\mathbf{G}}_{O\beta-1} \end{bmatrix}. \tag{6.4}$$

Therefore, by applying the convolution between the IDFT output of vector $\mathbf{x}_k$ and the filter impulse response represented by the Toeplitz matrix $\mathbf{G}$ we generate the output data vector $\mathbf{s}$ now of length $M = ON + \frac{N}{\beta}(K' - 1)$, as follows:

$$\mathbf{s} = \underbrace{\mathbf{G}\tilde{\mathbf{W}}^H}_{\bar{\mathbf{G}}}\mathbf{x} = \bar{\mathbf{G}}\mathbf{x} \tag{6.5}$$

Now, the symbols are delayed each N/β samples. Considering an OFDM symbol of length L as a reference, each symbol in the generalization of the filter bank is composed by $L/(\beta)$ complex symbols plus $L((\beta - 1)/\beta)$ zeros. These symbols are spread in the frequency domain through an L-point DFT and transmitted using a rate factor equal to β, to

obtain the same transmission capacity as OFDM. Figure 51 shows OFDM, FBMC/OQAM symbols and the ones from the proposed system with $\beta = 4$, all with the same duration T. Of course, to maintain the same density of transmitted symbols, FBMC/OQAM symbols are transmitted every $T/2$ while in our system every T/(β) with $\beta = 4$. That is, to maintain the same symbol transmission rate, the conventional FBMC system, for example, doubles the network/block density in time (K) in relation to OFDM when adopting OQAM. In this way, we define the number of multicarrier symbols for the networked systems is given by $K' = \beta K$ in order to maintain the same transmission capacity. We highlight that in all our comparisons the same symbol duration was adopted for all schemes. Basically,

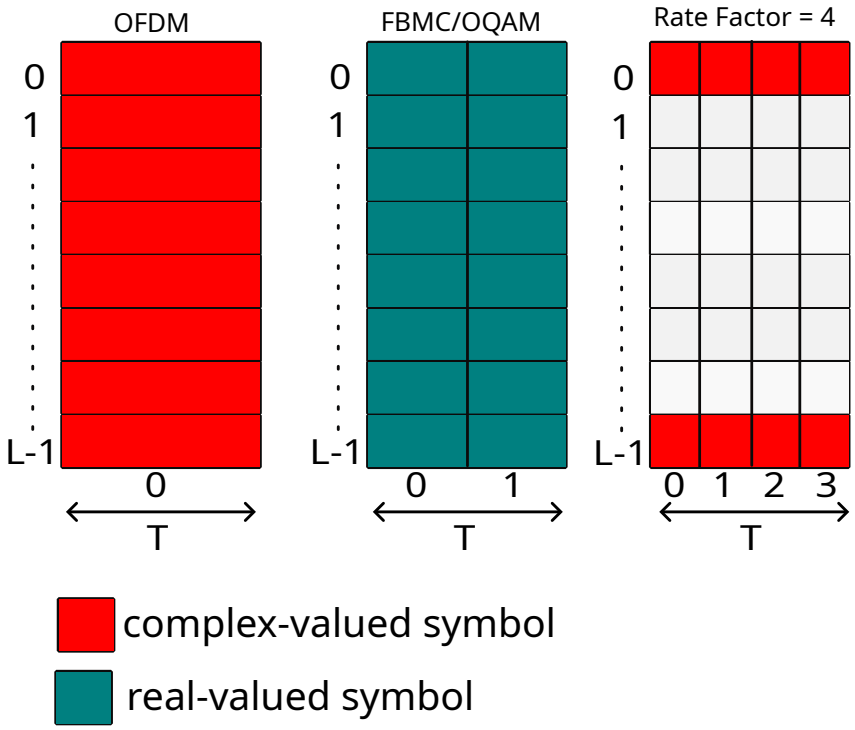

Figure 51 – Time-frequency grid for OFDM, FBMC/OQAM and 2D-FFT systems.

the system increases β times the density of the lattice/grid in time in relation to OFDM to maintain the transmission symbol rate. While the overall symbol density within a given interval is always the same, the rate factor parameter allows us to tune the system in order to shorten the symbols. These shorter symbols will make the system less susceptible to the Doppler effect and lower the PAPR, at a cost of greater computational complexity, since the system will transmit β times during the symbol period. An alternative view in terms of the transmission process is to analyze the symbol chains by the two PPN of Figure 12 and in the first matrix notation of the transmission of symbols via filter bank via matrices (equation (2.57)). We can see that after the N-IDFT, the $K' = \beta K$ symbols are split into β streams such that each stream has a time-frequency grid of dimensions $L \times K$. Each flow passes through the filter described via PPN and receives its respective delay to be summed, generating the transmitted signal $\mathbf{s}$ at a rate β. Thus, we use the PPN β times.

Figure 52 presents this structure for $\beta = 4$. If we consider the first version of the matrix equation derived in equation (2.57), we would have a summation with β terms where each term represents the filtering of $K'\beta$ multicarrier symbols by a PPN plus their respective delays. Note that for the second flow onwards there is a delay of N/β ($\beta = 4$) samples in relation to the previous flow. The structure of new matrix $\mathbf{G}$ itself does this process transparently. The representation as a sum of matrices delayed among themselves can be seen in [75].

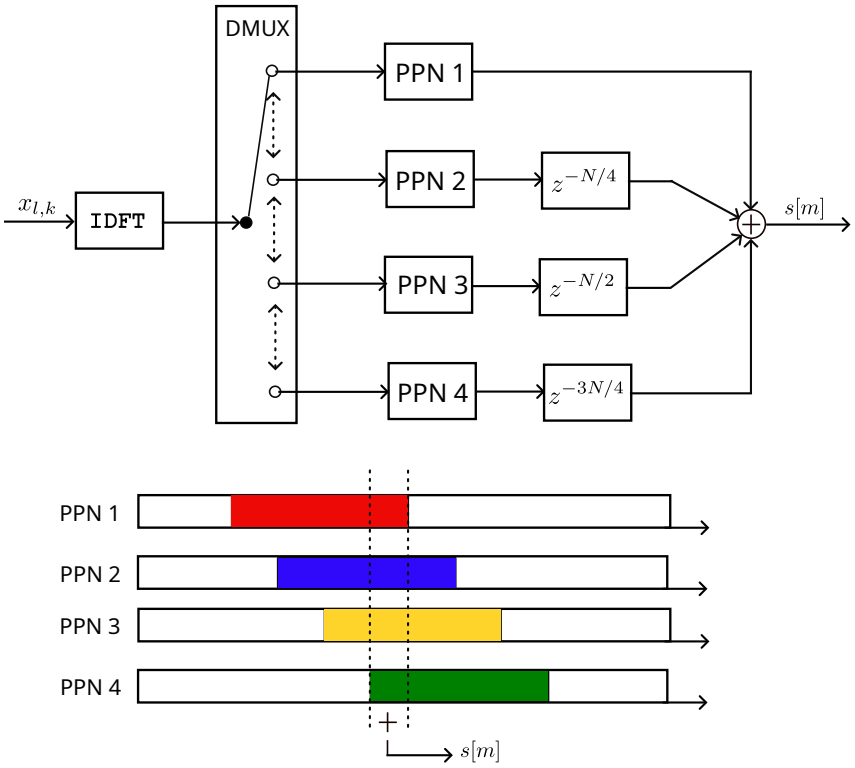

Figure 52 – Each colored block corresponds to $L/4$ information data spread over L subcarriers. In OFDM in a time slot, L complex symbols are transmitted. In our proprosed systems with the rate factor, L/β complex symbols are transmitted in β time slots.

Regarding the recovery of complex orthogonality, some subtle changes are observed. First, the frequency spread increases, and due to the change in data allocation, the compensation stage is now expressed by .

$$[\tilde{\mathbf{b}}]_{\tilde{l}} = \begin{cases} \sqrt{\frac{1}{[\tilde{\mathbf{c}}]_{\tilde{l}}}}, & \text{for } \tilde{l} = \left[0, \ldots, \frac{L}{2\beta} - 1; L - \frac{L}{2\beta} - 1, \ldots, L - 1\right] \\ 0, & \text{otherwise} \end{cases} \tag{6.6}$$

Second, generalizing for any value of β we have that the width of the selected pulse is now L/β. Thus, as the selected pulse starts at time $OL/2 - L/2\beta$, we arrive at a new

relationship between the overlap factor O and the rate factor β described by

$$OL - \left(\frac{O.L}{2} - \frac{L}{2\beta}\right) \leq L$$
$$O + \frac{1}{\beta} \leq 2 \tag{6.7}$$

For the conventional case with $\beta = 2$, we maintain our relationship that the overlap factor needs to be less than or equal to 1.5. However, note that for $\beta = 4$ and 8, we can increase the overlap factor to 1.75 and 1.875, respectively. Depending on the filter being used, this small increase over the filter's overlap factor can be useful. However, in general, this benefit of increasing β is not as significant. We will see below that the main advantages of generalization of the filter bank structure are in terms of PAPR and error performance in high mobility scenarios.

6.2 Error Performance Analysis

The theoretical analysis will be illustrated only for the proposed techniques (2D-FFT and DFT precoded filter bank) considering that the performance of the OFDM, FBMC and SC-FDMA techniques are already known in the literature. The overall equation and obtaining the SIR and SINR equations could be derived previously, however to encompass all the two proposed systems and with the rate factor β, it was decided to invest in this question only at the end, after the derivation of all the proposed waveforms. Thus, using the input-output ratio of the entire transmission system defined by the vector $\tilde{\mathbf{a}}$ and repeated here for convenience, we have the global transmission of data symbols given by

$$\tilde{\mathbf{a}} = \underbrace{\mathbf{C}^H \text{diag}\{\mathbf{e}\} \bar{\mathbf{G}}^H \mathbf{H} \bar{\mathbf{G}} \mathbf{C}}_{\mathbf{\Delta}} \mathbf{a} + \underbrace{\mathbf{C}^H \text{diag}\{\mathbf{e}\} \bar{\mathbf{G}}^H}_{\mathbf{\Upsilon}} \mathbf{n}. \tag{6.8}$$

Remembering that $\mathbf{C}$ is equal to $(\mathbf{I}_K \otimes \mathbf{C}_f)$ for DFT precoded FB and equal to $(\mathbf{I}_K \otimes \mathbf{C}_f)(\mathbf{W}_K^H \otimes \mathbf{I}_L)$ for 2D-FFT. We will only consider the MMSE-TF equalizer in the SINR analysis since the iterative nature of the interference cancellation algorithm and the IB-DFE makes it difficult to obtain this theoretical derivation. Considering the independent and identically distributed transmitted symbols of zero mean and unity power and without statistical relation to noise, the SINR can be calculated by

$$\text{SINR}_{l,k}(\mathbf{H}) = \frac{1}{\sum_{w=1}^{LK} \left| [\mathbf{\Delta} - \mathbf{I}_{LK'}]_{q,w} \right|^2 + \sigma_n^2 \sum_{w=1}^{M} \left| [\Upsilon]_{q,w} \right|^2} \tag{6.9}$$

with $q = L(k-1)+l$ describing the q-th position of the line corresponding to the subcarrier l and the time k. Through the SINR expression it is possible to calculate the instantaneous bit error probability (BEP) (i.e., the BEP for a given channel realization). Thus, assuming Gaussian approximation is used for the interference, the BEP to each channel realization

can be obtained according to [38]

$$\mathrm{BEP} = E_{\mathbf{H}}\left\{ \frac{1}{K'} \sum_{k=1}^{K'} \frac{1}{L/\delta} \sum_{\tilde{l}} \mathrm{BEP}_{\mathrm{AWGN}}\left\{ \mathrm{SINR}_{\tilde{l},k}(\mathbf{H}) \right\} \right\} \tag{6.10}$$

where $\mathrm{BEP}_{\mathrm{AWGN}}$ is the BEP for the case of an AWGN channel specified in [76] and the expectation $E_{\mathbf{H}}\{\,\cdot\,\}$ is obtained through a Monte Carlo simulation.

A time-varying channel, with strong Doppler spread, can lead to significant interference effects. To describe only the influence of a doubly selective channel, we will ignore the noise and remove the equalizer at $\mathbf{\Delta}$, resulting in $\bar{\mathbf{\Delta}} = \mathbf{C}^H \bar{\mathbf{G}}^H \mathbf{H} \bar{\mathbf{G}} \mathbf{C}$. Evaluating the entire received block, we can calculate the SIR dependent on the channel realization as follows:

$$\mathrm{SIR} = \frac{\left|\mathrm{diag}\{\bar{\mathbf{\Delta}}\}\right|^2}{\sum_{i=1}^{LK} \left|[\bar{\mathbf{\Delta}}]_{\underline{lk},i}\right|^2 - \left|\mathrm{diag}\{\bar{\mathbf{\Delta}}\}\right|^2}. \tag{6.11}$$

Doubly selective channels are characterized by off-diagonal non-null values in $\bar{\mathbf{\Delta}}$. On the other hand, diagonal elements describe the desired signal components. For 2D-FFT system, Figures 53 and 54 show how the SIR changes for ITU-T Pedestrian A and Vehicular A channels respectively, considering different velocity values and for a 32 subcarriers spaced each $F = 15\mathrm{KHz}$. For the Pedestrian A channel model it can be seen that even at high

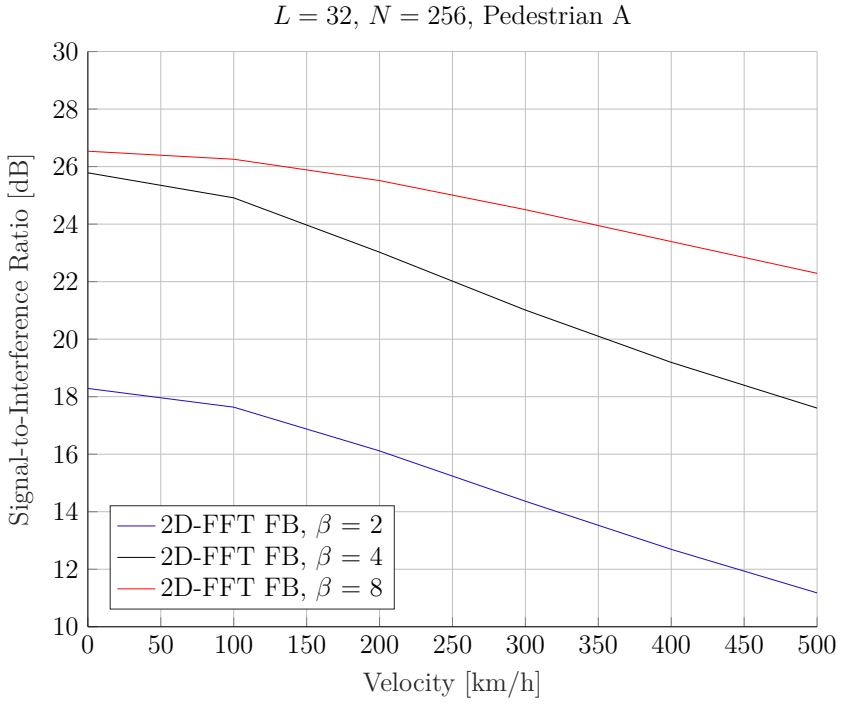

Figure 53 – SIR analysis against velocity for Pedestrian A channel model.

velocitys, such as 300 km/h, the SIR remains at a sufficiently high level, mainly in the cases where $\beta = 4$ and 8. We have a similar behaviour, for the Vehicular A channel, when

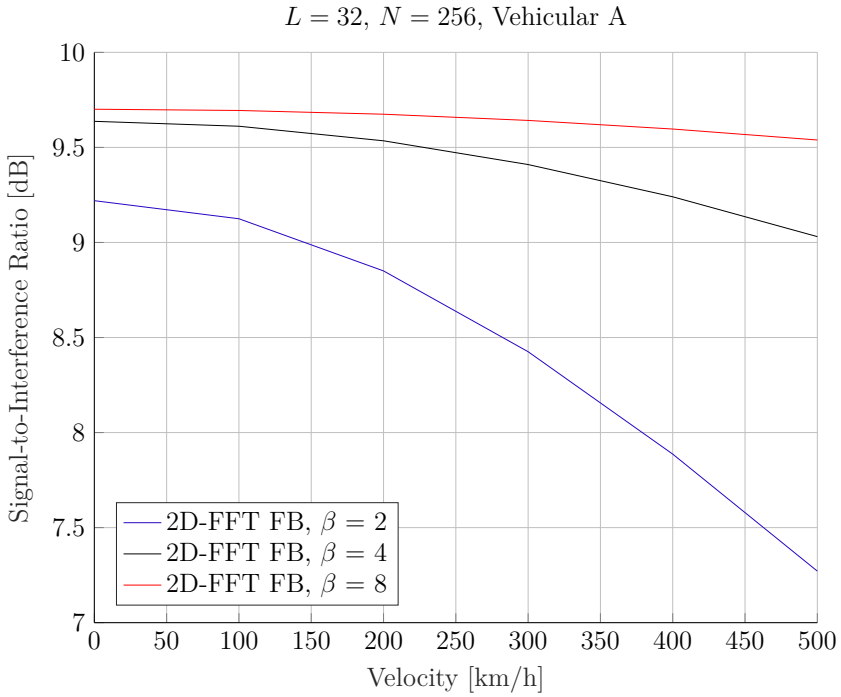

Figure 54 – SIR analysis against velocity for Vehicular A channel model.

compared to the previous scenario, but with a worse SIR performance due to the channel model being more selective, inducing more interference. Finally, it can be seen that for both cases, we have an increase in the SIR level when increasing β, with the SIR values decreasing more slowly when increasing velocity.

6.3 Numerical Analysis

We will now present the impact of the generalization of the systems proposed in this work in terms of BER and PAPR. Among the iterative receivers introduced, it was decided to apply the IB-DFE to 4 iterations due to its lower computational complexity. The considered β values are 2, 4 and 8 and the total number of subcarriers equals 1024, i.e. we will have $K' = 8\beta$ multicarrier symbols each with $L = 128$ subcarriers spaced apart by 15 KHz. The variation in the value of K' is necessary in order to maintain the same density of transmitted symbols for all values of β, since we transmit at a rate L/β. We highlight that in all our comparisons the same multicarrier symbol duration was adopted for all schemes. The truncated hermite filter was applied to all scenarios to obtain $O = 1.5$ so that the interference in the system is entirely due to the channel and noise. The theoretical BER curves for the one-tap equalizers were obtained using the equation (6.10) for both the DFT precoded and 2D-FFT filter bank schemes. We will analyze first only for the DFT precoded scheme in SISO scenarios and also with multiple antennas in reception. Then we compare these results with 2D-FFT and OTFS. The rest

of the parameters are practically the same as in the previous analyses, only with some additions that will be specified when necessary.

6.3.1 Rate factor in DFT precoded filter bank

Figure 55 presents the BER for DFT precoded filter bank scheme using 16-QAM, MMSE equalizer with the Vehicular A channel model for situations without and with mobility. Note that in no mobility, the system has the same BER for different values of the rate factor β. However, when mobility ($\vartheta = 300$ km/h) is considered it is possible to

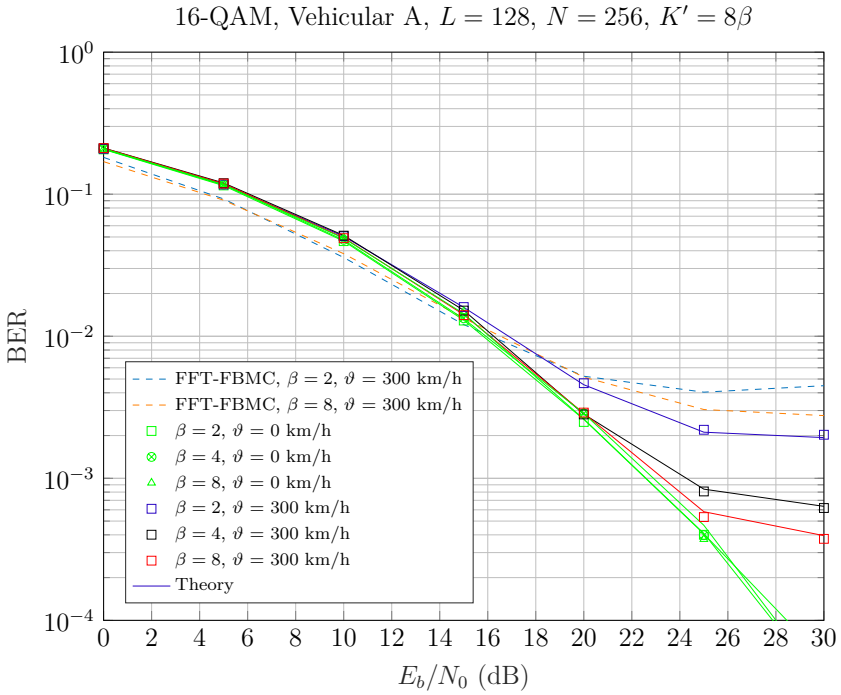

Figure 55 – BER for DFT precoded filter bank to 16-QAM with and without mobility using MMSE-TF equalizer.

observe a significant performance improvement for SNRs above 18 dB; moreover, $\beta = 4$ is enough to guarantee a good performance in this scenario. It is possible to see a 4 dB gain between $\beta = 2$ and $\beta = 4$ or 8 at a BER of approximately 3×10^{-3}. This improvement happens because with higher values of β multiple shorter symbols are transmitted, which can cope better with the fast variations induced by the Doppler effect. For comparison, in Figure 55 we also present curves for the system seen in [77], called FFT-FBMC, with $\beta = 2$ and 8 for 16-QAM with a velocity of 300 km/h. A total of 1024 subcarriers were also used, but with $L = 32$ and $K = 64$ - this configuration brings better results for FFT-FBMC. Unlike our generalized scheme that aims to reduce PAPR and improve performance in high mobility scenarios, the FFT-FBMC system only aims to restore the complex orthogonality using time spreading through an OFDM waveform (IDFT + cyclic prefix). Thus, even for $\beta = 2$ the DFT precoded has superior performance. Moreover, by increasing β for

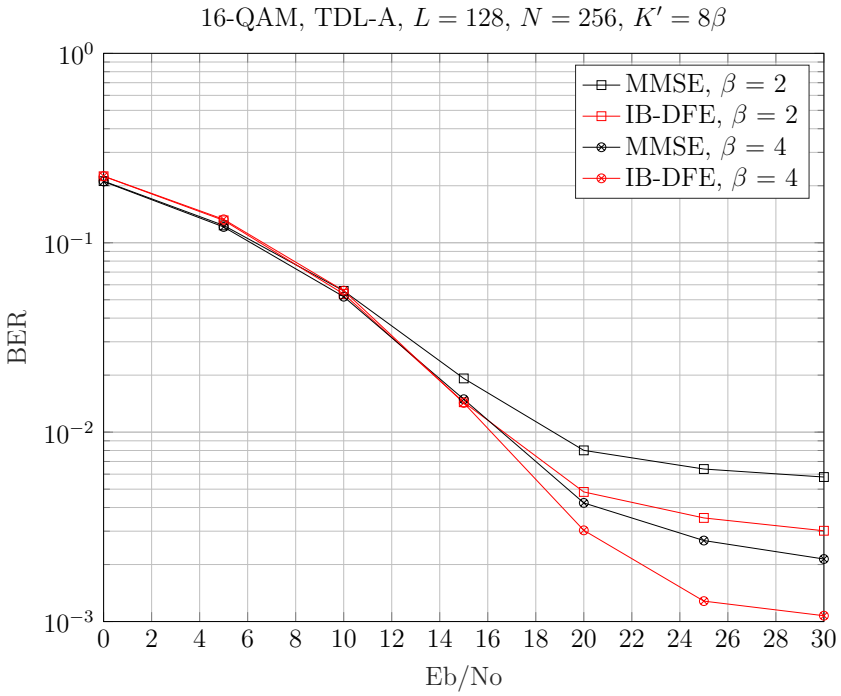

Figure 56 – BER for DFT precoded filter bank to TDL-A channel with velocity of 300 Km/h.

FFT-FBMC there is little improvement in terms of BER. Through frequency spreading pulses become shorter in time and, therefore, are more robust to time variations [38]. As for FFT-FBMC, where spreading is performed in time, the robustness is in terms of the delay spread; however, the Doppler spread must be low. For these reasons, it is more interesting to study the FFT-FBMC system with the rate factor in terms of the impact on the rejection of interference coming exclusively from the filter to recover the complex orthogonality. Finally, it is noted that the theoretical curves practically correspond to those simulated validating the performance of the system. The small variations between theoretical and simulated curves at high SNR values come from the fact that the channel interference is not purely Gaussian. In general, the larger the value of L, the more valid the Gaussian approximation for the interference will be.

Combining the rate variation with the IB-DFE equalizer in the mobility scenario, the error performance becomes even more significant, as shown in Figure 56. For this experiment, we used the TDL-A channel model, however, now with a very long delay spread of 2000 ns. Because of this large delay spread, performance is affected. However, note that the iterative equalizer does its job of eliminating residual channel interference. Again, there is a significant improvement due to the rate factor and this improvement is further leveraged by the iterative equalizer.

The explanation for this improvement can be demonstrated by analyzing the time-frequency grid. By increasing β the temporal duration of the transmitted symbols decreases.

Thus, the shorter the duration of a symbol, more symbols will be transmitted within the channel coherence time, and therefore, a greater number of symbols are transmitted with a constant channel impulse response, decreasing the Doppler effect.

6.3.1.1 Multiple antennas at reception

To exploit the available diversity and provide better error performance, multiple antennas can be employed at the receiver. This single-input multiple-output (SIMO) scheme, with one antenna on the transmitter and several on the receiver, can be suitable for uplink, where low-cost terminals are used as the transmitter and, for example, a base station is the receiver. Let us explore the impact of this waveform change using multiple antennas in receiver with iterative equalizer in a high mobility scenario. This diversity imposed on the reception was done via maximum ratio combination (MRC) where the output $\mathbf{y}$ is weighted before the one-tap equalizer to aggregate the signals. For Vehicular A channel model with velocity of 300 km/h, Figure 57 illustrate the error performance in this scenario with two antennas in reception. It is noticeable that the rate factor also

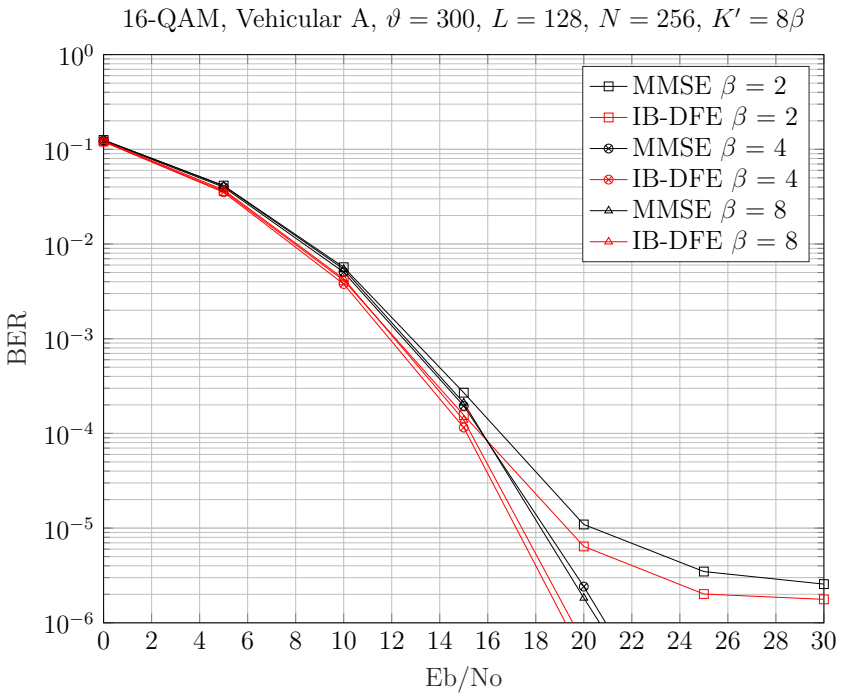

Figure 57 – BER for DFT precoded filter bank to Vehicular A channel with velocity of 300 Km/h and two antennas at the reception.

generates a considerable performance gain in this configuration and that for $\beta = 4$ and 8, the performance of the equalizers is practically the same as that of the MMSE equalizer. For the MMSE equalizer with $\beta = 4$ and BER of 2×10^{-6}, we have a gain of 5dB compared to the IB-DFE equalizer with $\beta = 2$. Figure 58 presents the same scenario, but for the TDL-A channel model with very long delay spread (2000ns). Again there is a significant

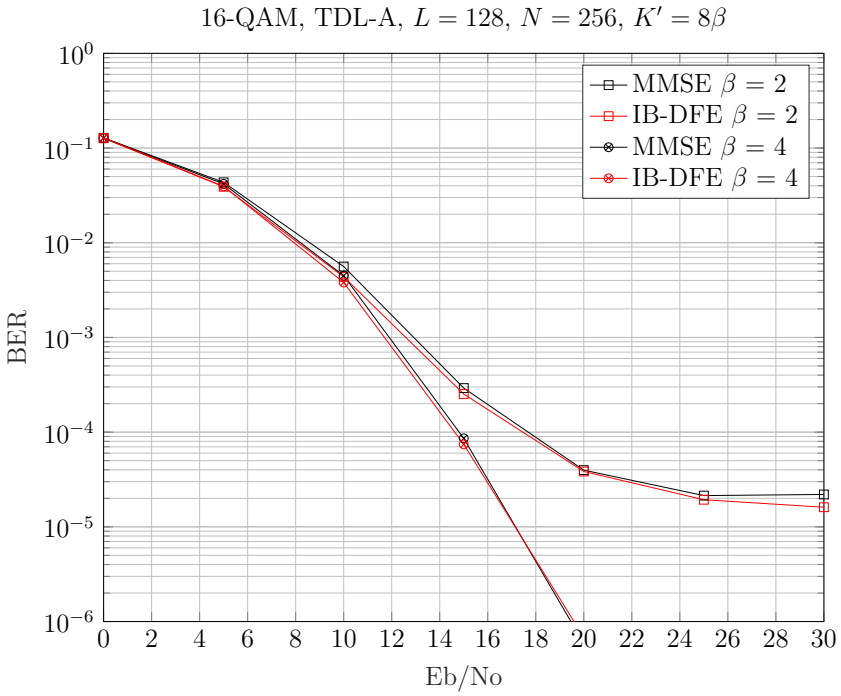

Figure 58 – BER for DFT precoded filter bank to 16-QAM, TDL-A channel with velocity of 300 Km/h and two antennas at the reception.

improvement due to the rate factor, where for a BER of 10^{-5} there is a difference of approximately 3 dB between $\beta = 2$ and 4. In this situation of multiple antennas with a more aggressive channel, it is observed that the inclusion of the more robust equalizer did not have as much effect. The improvement regarding the iterative equalizer was restricted to the SISO case for this scenario.

The generalized DFT precoded filter bank system presents robustness to doubly selective channels. The use of a more robust receiver with multiple antennas or with an iterative equalizer showed a considerable performance gain. In the mobility scenarios presented in this work, it was shown a good advantage of the iterative receiver in a SISO scenario allied with the rate factor, while for SIMO scenarios the rate factor prevailed for the good performance in terms of bit error rate. Due to its characteristics of low latency (due to a short prototype filter) and robustness to mobility scenarios, the proposed system is a great alternative to the uplink. Thus, according to the transmission scenario, the use of multiple antennas in the reception associated with the rate factor can be flexibly applied to obtain a better performance in the uplink.

6.3.2 Rate factor in 2D-FFT filter bank

The performance gain in high mobility scenarios was noticeable for the generalized DFT precoded filter bank in the presented situations. Filter bank generalization is also studied and applied to the 2D-FFT FB system. We limit our analysis to the Vehicular A

channel model. However, we add for comparison the OTFS system using the MMSE-DD equalizer and the Simplified First Order AMP (AMP-FO) technique proposed by [28]. The addition of this last receiver is interesting for comparison, as it is a robust and simpler algorithm than the conventional AMP algorithms, widely studied in OTFS systems. This receiver also operates iteratively, using 15 iterations and a damping factor of 0.6 as used in [29]. In addition to the IB-DFE, this same receiver is applied to the 2D-FFT scheme with these same parameters in order to demonstrate its compatibility with OTFS. As shown in this work, the IB-DFE equalizer is not applied to the OTFS system, due to the unreliable first estimates of the direct filter (TF domain) provided for the feedback filter in the iterative process.

Figure 59 shows the BER for 4-QAM modulation and a velocity of 400 km/h. Note that for $\beta = 8$ the DFT precoded filter bank system has lower performance than 2D-FFT with $\beta = 2$, showing the higher robustness of the 2D-FFT scheme to Doppler spread. Compared to OTFS with the computationally complex MMSE-DD equalizer, our proposed system using the low complexity MMSE-TF equalizer and $\beta = 4$ has similar error performance, thus validating the proposed study. Moreover, if we apply the proposed IB-DFE equalizer there is a performance gain of approximately 3 dB for a BER of 10^{-5} when compared to MMSE-DD OTFS. This makes it possible to use only 2 iterations for the IB-DFE and $\beta = 2$, thus reducing receiver complexity and obtaining a good error performance.

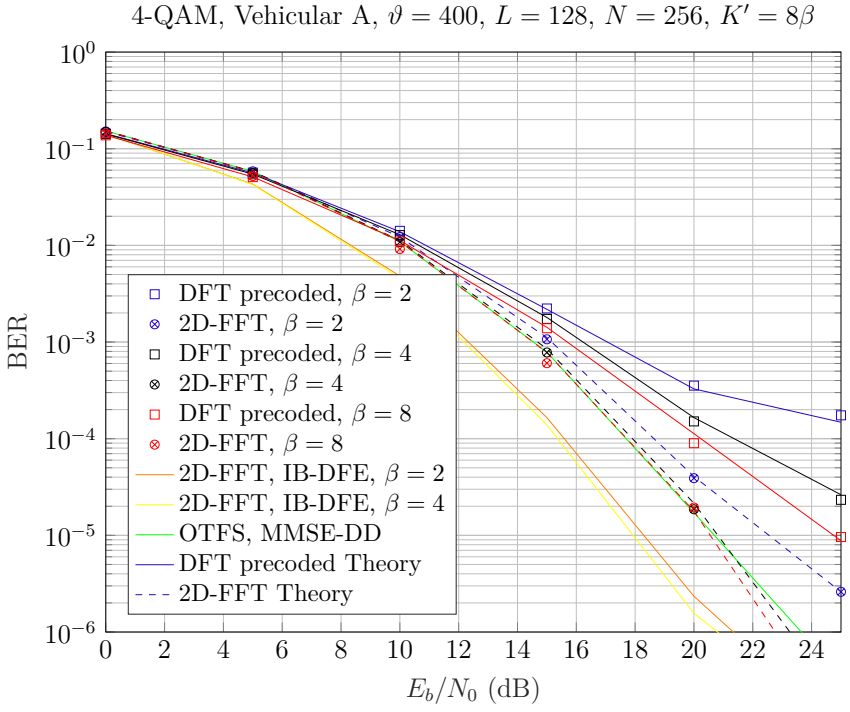

Figure 59 – Error performance comparison for 4-QAM and a velocity of 400 Km/h.

Figure 60 presents a direct comparison between the 2D-FFT and DFT precoded

filter bank systems with the one-tap MMSE equalizer in the TF domain, now for 16 QAM and velocity reduced to 300 km/h. The performance gain in the mobility scenario is again

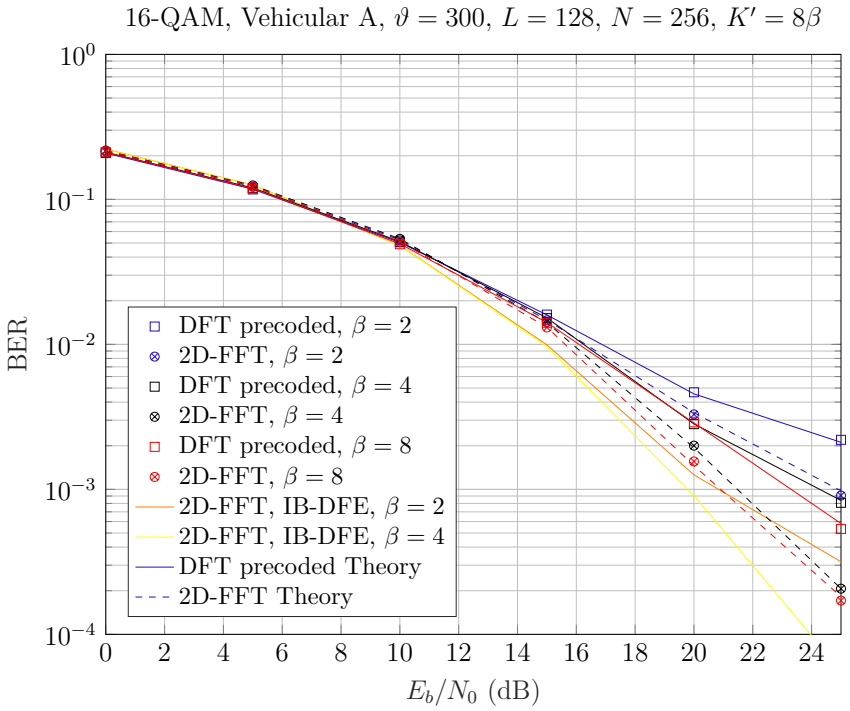

Figure 60 – Error performance comparison for MMSE-TF and IB-DFE to 16-QAM and a velocity of 300 km/h.

noted when the rate factor is varied for both systems. As we saw, such variation has a greater impact for the technique proposed in this work. The SIR analysis of Section 6.2 explains the results shown beforehand with respect to the variation of the rate factor β. From $\beta = 2$ to $\beta = 4$ there is a substantial performance gain, whereas from $\beta = 4$ to $\beta = 8$ the gain is reduced, as seen in Figures 54, 59 and 60. Taking into account the OTFS technique now, Figure 61 presents the BER curves for the same scenario presented in Figure 60. The 2D-FFT with MMSE-TF and IB-DFE, OTFS MMSE-DD and OTFS AMP-FO schemes were used for this comparison. As can see, the OTFS with AMP-FO technique slightly outperforms our schemes with one-tap MMSE equalizers for E_b/N_o lower than 16 dB. On the other hand, the IB-DFE equalizer with 4 iterations and $\beta = 4$ outperforms all others techniques for E_b/N_o greater than 17 dB. Note that the 2D-FFT scheme was implemented using the AMP-FO technique and obtained better BER performance than OTFS AMP-FO demonstrating the compatibility of the proposed scheme with OTFS. In the case of using the variation of the β factor with this receiver, the performance will certainly be even better. Finally, again the theoretical curves for the MMSE-TF equalizer calculated from SINR and BEP are very close to those simulated.

Due to the performance gain in high mobility scenarios for the DFT precoded filter bank, the rate factor was expected to have the same behavior for the 2D-FFT FB

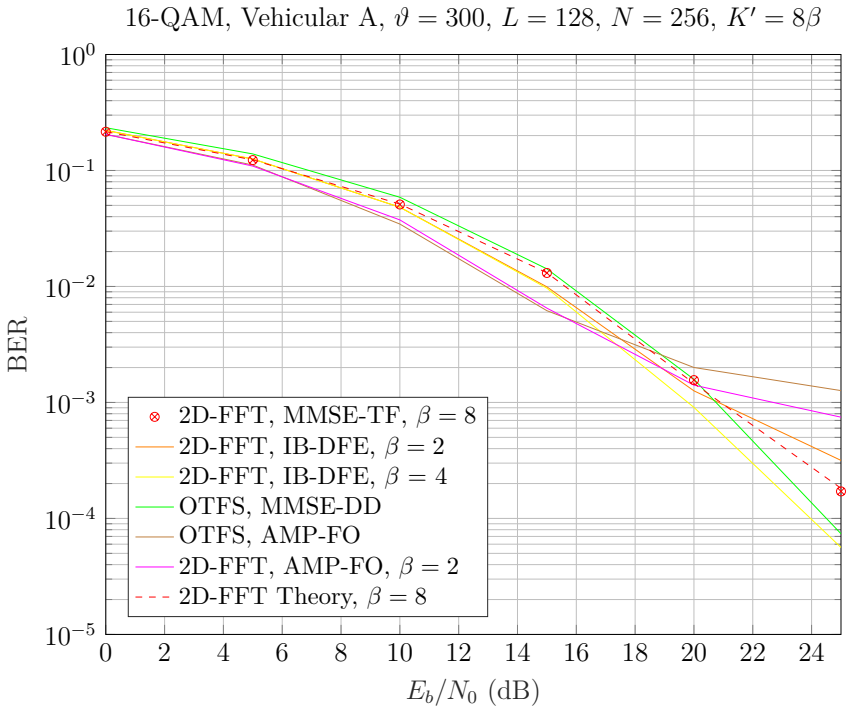

Figure 61 – Error performance comparison for 16-QAM and a velocity of 300 Km/h.

system. The performance gain appears, however, and an even larger scale obtaining satisfactory results even using a simple equalizer in the TF domain. It is possible to obtain performances similar to those obtained with much more complex receivers in the Doppler-delay domain using an equalizer with only one coefficient per subcarrier.

In terms of PAPR, Figure 62 illustrates a comparison CCDF of the PAPR considering the generalized structures and the OTFS system, for a 4-QAM signal constellation and $L = 128$ subcarriers. A uniform reduction of the PAPR is observed when we change β from 2 to 4 and 8. As seen in Section 6.1, by varying the rate factor less data is transmitted per symbol; however, this transmission is done in a faster way, guaranteeing the symbol density for all scenarios. Thus, we have a reduction in PAPR of about 3 dB between each variation of the rate factor β. This makes sense if we analyze that with the increase of the rate factor, L/β symbols are transmitted, i.e. for each variation of β we have a reduction of half of the symbols to be transmitted in each time interval. Thus, it is possible to use the rate factor to tune the PAPR of the 2D-FFT FB system to better cope with transmitters sensitive to high PAPR.

The table 10 presents the computational complexity of the receivers used in this work. Clearly, the one-tap equalizer in the TF domain MMSE-TF is the simplest. On the other hand, the MMSE solution in the DD domain, using the traditional matrix inversion, requires the greatest complexity. For the IB-DFE equalizer, due to the iterative process the term $\bar{i}$ is the maximum number of iterations used, while $(LK' \log(L/\beta) + (L/\beta)K' \log K')$ represents the complexity of SFFT. For the IIC hybrid receiver, LK' multiplications are

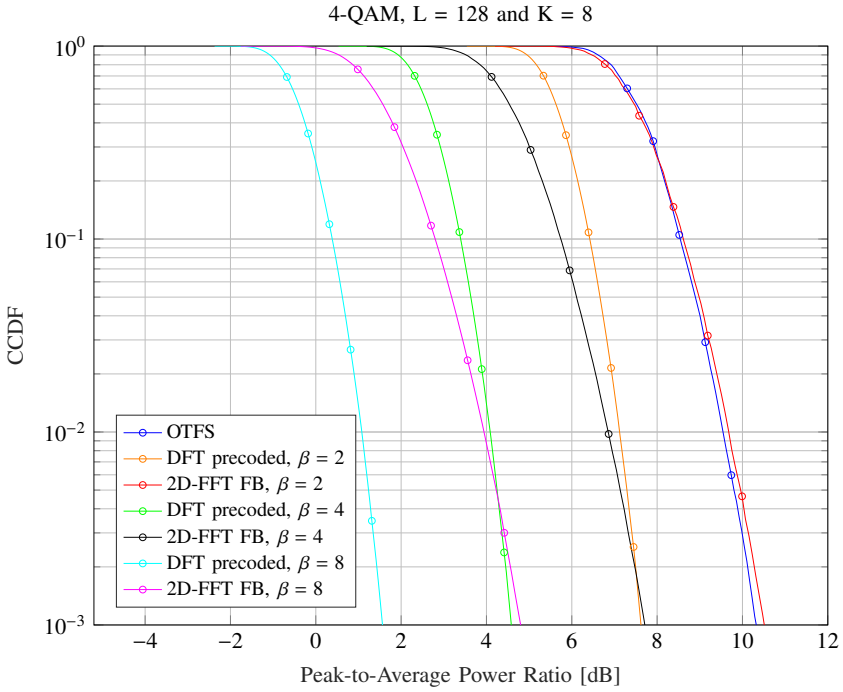

Figure 62 – PAPR analysis between waveforms.

Receiver	Complexity
MMSE - TF domain	$O(LK')$
MMSE - DD domain	$O(L^3K'^3)$
IB-DFE	$O(\bar{i}LK'\log(L/\beta) + \bar{i}(L/\beta)K'\log K')$
IIC	$O(LK' + \bar{i}(LK'/\beta)^2)$
AMP-FO	$O(\bar{i}LK'P + \bar{i}LK'Z)$

Table 10 – Computational complexity of the receivers.

required due to the MMSE-TF plus a cost of $\tilde{i}(LK')^2$ multiplying the matrix $\mathbf{\Delta}-$ diag $\{\mathbf{\Delta}\}$ by the vector $\hat{\mathbf{a}}$ if we consider $\bar{i}$. In addition to the size of the delay-Doppler grid, the complexity of the AMP-FO receiver is calculated as a function of the constelation size Z-QAM, the number of the channel taps P and also the number of iterations used in the algorithm [29]. Although the order of the AMP-FO and IB-DFE receivers are the same (linear), the computational implementation of AMP-FO has a much greater complexity due to the number of operations performed by the algorithm. Furthermore, a much larger number of iterations are required in AMP-FO than in IB-DFE for same-order error performance. A more effective analysis of the complexity of the AMP-FO should be studied. It is worth mentioning that if the receivers are being applied in the OTFS technique, the value of K' is replaced by K and we will not have division by β in the squared and cubed terms.

The rate factor (β) must be understood primarily as a frequency spreading factor. That is, L/β active data is spread at L points in frequency domain by the $\mathbf{C}_f$ precoding

matrix. Of course, to maintain the same transmitted symbol density of an L-OFDM system, the new system must operate at a rate (β) times higher than conventional OFDM. The interesting thing about using this transmission technique is that it allows the following:

- Lower PAPR, due to the effective reduction in the length of active symbols by the rate factor;
- Better performance in environments with mobility, due to the reduction of the Doppler effect;
- Flexibility waveform design, as the number of subcarriers with useful information is no longer fixed to half the number of subcarriers, but now depends on β.

7 Final considerations

The dispersive nature of the wireless communication channel meant that over time, a series of research topics were proposed to use it efficiently. In particular, the FBMC system is an interesting modulation scheme for future wireless systems because it has much lower OOB emissions compared to OFDM. The need for an efficient allocation of available time-frequency resources is an essential factor in new wireless systems that cover numerous scenarios. Filtering on each subcarrier allows this efficient allocation, however, the constraint of orthogonality to the real field in order to respect the Balian-Low theorem is an issue to be worked on and resolved. This brings us to the study of precoded systems to recover complex orthogonality in filter bank-based systems. In this context, we present a new structure based on the system proposed in [38]. This scheme called DFT precoded filter bank can be viewed as a hybrid between FBMC and SC-FDMA. The technique restores the complex orthogonality, the prototype filter has a spectrum well located in time and frequency with low OOB emission and a low PAPR is obtained. The scheme is built from the spread of data in the frequency domain through a DFT. Furthermore, the complex orthogonality is re-established by including a filter interference compensation factor combined with a data allocation strategy. Thus, complex data transmission is allowed on half of the subcarriers of a multicarrier symbol. Using the double rate transmission of FBMC/OQAM systems, the same transmission capacity of an OFDM symbol is obtained without the need for the phase term for OQAM. In addition, we present a new matrix analysis for filter bank systems that is extremely important for understanding the precoding process. Such notation is based on an implementation by polyphase networks, where we were able to extract the Fourier transform from the filter matrix. This allows us to better understand the filter compensation process behind precoding, the reason for avoiding critical sampling, and limiting the filter overlap factor.

All system derivations, theoretical analyses, SINR, SIR come from this notation. The compensation stage is a multiplicative factor, in this sense, the interference from the filter must also be of only one coefficient. Therefore, in the prototype filter and system design, we derive that the filter overlap factor should not be greater than 1.5 for perfect interference compensation. Thinking about systems that need low latency, a short filter like one with $O < 1.5$ is interesting to use. On the other hand, if it is important to obtain a better spectral localization, this factor needs to be increased, effectively generating interference in the system. Therefore, we present in this work two iterative receivers with the objective of obtaining better performance in terms of BER and also enabling the use of overlap factors greater than 1.5 while maintaining an acceptable BER level. While the first receiver is based only on minimizing residual channel interference, the second

receiver encompasses eliminating filter and channel interference at the expense of greater computational complexity. The system performance was also evaluated in scenarios with high Doppler spreading and using multiple antennas in the reception. A certain robustness of the system was observed in these scenarios with high speeds and that the increase of the spatial diversity in the reception significantly increases the performance.

Future wireless systems will be present in millimeter-waves band and high mobility environments such as high speed trains. Data transmission in this type of scenario where the channels vary in time and with higher Doppler dispersion is a challenge. Thus, we present a new precoded filter bank structure based on OTFS modulation, which has significant advantages in doubly selective channels. The proposed study focuses on the impact of interference rejection in a channel with large Doppler spreading. Allied to a PAPR similar to OTFS and a better spectral localization, the proposed system called 2D-FFT FB is a good alternative for emerging applications. Its structure was obtained with the initial objective of eliminating the filter's intrinsic interference from the use of pre-coding based on symbol spreading. The key point is that the pre-coding used to restore complex orthogonality is part of the ISFFT applied as pre-coding in the OTFS system. Thus, the analysis and addition of elements in the pre-coding was envisaged in order to obtain a new waveform that holds robustness in high mobility scenarios, preserving this complex orthogonality and maintaining a low PAPR. Furthermore, compared to OTFS, the cyclic prefix is removed, better spectral localization is obtained and a simple time-frequency domain equalization can be applied providing significantly superior error performance. Exploiting this behavior, we introduce a hybrid receiver that uses an equalization stage in the frequency domain combined with an interference canceller in the delay-Doppler domain. With this receiver, error performance is obtained at the same levels of receivers of the OTFS technique in the DD domain with less complexity.

From the imposed precoding combined with the data allocation strategy, complex orthogonality is restored and the use of OQAM modulation is avoided. In this way, the scheme is no longer tied to double-rate transmission, allowing flexibility in the structure of the filter bank. This is done by introducing the rate factor through the variable β. Thus, the impact of frequency spreading for different values of β in high mobility scenarios was explored. In fact, the number of subcarriers with useful information is no longer fixed to half the number of subcarriers, but now depends on β. In this sense, the data spread length in the frequency domain is greater. It was noted that the increase in frequency spreading by the β factor increased the Doppler robustness, bringing better error performance in these high mobility scenarios, especially in the 2D-FFT FB. It was observed that using $\beta = 4$ and a one-tap equalizer in the TF domain, performance is achieved at the same levels of more complex receivers in the DD domain studied in OTFS. Also, by varying the rate factor, less data is transmitted per symbol; however, this transmission is done faster, ensuring symbol density for all scenarios. Thus, we have a reduction in PAPR of about 3

dB between each change in the rate factor β. Finally, the generalization of the systems allowed increasing the filter overlap factor O to values just above 1.5, guaranteeing the complete cancellation of the filter interference. The key point of this generalization and application of rates other than the double rate ($\beta = 2$) of FBMC/OQAM based systems, is performance gain in high mobility scenarios. In fact, for the 2D-FFT FB system, which by itself presents such a characteristic, its application intensified this robustness even more. It is worth mentioning again that closed solutions of SIR, SINR and BER were derived validating the results obtained through simulations. It is noteworthy that the articles produced have more complete analysis and more detailed conclusions about the results obtained in this work - especially those of chapter 4, 5 and 6.

7.1 Future perspectives

This work opens several aspects to be addressed in the future, such as an expansion to the case of using MIMO techniques and more aggressive channels in terms of time spreading. The channel estimation process proves to be quite challenging when considering reception in the DD domain in OTFS. The investigation of this process considering the equalization in the TF domain as well as the errors in this process are also studies to be investigated. The application of other receivers proposed for the OTFS technique, such as those based on message passing algorithm (MPA), is an interesting topic to work on. Further comparisons can be made in terms of performance, complexity and compatibility with the system proposed in this work. Obtaining good results in the TF domain for the 2D-FFT FB is due to the filtering process on each subcarrier. This aspect can be analyzed in detail in later works. A more detailed study of frequency scattering in relation to the mobile communication channel can also be better explored. The complexity analysis and a more concise simplification in relation to the precoding process, more precisely the DFT with the multicarrier core represented by the IDFT, is another interesting topic to be addressed. Finally, it would be interesting to compare the proposed structure with other waveforms and the use of filters designed for smaller overlap factors in order to benefit from the extended rate limit.

Bibliography

1 BELLANGER, M. G. Specification and design of a prototype filter for filter bank based multicarrier transmission. In: CITESEER. *icassp*. [S.l.], 2001. v. 1, p. 2417–2420.

2 ZAKARIA, R. *Transmitter and receiver design for inherent interference cancellation in MIMO filter-bank based multicarrier systems*. Tese (Doutorado), 2012.

3 DEMESTICHAS, P. et al. 5G on the horizon: Key challenges for the radio-access network. *IEEE vehicular technology magazine*, IEEE, v. 8, n. 3, p. 47–53, 2013.

4 TULLBERG, H. et al. The METIS 5G system concept: Meeting the 5G requirements. *IEEE Communications magazine*, IEEE, v. 54, n. 12, p. 132–139, 2016.

5 SHAFI, M. et al. 5G: A tutorial overview of standards, trials, challenges, deployment, and practice. *IEEE journal on selected areas in communications*, IEEE, v. 35, n. 6, p. 1201–1221, 2017.

6 RAPPAPORT, T. S. et al. Millimeter wave mobile communications for 5G cellular: It will work! *IEEE access*, IEEE, v. 1, p. 335–349, 2013.

7 ROH, W. et al. Millimeter-wave beamforming as an enabling technology for 5G cellular communications: Theoretical feasibility and prototype results. *IEEE communications magazine*, IEEE, v. 52, n. 2, p. 106–113, 2014.

8 SARI, H.; KARAM, G.; JEANCLAUDE, I. Transmission techniques for digital terrestrial TV broadcasting. *IEEE communications magazine*, IEEE, v. 33, n. 2, p. 100–109, 1995.

9 GROUP, I. . W. et al. Ieee standard for local and metropolitan area networks-part 16: Air interface for fixed broad-band wireless access systems. *IEEE Std. 802.16-2004*, 2004.

10 WANNSTROM, J. LTE-advanced. *3GPP, June*, 2013.

11 38.802, G. T. Study on new radio access technology, physical layer aspects (release 14). 2017.

12 SAAD, W.; BENNIS, M.; CHEN, M. A vision of 6G wireless systems: Applications, trends, technologies, and open research problems. *IEEE network*, IEEE, v. 34, n. 3, p. 134–142, 2019.

13 SIOHAN, P.; SICLET, C.; LACAILLE, N. Analysis and design of OFDM/OQAM systems based on filterbank theory. *IEEE transactions on signal processing*, IEEE, v. 50, n. 5, p. 1170–1183, 2002.

14 STITZ, T. H. Filter bank techniques for the physical layer in wireless communications. *Tampere University of Technology publications*, v. 919, 2010.

15 FARHANG-BOROUJENY, B. OFDM versus filter bank multicarrier. *IEEE signal processing magazine*, IEEE, v. 28, n. 3, p. 92–112, 2011.

16 BELLANGER, M. et al. FBMC physical layer: a primer. *PHYDYAS, January*, v. 25, n. 4, p. 7–10, 2010.

17 BALIAN, R. Un principe d'incertitude fort en théorie du signal ou en mécanique quantique. *CR Acad. Sci. Paris*, v. 292, n. 2, p. 1357–1361, 1981.

18 PISCHELLA, M.; RUYET, D. L. *Digital Communications 2: Digital Modulations*. [S.l.]: John Wiley & Sons, 2015. v. 2.

19 BELLANGER, M. Transmit diversity in multicarrier transmission using OQAM modulation. In: IEEE. *2008 3rd International Symposium on Wireless Pervasive Computing*. [S.l.], 2008. p. 727–730.

20 PEREZ-NEIRA, A. I. et al. MIMO signal processing in offset-QAM based filter bank multicarrier systems. *IEEE Transactions on Signal Processing*, IEEE, v. 64, n. 21, p. 5733–5762, 2016.

21 TAHERI, S. et al. Evaluation of preamble based channel estimation for MIMO-FBMC systems. *ZTE Communications*, v. 14, n. 4, p. 3–10, 2019.

22 DEMIR, A. F. et al. Waveform design for 5G and beyond. *arXiv preprint arXiv:1902.05999*, 2019.

23 MYUNG, H. G.; LIM, J.; GOODMAN, D. J. Single carrier FDMA for uplink wireless transmission. *IEEE vehicular technology magazine*, IEEE, v. 1, n. 3, p. 30–38, 2006.

24 HADANI, R. et al. Orthogonal time frequency space modulation. In: IEEE. *2017 IEEE Wireless Communications and Networking Conference (WCNC)*. [S.l.], 2017. p. 1–6.

25 MURALI, K.; CHOCKALINGAM, A. On OTFS modulation for high-doppler fading channels. In: IEEE. *2018 Information Theory and Applications Workshop (ITA)*. [S.l.], 2018. p. 1–10.

26 HADANI, R.; MONK, A. OTFS: A new generation of modulation addressing the challenges of 5G. *arXiv preprint arXiv:1802.02623*, 2018.

27 SURABHI, G.; CHOCKALINGAM, A. Low-complexity linear equalization for OTFS modulation. *IEEE communications letters*, IEEE, v. 24, n. 2, p. 330–334, 2019.

28 WU, S. et al. Low-complexity iterative detection for large-scale multiuser MIMO-OFDM systems using approximate message passing. *IEEE Journal of Selected Topics in Signal Processing*, IEEE, v. 8, n. 5, p. 902–915, 2014.

29 BANDEIRA, D. et al. Performance evaluation of low-complexity algorithms for orthogonal time-frequency space modulation. *Journal of Communication and Information Systems*, v. 35, n. 1, p. 138–149, 2020.

30 ZHANG, H.; ZHANG, T. A low-complexity message passing detector for OTFS modulation with probability clipping. *IEEE wireless communications letters*, IEEE, v. 10, n. 6, p. 1271–1275, 2021.

31 ZEMEN, T.; HOFER, M.; LOESCHENBRAND, D. Low-complexity equalization for orthogonal time and frequency signaling (OTFS). *arXiv preprint arXiv:1710.09916*, 2017.

32 RAVITEJA, P. et al. Interference cancellation and iterative detection for orthogonal time frequency space modulation. *IEEE Transactions on Wireless Communications*, IEEE, v. 17, n. 10, p. 6501–6515, 2018.

33 TIWARI, S.; DAS, S. S.; RANGAMGARI, V. Low complexity LMMSE receiver for OTFS. *IEEE communications letters*, IEEE, v. 23, n. 12, p. 2205–2209, 2019.

34 LÉLÉ, C.; SIOHAN, P.; LEGOUABLE, R. The alamouti scheme with CDMA-OFDM/OQAM. *EURASIP Journal on Advances in Signal Processing*, Springer, v. 2010, p. 1–13, 2010.

35 NISSEL, R.; BLUMENSTEIN, J.; RUPP, M. Block frequency spreading: A method for low-complexity MIMO in FBMC-OQAM. In: IEEE. *2017 IEEE 18th International Workshop on Signal Processing Advances in Wireless Communications (SPAWC)*. [S.l.], 2017. p. 1–5.

36 ZAKARIA, R.; RUYET, D. L. A novel filter-bank multicarrier scheme to mitigate the intrinsic interference: Application to MIMO systems. *IEEE Transactions on Wireless Communications*, IEEE, v. 11, n. 3, p. 1112–1123, 2012.

37 DEMMER, D. et al. Block-filtered OFDM: a novel waveform for future wireless technologies. In: IEEE. *2017 IEEE International Conference on Communications (ICC)*. [S.l.], 2017. p. 1–6.

38 NISSEL, R.; RUPP, M. Pruned DFT-Spread FBMC: Low PAPR, low latency, high spectral efficiency. *IEEE Transactions on Communications*, IEEE, v. 66, n. 10, p. 4811–4825, 2018.

39 SALTZBERG, B. Performance of an efficient parallel data transmission system. *IEEE Transactions on Communication Technology*, IEEE, v. 15, n. 6, p. 805–811, 1967.

40 DINIZ, P. S.; SILVA, E. A. D.; NETTO, S. L. *Digital signal processing: system analysis and design*. [S.l.]: Cambridge University Press, 2010.

41 GOLDSMITH, A. *Wireless communications*. [S.l.]: Cambridge university press, 2005.

42 HIROSAKI, B. An orthogonally multiplexed qam system using the discrete fourier transform. *IEEE Transactions on Communications*, IEEE, v. 29, n. 7, p. 982–989, 1981.

43 PELED, A.; RUIZ, A. Frequency domain data transmission using reduced computational complexity algorithms. In: IEEE. *Acoustics, Speech, and Signal Processing, IEEE International Conference on ICASSP'80*. [S.l.], 1980. v. 5, p. 964–967.

44 LATHI, B.; DING, Z. Sistemas de comunicações analógicos e digitais modernos. *LTC, Rio de Janeiro*, 2012.

45 GRAY, R. M. Toeplitz and circulant matrices: A review (foundations and trends in communications and information). *Now Publishers Inc., Hanover, MA*, 2006.

46 TU, J. C. *Theory, design and application of multi-channel modulation for digital communications*. Tese (Doutorado) — Stanford University, 1991.

47 MEDJAHDI, Y. *Interference modeling and performance analysis of asynchronous OFDM and FBMC wireless communication systems*. Tese (Doutorado) — Conservatoire national des arts et metiers-CNAM, 2012.

48 LIM, D.-W.; HEO, S.-J.; NO, J.-S. An overview of peak-to-average power ratio reduction schemes for OFDM signals. *journal of communications and networks*, KICS, v. 11, n. 3, p. 229–239, 2009.

49 ABDOLI, J.; JIA, M.; MA, J. Filtered OFDM: A new waveform for future wireless systems. In: IEEE. *2015 IEEE 16th International Workshop on Signal Processing Advances in Wireless Communications (SPAWC)*. [S.l.], 2015. p. 66–70.

50 WILD, T.; SCHAICH, F.; CHEN, Y. 5G air interface design based on universal filtered (UF-) OFDM. In: IEEE. *2014 19th International Conference on Digital Signal Processing*. [S.l.], 2014. p. 699–704.

51 FEICHTINGER, H. G.; STROHMER, T. *Gabor analysis and algorithms: Theory and applications*. [S.l.]: Springer Science & Business Media, 2012.

52 ZAKARIA, R.; RUYET, D. L. A novel FBMC scheme for spatial multiplexing with maximum likelihood detection. In: IEEE. *2010 7th International Symposium on Wireless Communication Systems*. [S.l.], 2010. p. 461–465.

53 BELLANGER, M.; BONNEROT, G.; COUDREUSE, M. Digital filtering by polyphase network: Application to sample-rate alteration and filter banks. *IEEE Transactions on Acoustics, Speech, and Signal Processing*, IEEE, v. 24, n. 2, p. 109–114, 1976.

54 CHANG, B. S. *New precoding and equalization techniques for multicarrier systems*. Tese (Doutorado), 2012.

55 HAAS, R.; BELFIORE, J.-C. A time-frequency well-localized pulse for multiple carrier transmission. *Wireless personal communications*, Springer, v. 5, n. 1, p. 1–18, 1997.

56 NISSEL, R.; SCHWARZ, S.; RUPP, M. Filter bank multicarrier modulation schemes for future mobile communications. *IEEE Journal on Selected Areas in Communications*, IEEE, v. 35, n. 8, p. 1768–1782, 2017.

57 NISSEL, R.; RUPP, M.; MARSALEK, R. FBMC-OQAM in doubly-selective channels: A new perspective on MMSE equalization. In: IEEE. *2017 IEEE 18th International Workshop on Signal Processing Advances in Wireless Communications (SPAWC)*. [S.l.], 2017. p. 1–5.

58 ZHOU, Z. et al. Learning to equalize OTFS. *IEEE Transactions on Wireless Communications*, IEEE, 2022.

59 RAVITEJA, P. et al. Practical pulse-shaping waveforms for reduced-cyclic-prefix OTFS. *IEEE Transactions on Vehicular Technology*, IEEE, v. 68, n. 1, p. 957–961, 2018.

60 DANG, U. L. et al. On time domain co-channel interference suppression for sc-fdma transmission. In: IEEE. *Wireless Communications and Networking Conference (WCNC), 2011 IEEE*. [S.l.], 2011. p. 1253–1258.

61 DOUCET, A.; WANG, X. Monte carlo methods for signal processing: a review in the statistical signal processing context. *IEEE Signal Processing Magazine*, IEEE, v. 22, n. 6, p. 152–170, 2005.

62 LTE, E. Evolved universal terrestrial radio access (e-utra); base station (bs) radio transmission and reception (3gpp ts 36.104 version 8.6. 0 release 8), july 2009. *Etsi ts*, v. 136, n. 104, p. V8, 2009.

63 MOLISCH, A. F. *Wireless communications*. [S.l.]: John Wiley & Sons, 2012.

64 NA, D.; CHOI, K. Low PAPR FBMC. *IEEE Transactions on Wireless Communications*, IEEE, v. 17, n. 1, p. 182–193, 2017.

65 DENT, P.; BOTTOMLEY, G. E.; CROFT, T. Jakes fading model revisited. *Electronics letters*, v. 13, n. 29, p. 1162–1163, 1993.

66 Benvenuto, N.; Tomasin, S. Iterative design and detection of a DFE in the frequency domain. *IEEE Transactions on Communications*, v. 53, n. 11, p. 1867–1875, 2005.

67 MOLISCH, A. F.; TOELTSCH, M.; VERMANI, S. Iterative methods for cancellation of intercarrier interference in OFDM systems. *IEEE Transactions on Vehicular Technology*, IEEE, v. 56, n. 4, p. 2158–2167, 2007.

68 JUNIOR, R. P. et al. A novel DFT precoded filter bank system with iterative equalization. *IEEE Wireless Communications Letters*, v. 10, n. 3, p. 478–482, 2021.

69 CHANG, B. S. et al. A simplified widely linear iterative equalizer for SC-FDE systems. In: IEEE. *Wireless Days, 2017*. [S.l.], 2017. p. 159–162.

70 JUNIOR, R. P. et al. Equalização largamente linear aplicada a supressão de interferências em sistemas sc-fde. 2018.

71 ZAKARIA, R.; RUYET, D. L. Intrinsic interference reduction in a filter bank-based multicarrier using QAM modulation. *Physical Communication*, Elsevier, v. 11, p. 15–24, 2014.

72 MAHAMA, S. et al. Iterative interference cancellation in FBMC-QAM systems. In: IEEE. *2019 IEEE Wireless Communications and Networking Conference (WCNC)*. [S.l.], 2019. p. 1–5.

73 MEREDITH, J. Study on channel model for frequency spectrum above 6 GHz. *3GPP TR 38.900, Jun, Tech. Rep.*, 2016.

74 SURABHI, G.; AUGUSTINE, R. M.; CHOCKALINGAM, A. Peak-to-average power ratio of OTFS modulation. *IEEE Communications Letters*, IEEE, v. 23, n. 6, p. 999–1002, 2019.

75 PEREIRA, R. et al. A generalized DFT precoded filter bank system. *IEEE Wireless Communications Letters*, IEEE, 2022.

76 NISSEL, R.; ADEMAJ, F.; RUPP, M. Doubly-selective channel estimation in FBMC-OQAM and OFDM systems. In: IEEE. *2018 IEEE 88th Vehicular Technology Conference (VTC-Fall)*. [S.l.], 2018. p. 1–5.

77 DEMMER, D. et al. Study of OFDM precoded filter-bank waveforms. *IEEE Transactions on Wireless Communications*, IEEE, v. 18, n. 6, p. 2889–2902, 2018.